

SYSTEMATIC EFFECTS OF LOCAL LARGE SCALE
STRUCTURE ON THE MEASURED EXPANSION
HISTORY OF THE UNIVERSE

A Dissertation

Presented to the Faculty of the Graduate School

of Cornell University

in Partial Fulfillment of the Requirements for the Degree of

Doctor of Philosophy

by

Riva Ashley Vanderveld

August 2007

© 2007 Riva Ashley Vanderveld

ALL RIGHTS RESERVED

SYSTEMATIC EFFECTS OF LOCAL LARGE SCALE STRUCTURE ON THE MEASURED EXPANSION HISTORY OF THE UNIVERSE

Riva Ashley Vanderveld, Ph.D.

Cornell University 2007

We discuss some of the ways that local cosmological inhomogeneity has been found to affect our interpretation of the measurements of the redshifts and luminosity distances of Type Ia supernovae, so that we may ask: Can a matter dominated universe, with gravity governed by general relativity, appear to be accelerating? This discussion focuses on the systematic corrections to measured cosmological parameters that one would find as a result of the “fitting problem”, wherein the fitting of data to what we would see in a homogeneous universe introduces errors due to the nonlinearity of general relativity. It has been suggested that this fitting effect could explain the supernova data without introducing dark energy or modifications of general relativity. We explore this claim within the context of several cosmological scenarios, all of which use standard general relativity and are dust dominated, with no dark energy. First, we use the spherically-symmetric Lemaître-Tolman-Bondi cosmological models, then we look at a simple model for cosmological voids and sheets, and finally we treat the problem in full three dimensional generality. In each of these contexts, we analyze the systematic corrections to the luminosity distances and redshifts of Type Ia supernovae that result from local large scale structure. We then find how such corrections affect the properties of the Universe that we infer from this measured luminosity distance-redshift re-

lation. We show how, in principle, a very large degree of inhomogeneity can trick us into thinking that the expansion of the Universe is accelerating when it is not. However, within the confines of more realistic models, such effects are shown to be small. In the full three dimensional case, we find that the error in the best-fit cosmological constant is approximately $\Delta\Omega_\Lambda \approx 0.004$ for a large sample of supernovae at small redshifts, between $z_{min} = 0.02$ and $z_{max} = 0.15$. Although this error is not large enough to explain the measured cosmological constant value $\Omega_\Lambda \approx 0.7$, it is still a potentially significant systematic error that has not been accounted for previously.

BIOGRAPHICAL SKETCH

Riva Ashley Vanderveld, being the first child of Rheanna and Ronald Vanderveld, was born on a crisp autumn evening in 1980 at the Loyola University Medical Center in Chicago, Illinois, after her mother selflessly endured ten months of pregnancy and 36 hours of labor. Hereafter, the new child would be referenced simply by the nickname “Ali”, so as to profoundly confuse anyone who would ever try to look her up in a phone book. Five years later, Rheanna and Ronald produced young Ali’s eventual best friend, a brother named John, and the family moved to Cincinnati, Ohio.

At the age of seven, Ali discovered music, a passion that would sustain and center her throughout her life, when she first studied the violin and then the piano. She would later go on to study several other musical instruments, including most notably the French horn, which she continues to attempt to play to this very day.

Around 1993, the Vanderveld family moved back to the Chicago suburbs, and their lives became much more difficult. Times were very tough, both financially and emotionally, and this is when the bond between John and Ali first emerged. This is also when the teenage Ali developed a deep appreciation of hip-hop and rap music.

Ali graduated from Adlai Stevenson High School in Lincolnshire, Illinois, in the fall of 1998, torn between her love of music and her apparent aptitude in the areas of math and science. Shunning an invitation to audition at Juilliard music school, she brashly chose to study physics instead. She went on to an atypical and chaotic three years of undergraduate education at the University of Illinois at Urbana-Champaign. She was legally emancipated from her parents and spent

this time coming to terms with her difficult adolescence; this was a draining, but defining, period in Ali's life. Even though she was forced to work four jobs to pay her way through school, the tenacious young woman still managed to attend several house parties, and it was at one such gathering wherein she met the love of her life: a man named John Dailey, Jr.

After graduation from the University of Illinois, John and Ali had their first child: a blue-gray domestic shorthair cat that they named Isaac. Ali then continued her studies at Cornell University in Ithaca, New York, in the field of Mechanical Engineering. After a few short months, the keen student realized her horrible mistake and transferred back into physics, eventually settling into the beginning of a glamorous career as a theoretical cosmologist. In August of 2005, Ali married John Dailey and the couple lived happily ever after. In August of 2007, she receives her Ph.D. in physics.

To my best friend at my most difficult time, to Max.

ACKNOWLEDGEMENTS

First of all, I have to thank Ira Wasserman, who has taught me practically everything that I know about how to be a scientist. Why he foolishly chose to take me on as a student, despite how poorly prepared I was for graduate school, will forever remain a mystery to me. I have always been grateful, though, for his unending patience and his amazing pedagogical style (that, despite what he says, is not at all like that torture where they shove bamboo under your fingernails). I am also thankful that Ira forced Éanna Flanagan to watch over me during his sabbatical, because this left me with the great fortune to have two advisors, both with fantastic ideas that I could steal and present as my own. Ira and Éanna, I have also appreciated your patience with my continued inability to do math. To my experimentalist committee member Jim Alexander, thank you for taking the time and effort to be on my committee, and for allowing me to pass my exams. Also, thank you for allowing me to join the physics department in the first place.

There are several other professors who have helped me greatly throughout my education. I am thankful to have the continuing influence of Karin Dahmen, who gently introduced me to the wonders of scientific research, and who continues to write me all of those letters of recommendation. I am also thankful to have had Jeremiah Sullivan as my undergraduate academic advisor. Also, thanks go to Carl Franck for all of the helpful discussions and advice.

There are many other people at Cornell to whom I owe thanks. Special thanks go to Deb Hatfield, Sherry Falletta, Monica Armstrong, Lisa Margosian, and all other administrative employees of the Cornell physics and astronomy departments. I am also sincerely grateful to Tony Ingraffea and the Cornell Theory Center, for giving my husband a job that he loves so much that he had sort of hoped that I

would never graduate. I must also thank the office-mates who have further tried to impede my graduation during the past few years: Marko, Matt, Zach, Andy, Taner, and Dave.

I also acknowledge the financial support that I have received throughout my graduate education, through the National Science Foundation Graduate Research Fellowship, from the Cornell NASA Space Grant Program, and from the American Association of University Women.

Before I came to Cornell, my life hit a rough patch, and so this section would be incomplete if I did not thank all of the people that helped me during that time. I am sincerely grateful to have had such an amazing support system at the University of Illinois during the emancipation process. Particular thanks go to Deans Abby Broga and Sister Marie. Also deserving of gratitude, are all of the families who chose to take me in during those times when I was “homeless”, i.e. when I lived in the University of Illinois dormitories and they closed for school holidays. So thank you Alissa Nickow, Bridget O’Connell, Lisa Dieter, Jenny Katehos, Libby Bond, Christy Healan, and the Daileys. These families treated me like I was family when I did not have my own to go to, and invited me into their homes for spring break, summer break, Thanksgiving, and Christmas.

I would also like to thank my own family, starting with my parents. I realize now just how much they really do love me, and that they tried to take care of me despite some exceptionally difficult circumstances. But I am also appreciative of my extended family, who has recently helped me realize that my lot in life is not as bad as I had thought. In the past few years that I have gotten to know them, my life has been enriched by the love and support of my cousins, uncles, and aunts, especially the Del Valles: Lissy, John, Joy, and Chase. I am also very grateful to

have my husband John and his family in my life now. John has been an amazing supporter throughout my graduate studies, and Mary and John Dailey, Sr., have tried to treat me as their own daughter. John, thank you for taking such good care of me after my knee surgeries, and for cooking me all of those dinners and washing all of those dishes. Also, I thank my best animal friends Max (who is recently deceased) and Isaac for always being there for me to pet and play with.

Finally, I owe everything that I've accomplished in life to my brother, John. Literally, none of this would have been possible without his love and support. Words cannot describe how much he means to me.

TABLE OF CONTENTS

1	Introduction	1
1.1	The Luminosity Distance-Redshift Relation	1
1.1.1	Measuring Acceleration and Dark Energy with Type Ia Supernovae	2
1.1.2	The Fitting Problem	4
1.2	Acceleration from Errors in Fit Assumptions: Two Illustrative Examples	6
1.2.1	Spatial Curvature	6
1.2.2	The Empty Beam Approximation	7
1.3	Overview of Thesis	11
2	Effects of Inhomogeneity in Spherical Symmetry*	13
2.1	Introduction	13
2.2	The Forward Problem	16
2.2.1	Lemaître-Tolman-Bondi Models	16
2.2.2	The Weak Singularity at $r = 0$	19
2.2.3	Proof of $q_0 \geq 0$ Directly from LTB Solutions	24
2.2.4	Models of Iguchi, Nakamura and Nakao	26
2.2.5	Achieving a Negative Apparent Deceleration Parameter at Nonzero Redshifts	28
2.3	The Inverse Problem	31
2.3.1	General Properties	31
2.3.2	Manufacturing Transcritical Solutions	40
2.4	Conclusions	47
3	Systematic Effects of Cosmological Voids and Sheets	51
3.1	Introduction	51
3.2	Model Dynamics	52
3.3	Motion of a Single Light Ray	58
3.3.1	First Order Results	61
3.3.2	Second Order Results	63
3.4	Effect on the Luminosity Distance	65
3.4.1	Mean Effect	66
3.4.2	Variance Estimate	68
3.5	Conclusions	69
4	Systematic Effects in General Three Dimensional Models[†]	71
4.1	Introduction	71
4.2	Post-Newtonian Expansion of the Local FRW Metric	76

*This chapter is published in Vanderveld, Flanagan, and Wasserman (2006).

[†]This chapter is published in Vanderveld, Flanagan, and Wasserman (2007).

4.3	Computation of Luminosity Distance and Redshift	80
4.3.1	Computing $D_L(z)$ in a General Spacetime	80
4.3.2	Computing $D_L(z)$ to First Post-Newtonian Order	82
4.4	Adding Density Perturbations	85
4.4.1	Basic Method	85
4.4.2	Unperturbed Quantities	88
4.4.3	Second Order Perturbed Optics	89
4.5	The Perturbation to the Inferred Cosmological Constant	97
4.5.1	Finding the Best-Fit FRW Model	97
4.5.2	Variance	103
4.6	Consistency with Prior Results	106
4.7	Conclusions	112
5	Summary of Results	115
5.1	Models Used in this Study	115
5.2	Systematic Corrections to $D_L(z)$ and Their Impact on the Assessment of Acceleration	116
A	Details of the Calculation in Chapter 4	118
A.1	Combining the Redshift and Luminosity Distance Relations	118
A.2	Newtonian Second-Order Perturbation Theory	121
A.3	Averaging the Luminosity Distance-Redshift Relation	122
A.4	Transforming from the Standard Post-Newtonian Gauge to the Synchronous Gauge	126
	Bibliography	130

LIST OF FIGURES

1.1	The inferred deceleration parameter q versus redshift z for several values of Ω_k , when the supernova data are interpreted within the framework of a flat cosmological model. Shown here are results for the models where $\Omega_k = 0.2, 0.4, 0.6,$ and 0.8	8
1.2	The effective deceleration parameter q versus redshift z in the empty beam approximation.	10
2.1	The effective deceleration parameter q versus redshift z for several quadratic bang time models which have a minimum q of approximately negative one. Plotted here are the data for models with $(\lambda, D) = (0.094, 0.14), (0.20, 0.29), (0.46, 0.62), (0.75, 0.91),$ and $(1.0, 1.2)$	30
2.2	Several measures of the feasibility of quadratic bang time models, plotted versus D for $\lambda = 1, 0.751, 0.589,$ and 0.455 . From top to bottom, we have plotted $\Delta z_{neg}, \Delta z_{q<-1},$ and $z_{max},$ all versus D . . .	32
2.3	Results for our candidate transcritical model with $K = 1, p = 2, n = 3,$ and $\tilde{r}_1 = 1.05,$ out to $z = 1000$. The left panel shows $r_{FRW}(z)/r_{FRW}^{(0)}(z)$ (dotted), $h(z) \equiv H(z)/[H_0(1+z)^{3/2}]$ (short dashed), and $w_{eff}(z)$ (solid). The reference model corresponding to $r_{FRW}^{(0)}(z)$ is the spatially flat Λ CDM model with $\Omega_M = 0.27$. The right panel shows V (short dashed), $1 - d \ln r_{FRW}/d \ln(1+z)$ (dotted), and t_0 (solid).	46
2.4	Distance moduli relative to spatially flat Λ CDM with $\Omega_M = 0.27$ for models with $K = 1$ and $(n, p) = (3, 2)$ (solid), $(n, p) = (3, 4)$ (dotted), $(n, p) = (2, 2)$ (dashed), and $(n, p) = (2, 4)$ (dash-dot), with $\tilde{r}_1 = 1.05$ for the lower set of curves, and $\tilde{r}_1 = 1.5$ for the upper set.	48
4.1	The best-fit cosmological constant density Ω_Λ plotted as a function of the maximum redshift z_{max} , for the choices $z_{min} = 0.01, 0.02,$ and 0.03 . The horizontal dash-dot line shows the actual model value $\Omega_\Lambda = 0$	73
4.2	The function $1+f(r)$ plotted versus $k_{eq}r$, where k_{eq} is the wavenumber of the dominant perturbation mode.	95
4.3	The relative size of the perturbation $\log[\Delta D_L(z) /D_{L(0)}(z)]$ plotted versus $\log(z)$, assuming that the dominant perturbation wavelength is 10^3 times smaller than the Hubble scale: $k_{eq}/H_0 = 10^3$	96

LIST OF TABLES

- 4.1 Best-fit parameters in the continuum limit for a few values of the source catalog limiting redshifts z_{min} and z_{max} , also for the choice that the dominant perturbation wavelength is 10^3 times smaller than the Hubble scale: $k_{eq}/H_0 = 10^3$ 103
- 4.2 Best-fit parameters for 20 catalogs of N=100 samples each, for a few values of the source catalog limiting redshifts z_{min} and z_{max} . We have also made the choice that the dominant perturbation wavelength is 10^3 times smaller than the Hubble scale: $k_{eq}/H_0 = 10^3$. . . 104

Chapter 1

Introduction

1.1 The Luminosity Distance-Redshift Relation

In the past decade, the measurement of the luminosity distances and redshifts of Type Ia supernovae has led to a complete overhaul of our perception of the Universe [1, 2]. These observations have fostered the belief that the expansion of the Universe is accelerating, a phenomenon that would require the introduction of radically new physics.

The luminosity distance of a light source,

$$D_L = \sqrt{\frac{L}{4\pi F}}, \quad (1.1)$$

is related to the source's emitted luminosity L and the received flux F . This gives a very natural measure of distance, given that we know the emitted luminosity. Type Ia supernovae have been found to be a good source for this purpose, because of our apparent ability to measure L . The progenitor of this type of supernova is thought to be a carbon-oxygen white dwarf that is accreting material from a companion. This process continues until a thermonuclear explosion is triggered before the white dwarf approaches a critical mass, the Chandrasekhar limit, of approximately 1.44 solar masses. As a result of this common mass scale, these explosions are relatively homogeneous and predictable. Accordingly, it appears as though there is a correlation between the peak brightnesses and the overall timescales of their light curves [3].

Type Ia supernovae are very bright, with peak bolometric luminosities of 10^{43} ergs per second, an energy output rate that is 5 billion times larger than that of the Sun. The rise times and decay times of their light curves are $\sim 15 - 20$ days and ~ 2 months, respectively [4]. They also have a very distinct spectrum, with a pronounced Si-II absorption line and no hydrogen lines.

Another natural measure of cosmological distance to a source is the redshift of the light received,

$$z = \frac{\lambda_{obs} - \lambda_{em}}{\lambda_{em}} , \quad (1.2)$$

where λ_{em} is the emitted wavelength and λ_{obs} is the observed wavelength. This is measured by looking at either key spectral lines or the apparent color of the observed object. For every source in a given catalog of Type Ia supernovae, we can measure D_L and z , so that we find the function $D_L(z)$. We then fit $D_L(z)$ to cosmological models. The models used are typically homogeneous and expanding, employing the Friedmann-Robertson-Walker (FRW) metric with the line element

$$ds^2 = -dt^2 + a^2(t)\delta_{ij}dx^i dx^j , \quad (1.3)$$

where $a(t)$ is the scale factor, and where we have set $c = G = 1$. The scale factor is typically normalized such that $a(t_0) = 1$ today, where t_0 is the present time.

1.1.1 Measuring Acceleration and Dark Energy with Type Ia Supernovae

In a given FRW cosmological model, the expansion history $a(t)$ is related to $D_L(z)$. However, knowledge of $D_L(z)$ is not sufficient to tell us the correct underlying

physical model, as there is a large degree of degeneracy [5]. In other words, it is possible that very different cosmological models can yield similar results for $D_L(z)$.

For FRW models that are governed by general relativity, the Einstein equation gives us the behavior of $a(t)$; for a review, see [6]. For example, for a flat universe,

$$a(t) = \left(\frac{t}{t_0} \right)^{2/3(1+w)}, \quad (1.4)$$

where w is the equation of state parameter that relates the pressure of the fluid in the Universe to its density: $p = w\rho$. The scale factor $a(t)$ is then related to the Hubble rate and the deceleration parameter. For a general model, these are defined to be

$$H \equiv \frac{\dot{a}}{a} \quad (1.5)$$

and

$$q \equiv -\frac{a\ddot{a}}{\dot{a}^2}, \quad (1.6)$$

respectively. Because of the proportionality to \ddot{a} , the sign of the deceleration parameter tells us whether the expansion of the Universe is accelerating or decelerating, positive q denoting deceleration and negative q denoting acceleration.

Fitting FRW models to the observed $D_L(z)$ can tell us about the contents of the Universe, if we make certain assumptions about the underlying model. Assuming general relativity, it turns out that the data are well fit by a flat model containing pressureless matter with a density ρ_M such that $\Omega_M = \rho_M/\rho_c \approx 0.3$, and a cosmological constant with the density ρ_Λ such that $\Omega_\Lambda = \rho_\Lambda/\rho_c \approx 0.7$, where $\rho_c = 3H_0^2/8\pi G$ is the critical density for flatness and $H_0 \approx 70$ (km/s)/Mpc is the Hubble rate today. There is further evidence for this ‘‘concordance’’ model from other cosmological observations, including the Cosmic Microwave Background

(CMB) data [7]. The luminosity distance redshift relation of this model is that of a flat universe,

$$D_L(z) = (1+z) \int_0^z \frac{dz'}{H(z')}, \quad (1.7)$$

where the Hubble rate is that of a Λ CDM model, i.e. a model containing only pressureless matter and a cosmological constant,

$$H^2(z) = H_0^2 [\Omega_M(1+z)^3 + \Omega_\Lambda]. \quad (1.8)$$

This model is presently undergoing accelerated expansion.

This result, that the data are best fit by a presently accelerating model, is the crux of the “dark energy problem”, as there is still a lack of a satisfactory explanation for the physics behind this acceleration. There are fundamental issues with having a cosmological constant of the measured size, and so many alternate explanations for the seemingly anomalous supernova data have been put forward. Most of these alternatives entail a modification of general relativity on cosmological scales or the addition of a new field with exotic properties, called dark energy; for reviews, see [8, 9]. After a decade of work in this area, it has proven to be quite difficult to find well motivated models that can match all of the presently available cosmological data.

1.1.2 The Fitting Problem

Due to these difficulties, there have also been recent attempts to explain this seemingly anomalous cosmic acceleration as a consequence of inhomogeneity, introducing no new physics. It has been suggested that small-scale density perturbations

could cause the appearance of accelerated expansion without the need to introduce any form of dark energy, which is an appealing prospect [10, 11, 12, 13, 14]. It is already well known that inhomogeneity in the matter distribution along the line of sight affects distance measurements in many ways, through Doppler shifts, gravitational redshifts, gravitational lensing, and a variety of other effects. However, could such effects lead to a systematic error that could actually trick us into thinking that the expansion of the Universe is accelerating?

The concept that inhomogeneity can systematically modify our interpretation of cosmological measurements was first realized by Ellis with the introduction of the “fitting problem” [15, 16]. The basic idea is this: Due to the nonlinearity of the Einstein equation, the operators for taking spatial averages and for time evolution do not commute. This means that, although our universe is homogeneous in the mean, it will likely not have the same time evolution as that of the corresponding homogeneous universe. Nevertheless, we routinely fit distance data to FRW models, a procedure that introduces errors into the inferred properties of our Universe, and these errors will be present even for very large samples of Type Ia supernovae. In other words, fitting supernova data from our inhomogeneous universe to FRW models can lead to systematic errors in our appraisal of its behavior.

Our preconceived notions with regard to how we should model and interpret supernova data can significantly affect our understanding of the nature of the expansion history, and therefore the contents of, the Universe. As we will show in the next section, fitting cosmological data is a very model-dependent procedure. By making false assumptions with regard to things like the spatial curvature or to the spatial distribution of matter, we could conceivably be tricked into thinking

that the expansion of the Universe is accelerating, when in fact it is not.

1.2 Acceleration from Errors in Fit Assumptions: Two Illustrative Examples

We will now look at two very simple examples that will illustrate how faulty assumptions made in the course of interpreting supernova data can lead us to believe that the expansion of the Universe is accelerating, when it is actually matter dominated, with no dark energy and with gravitation governed by general relativity.

1.2.1 Spatial Curvature

There are many reasons to believe that our Universe is flat, the most notable evidence for flatness being the first peak of the anisotropy spectrum of the CMB radiation. However, for the sake of example, let us assume for a moment that the Universe has a significant amount of spatial curvature. Then we can ask: What would happen if we interpreted the supernova data of such a universe while erroneously assuming that it is flat [17]?

The luminosity distance of an open, but still homogeneous, universe which contains only pressureless matter is

$$D_L(z) = \frac{1+z}{H_0\sqrt{\Omega_k}} \sinh \left[\sqrt{\Omega_k} \int_0^z \frac{dz'}{\sqrt{\Omega_M(1+z')^3 + \Omega_k(1+z')^2}} \right], \quad (1.9)$$

where Ω_M and $\Omega_k = 1 - \Omega_M$ are the densities of matter and of curvature, respectively, and H_0 is the Hubble parameter today. On the other hand, the luminosity

distance of a flat universe is given by Eq. (1.7). If the supernova data for $D_L(z)$ are interpreted within the framework of a flat universe, one can find the effective Hubble rate by inverting Eq. (1.7). This yields

$$H(z) = \left[\frac{d}{dz} \left(\frac{D_L(z)}{1+z} \right) \right]^{-1}, \quad (1.10)$$

which then leads to the associated deceleration parameter

$$q(z) = -1 + \left[\frac{1+z}{H(z)} \right] \frac{dH(z)}{dz}, \quad (1.11)$$

where $q < 0$ would imply that the expansion of the Universe is accelerating.

By using the luminosity distance-redshift relation, i.e. Eq. (1.9), in Eqs. (1.10) and (1.11), we find that a large enough Ω_k can lead to a negative apparent deceleration parameter. As an expansion in the redshift, we find

$$\begin{aligned} q(z) = & \frac{1}{2}(1 - \Omega_k) - \frac{1}{2}\Omega_k(1 + \Omega_k)z + \frac{1}{4}\Omega_k(3 + \Omega_k - 2\Omega_k^2)z^2 \\ & - \frac{1}{8}\Omega_k(7 - 4\Omega_k - 7\Omega_k^2 + 4\Omega_k^3)z^3 + O(z^4). \end{aligned} \quad (1.12)$$

We display this result, to order z^4 , for several values of Ω_k in Figure 1.1. One can clearly see that erroneously assuming flatness can lead to the appearance of accelerated expansion for nonzero redshifts, when in fact the Universe is matter dominated and the expansion is decelerating.

1.2.2 The Empty Beam Approximation

Now we will assume that the Universe really is flat, but has structure on large scales. The “empty beam approximation” was developed several decades ago in an attempt to analytically model the effect that large scale structure has on distance

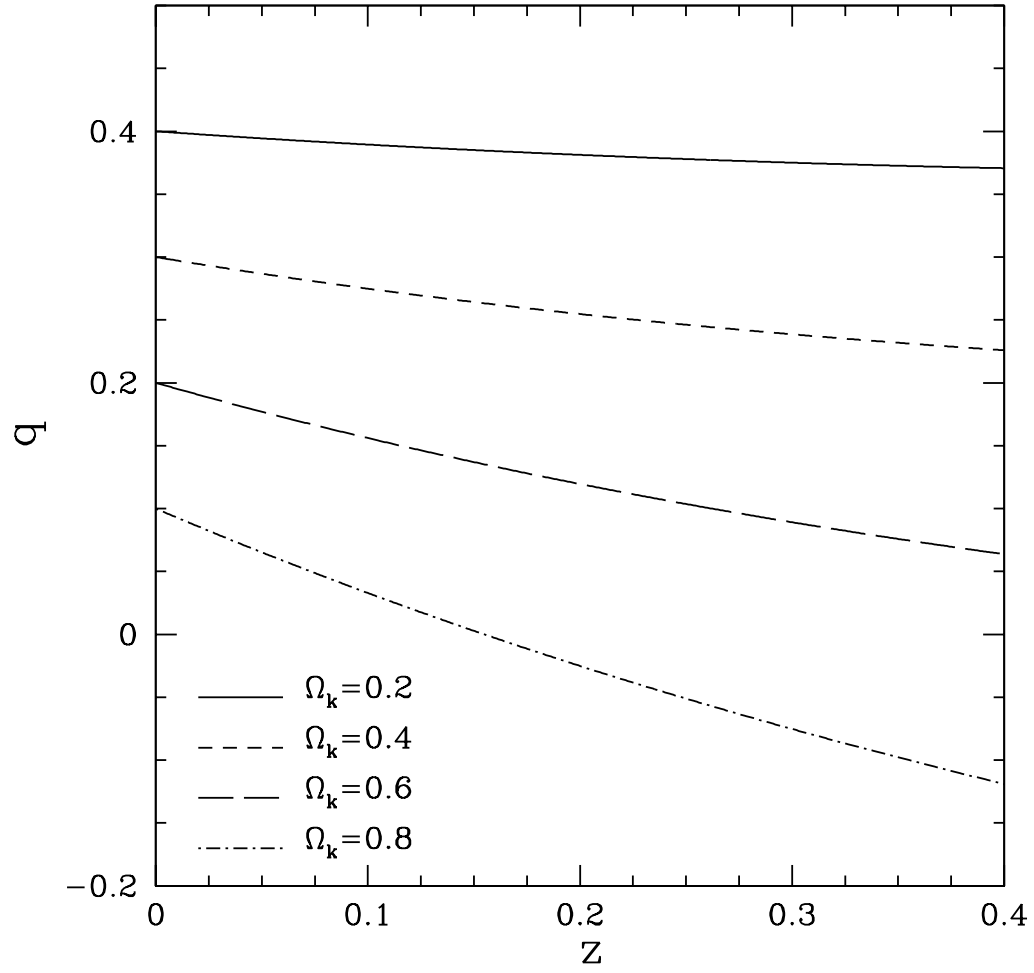


Figure 1.1: The inferred deceleration parameter q versus redshift z for several values of Ω_k , when the supernova data are interpreted within the framework of a flat cosmological model. Shown here are results for the models where $\Omega_k = 0.2, 0.4, 0.6,$ and 0.8 .

measurements [18, 19]. The idea is to assume that matter is so tightly clumped that the light that we receive from distant sources has passed only through empty space. This will mean that there will be less focusing from gravitational lensing, and hence objects will appear to be farther away than they really are. If we assume an FRW model for all of our data analysis, we would then perceive that the Universe is expanding faster than it really is.

In a flat and matter dominated universe, the luminosity distance in this approximation is [18]

$$D_L(z) = \frac{2}{5H_0} \left[(1+z)^2 - \frac{1}{\sqrt{1+z}} \right]. \quad (1.13)$$

Plugging this into Eq. (1.10), and then plugging the resulting Hubble parameter into Eq. (1.11), we find the apparent deceleration parameter to be

$$q(z) = 1 - \left[\frac{8(1+z)^{5/2} - 3}{4(1+z)^{5/2} + 6} \right], \quad (1.14)$$

which is plotted in Figure 1.2. Although $q_0 \equiv q(z=0) = 1/2$, as expected in a flat and matter dominated universe, the deceleration parameter becomes negative for nonzero redshifts. It turns out that this approximation is a gross oversimplification, but it nonetheless displays an important point, namely that inhomogeneity can affect luminosity distances in a way that could potentially mimic dark energy.

In reality, we expect the deviations from flatness and the effects of inhomogeneity to be small. However, in the following chapters we will see that significant systematic errors can still arise as a result of fitting the luminosity distance-redshift relation of an inhomogeneous universe to that of an FRW model.

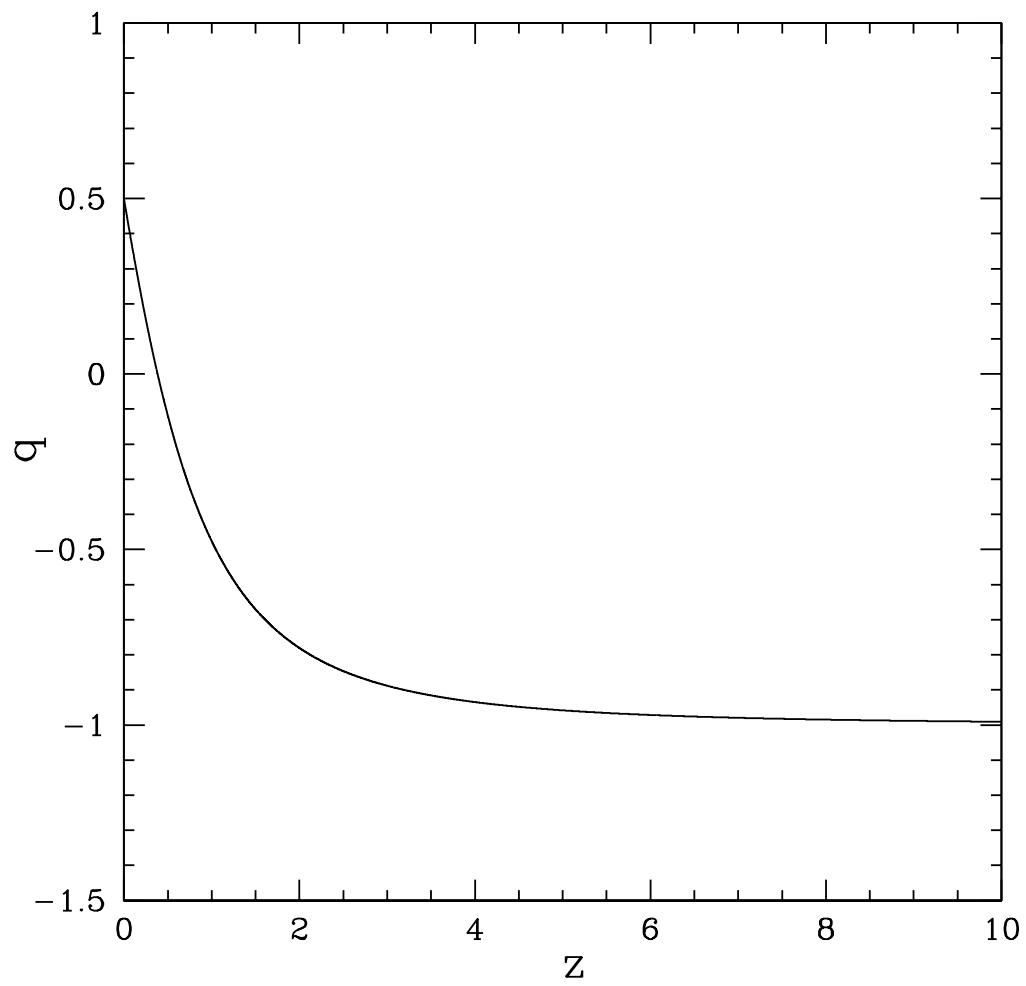


Figure 1.2: The effective deceleration parameter q versus redshift z in the empty beam approximation.

1.3 Overview of Thesis

The purpose of this thesis is to explore how local large scale structure can affect our efforts to measure the luminosity distance-redshift relation and subsequently deduce the contents and behavior of the Universe. To this end, we will use a series of models of structure formation that are all in the context of matter dominated cosmologies, with gravity via general relativity. For these models, we will compute the systematic effect that local inhomogeneity has on the luminosity distances and redshifts of Type Ia supernovae. We will then relate the resulting perturbed $D_L(z)$ to FRW models, so that we may find how these corrections affect our assessment of the acceleration of the Universe.

In Chapter 2, we use the spherically-symmetric, yet inhomogeneous, Lemaître-Tolman-Bondi (LTB) [20] cosmological models to ask if apparent accelerated expansion is possible in a matter dominated universe, in principle. We find that fitting the luminosity distance-redshift relation of LTB models to those of FRW models can indeed lead to the appearance of acceleration for nonzero redshifts.

As LTB models are only toy models, we then explore a more physically reasonable model for structure formation in Chapter 3. In this chapter, we construct cosmological voids and sheets by cutting spherical regions out of an FRW universe, and then spreading the excised matter into thin shells along the boundaries of the voids. In the Newtonian limit, we find that the effects of this type of inhomogeneity are negligible.

We explore the full three dimensional problem in Chapter 4. We again consider a flat and matter dominated universe, wherein we compute the luminosity distance

and redshift to second order in the density perturbation $\delta = \delta\rho/\rho$ and to third order in the fluid velocity v/c . We find that, in this more realistic framework, such errors are not large enough to explain the measurements that $\Omega_\Lambda \sim 0.7$. However, for nearby supernovae, these errors are still an important source of systematic uncertainty in the best-fit cosmological parameters.

Finally, we provide a summary of results in Chapter 5.

Chapter 2

Effects of Inhomogeneity in Spherical Symmetry*

2.1 Introduction

Since it has proven to be quite complicated to analyze the full three dimensional fitting problem analyzed by Kolb *et al.* [10, 11], a useful class of models to explore are the spherically-symmetric, yet inhomogeneous, LTB [20] cosmological models, containing only cold dark matter, or “dust”, and wherein it is often, but not always, assumed that we live at the symmetry center. In this way, we can confront the simpler and more general question: Are there any models based on general relativity and cold dark matter which can match the observations? We cannot completely address this question with LTB models, which are unrealistic since they place us near the center of the Universe, but these models are nevertheless useful toy models to address this general question. More specifically, in the LTB models we can ask if a centrally located observer can mistakenly interpret astronomical observations of redshifts and luminosity distances as requiring acceleration of the expansion of the Universe. We find that the answer is “yes”, and this implies that the mechanism studied by Kolb *et al.* is somewhat more plausible and requires more study.

Other papers have used LTB models in analyzing whether or not subhorizon

*This chapter is published in Vanderveld, Flanagan, and Wasserman (2006).

perturbations could “backreact” and drive accelerated expansion. Nambu *et al.* take averages to find effective expansion parameters of specific illustrative example models [21], Moffat looks at examples [22], Mansouri constructs a model that consists of a local LTB patch which is embedded into a background FRW space-time [23], and Chuang *et al.* numerically produce examples of LTB models with apparent acceleration [24]. Alnes *et al.* [25] argue against acceleration, but only by looking at a class of example models.

It has been claimed that it is possible to find LTB cosmological models that have $q_0 < 0$, where $q_0 \equiv q(z = 0)$ is the deceleration parameter measured by the central observer. However, there are general theorems that prohibit such behavior [26, 27]. In Section 2.2, we will first give a general review of LTB models and then we will discuss this contradiction and its resolution: there is a local singularity at the symmetry center of models with $q_0 < 0$, corresponding to a non-vanishing radial central density gradient and divergent second derivatives of the density. We will prove that excluding this singularity will necessarily lead to a positive value for q_0 . This singularity is not taken into account in any of the above papers, and most of them look at models which are singular at the center [21, 22, 23, 24].

We will also show that it is possible to construct models without a central singularity in which one would measure negative deceleration parameters $q(z)$, and therefore would measure regions of acceleration, at nonzero redshifts z . We will do this by choosing the LTB model and computing the resulting luminosity distance and ultimately $q(z)$; we call this the “forward problem”. As we discuss in Section 2.2 below, LTB models are characterized by two free functions of radius r , a bang time function $t_0(r)$ and an energy function $E(r)$. We focus on LTB models

with zero energy functions but non-zero bang time functions, because we do not expect the former to produce acceleration. This is because, as we will show, the energy function is associated with the growing mode of linear theory, whereas the bang time function is associated with the shrinking mode.

In Section 2.3, we will explore the “inverse problem”, where one chooses the luminosity distance as a function of redshift and then attempts to find a corresponding LTB model, which may or may not exist. Here, too, we only consider $E(r) = 0$. We show that there are numerous pitfalls to this method, as other singular behaviors arise which generally limit the range of redshifts for which this class of models could reproduce the observed supernova data. For a given luminosity distance $D_L(z) \equiv r_{FRW}(z)(1+z)$, there is a critical redshift z_{crit} where $d \ln r_{FRW}(z)/d \ln(1+z) = 1$. For almost all choices of $D_L(z)$, any attempt to find a corresponding zero energy LTB model will fail at some redshift smaller than z_{crit} when a singularity is encountered. There are exceptions which pass through a “critical point” at $z = z_{\text{crit}}$, the simple FRW model being one obvious example of such a “transcritical” solution. We show how others may be constructed. These models show redshift domains with enhanced apparent deceleration as well as acceleration, but do not appear to be consistent with observational data on $D_L(z)$.

Several papers have already computed how the dependence of the luminosity distance on redshift is distorted in LTB models due to purely radial inhomogeneities, and have claimed that we could be tricked into thinking that we are in a homogeneous accelerating universe when we are really in a dust-dominated inhomogeneous universe [28, 29, 30, 31]. However, this claim has not until now

been correctly justified, since all previous papers neglected the central singularity and the critical point.

2.2 The Forward Problem

2.2.1 Lemaitre-Tolman-Bondi Models

Using the notation of C el erier [30], the LTB spacetime [20] has the line element

$$ds^2 = -dt^2 + \frac{R'^2(r, t)}{1 + 2E(r)} dr^2 + R^2(r, t) (d\theta^2 + \sin^2 \theta d\phi^2) \quad (2.1)$$

where primes denote derivatives with respect to the radial coordinate r , and $E(r)$ is a free function, called the “energy function”. We define the function $k(r)$ by $k(r) \equiv -2E(r)/r^2$. If $k(r) = 0$, the Einstein equations admit the solution

$$R(r, t) = (6\pi G\tilde{\rho})^{1/3} r [t - t_0(r)]^{2/3} , \quad (2.2)$$

where $t_0(r)$ is another free function, often referred to as the “bang time” function, and $\tilde{\rho}$ is a fixed parameter. If $k(r) < 0$ for all r , we have the parametric solution

$$\begin{aligned} R &= \frac{4\pi G\tilde{\rho}r}{-3k(r)} (\cosh u - 1) \\ t - t_0(r) &= \frac{4\pi G\tilde{\rho}}{3[-k(r)]^{3/2}} (\sinh u - u) , \end{aligned} \quad (2.3)$$

and if $k(r) > 0$ for all r , we have the solution

$$\begin{aligned} R &= \frac{4\pi G\tilde{\rho}r}{3k(r)} (1 - \cos u) \\ t - t_0(r) &= \frac{4\pi G\tilde{\rho}}{3[k(r)]^{3/2}} (u - \sin u) . \end{aligned} \quad (2.4)$$

These are Eqs. (18), (19), and (20) of C el erier [30], but specialized to the choice $M(r) = 4\pi r^3 \tilde{\rho}/3$ by choosing the radius coordinate appropriately, where $M(r)$ is

the mass function used by C el erier, and where $\tilde{\rho}$ is a constant.¹ The energy density of the matter in these models is given by

$$\rho(r, t) = \frac{\tilde{\rho} r^2}{R' R^2}. \quad (2.5)$$

We define $\rho_0(t) = \rho(0, t)$ to be the central density, and from Eqs. (2.2) - (2.4) we find

$$\rho_0(t) = \frac{1}{6\pi G [t - t_0(0)]^2}. \quad (2.6)$$

Throughout this chapter we will restrict attention to an observer located at $r = 0$ and at $t = t_o$, where t_o is the observation time, not to be confused with the bang time $t_0(r)$. We also choose units such that $\tilde{\rho} = \rho_0(t_o)$, and we choose the origin of time such that $t_0(0) = 0$. A light ray directed radially inward follows the null geodesic

$$dt = -\frac{R'(r, t)}{\sqrt{1 - k(r)r^2}} dr \quad (2.7)$$

and has a redshift given by

$$\frac{dz}{dr} = (1 + z) \frac{\dot{R}'[r, t(r)]}{\sqrt{1 - k(r)r^2}} \quad (2.8)$$

where overdots denote partial derivatives with respect to time and where $t(r)$ is evaluated along light rays that are moving radially inward according to Eq. (2.7).

Equations (2.5) and (2.8) give us two important restrictions on the derivatives of $R(r, t)$: (i) in order for the density to remain finite, we require $R' > 0$, which excludes shell-crossing, and (ii) in order to have a monotonically increasing $z(r)$, we require $\dot{R}' > 0$.

¹Note that the mass function $M(r)$ which appears in Bondi [20], which we denote by $M_B(r)$, is related to C el erier's $M(r)$ by $M'_B(r) = M'(r)/\sqrt{1 + 2E(r)}$, and so our radial coordinate specialization in Bondi's notation is $M'_B(r) = 4\pi r^2 \tilde{\rho} / \sqrt{1 - 2k(r)r^2}$.

The luminosity distance measured by the observer at $r = 0$ and at $t = t_o$ is given by [30]

$$D_L(z) = (1 + z)^2 R, \quad (2.9)$$

where z and R are evaluated along the radially-inward moving light ray. It is not obvious how to define the deceleration parameter in an inhomogeneous cosmology, and Hirata and Seljak [27] explore several definitions. In this chapter, we restrict our attention to the deceleration parameter that would be obtained from measurements of luminosity distances and redshifts assuming a spatially flat FRW cosmology.² We can deduce the effective Hubble expansion rate $H(z)$ of the flat FRW model which would yield the same luminosity distances by inverting the FRW relation

$$D_L(z) = (1 + z) \int_0^z \frac{dz'}{H(z')} \quad (2.10)$$

to find

$$H(z) = \left[\frac{d}{dz} \left(\frac{D_L(z)}{1 + z} \right) \right]^{-1}. \quad (2.11)$$

We can then calculate the associated deceleration parameter

$$q(z) = -1 + \left[\frac{1 + z}{H(z)} \right] \frac{dH(z)}{dz} \quad (2.12)$$

and the effective equation of state parameter

$$w_{\text{eff}}(z) \equiv \frac{2}{3} \left[q(z) - \frac{1}{2} \right] = \frac{2(1 + z)}{3} \frac{d}{dz} \ln \left[\frac{H(z)}{(1 + z)^{3/2}} \right]. \quad (2.13)$$

If we know $t_0(r)$ and $E(r)$, then we can find $R(r, t)$ very simply by using the appropriate solution above, chosen from Eqs. (2.2), (2.3), and (2.4). We then solve the differential equations (2.7) and (2.8) to find $t(z)$ and $r(z)$, starting from the

²More generally, an observer might fit data on $D_L(z)$ to FRW models with arbitrary spatial curvature, including flat ones.

initial conditions $r = 0$ and $t = t_o$. We insert these $t(z)$ and $r(z)$ into the right hand side of Eq. (2.9) to obtain $D_L(z)$, and then use Eqs. (2.11) and (2.12) to find $H(z)$ and $q(z)$. We will use this procedure later in this section with a class of models as an illustrative example.

2.2.2 The Weak Singularity at $r = 0$

There have been many claims that there exist LTB cosmological models in which $q_0 \equiv q(z = 0) < 0$ [21, 22, 23, 24, 28, 29, 30, 31]. For example, Iguchi *et al.* [31] look at two different classes of LTB models: (i) models with $k(r) = 0$ and a pure “BigBang time inhomogeneity” and (ii) models with $t_0(r) = 0$ and a pure “curvature inhomogeneity”. In either case, they try to reproduce the luminosity distance function of a flat FRW universe with a matter density $\Omega_M = 0.3$ and a cosmological constant density $\Omega_\Lambda = 0.7$, namely

$$D_L(z) = \frac{1+z}{H_0} \int_0^z \frac{dz'}{\sqrt{\Omega_M (1+z')^3 + \Omega_\Lambda}} . \quad (2.14)$$

They appear to be successful up until they find $R' < 0$ or $\dot{R}' < 0$ at a redshift $z \sim 1$ (we will discuss these pathologies in the next section). Thus, they appear to successfully find models where $q_0 < 0$.

On the other hand, the local expansions of Flanagan [26] and of Hirata and Seljak [27] show that q_0 is constrained to be positive for arbitrary inhomogeneous dust-dominated cosmologies that are not necessarily spherically-symmetric. In particular, Flanagan expands the luminosity distance as

$$D_L = A(\theta, \phi)z + B(\theta, \phi)z^2 + \mathcal{O}(z^3) , \quad (2.15)$$

where θ and ϕ are spherical polar coordinates as measured in the local Lorentz frame of the observer. He then defines the central deceleration parameter as

$$q_0 \equiv 1 - 2H_0^{-2} \langle A^{-3} B \rangle , \quad (2.16)$$

where angle brackets denote averages over θ and ϕ , and $H_0 = \langle A^{-1} \rangle$. Using local Taylor series expansions and assuming that the pressure is zero, he finds

$$q_0 = \frac{4\pi}{3H_0^2} \rho + \frac{1}{3H_0^2} \left[\frac{7}{5} \sigma_{\alpha\beta} \sigma^{\alpha\beta} - \omega_{\alpha\beta} \omega^{\alpha\beta} \right] \quad (2.17)$$

where $\sigma_{\alpha\beta}$ and $\omega_{\alpha\beta}$ are the shear and vorticity tensors. The first term of this expression is obviously positive, and the terms in the brackets vanish in LTB models by spherical symmetry. Thus there is a contradiction: general theorems prove that q_0 is positive in these inhomogeneous models, whereas the analysis of specific examples appears to show that it is possible to construct models in which q_0 can be negative. Here we present the resolution of this contradiction, that there exists a weak local singularity which is excluded at the start from the computations of Flanagan and Hirata and Seljak, but which is present in models giving $q_0 < 0$. We will show that the exclusion of this singularity inevitably leads to models with a positive q_0 .

We expand the density (2.5) to second order in r as

$$\rho(r, t) = \rho_0(t) + \rho_1(t)r + \rho_2(t)r^2 + \mathcal{O}(r^3) . \quad (2.18)$$

The weak singularity occurs when $\rho_1(t)$ is nonzero, in which case the gravitational field is singular since $\square \mathcal{R} \rightarrow \infty$ as $r \rightarrow 0$, where \mathcal{R} is the Ricci scalar. In other words, second derivatives of the density diverge at the origin, independent of where observers may be located. This is true both in flat spacetime and in the curved

LTB metric when we have a density profile of the form (2.18). The singularity is weak according to the classification scheme of the literature on general relativity [32]. This singularity is excluded from the start in the analyses of Flanagan [26] and Hirata and Seljak [27] which assume that the metric is smooth.

We now determine the conditions for a weak singularity to occur. We define the variable

$$a(r, t) = \frac{R(r, t)}{r} ; \quad (2.19)$$

this is analogous to the FRW scale factor $a(t)$, in the sense the metric takes the form

$$ds^2 = -dt^2 + a^2(r, t) \left\{ \frac{[1 + ra'(r, t)/a(r, t)]^2}{1 - k(r)r^2} dr^2 + r^2 (d\theta^2 + \sin^2 \theta d\phi^2) \right\} . \quad (2.20)$$

We expand this function as

$$a(r, t) = a_0(t) + a_1(t)r + a_2(t)r^2 + \mathcal{O}(r^3) . \quad (2.21)$$

Comparing this to the formula (2.2) for $R(r, t)$, we find for the zeroth order expansion coefficient

$$a_0(t) = [6\pi G\rho_0(t_o)]^{1/3} t^{2/3} . \quad (2.22)$$

We define $H_0 = \dot{a}_0(t_o)/a_0(t_o)$, and our choice of units above imply $a_0(t_o) = 1$.

Using Eqs. (2.19) and (2.21) in the expression (2.5) for the density gives

$$\rho(r, t) = \frac{\rho_0(t_o)}{a_0^2(t)} - 4\frac{\rho_0(t_o)a_1(t)}{a_0^3(t)}r + \mathcal{O}(r^2) . \quad (2.23)$$

Since $a_0(t) \neq 0$ by Eq. (2.22), we see that having a non-singular model requires $a_1(t) = 0$, or equivalently $R''(r = 0, t) = 0$.

It is straightforward to see that if $a_1 = 0$, then $q_0 \geq 0$, and that if $a_1(t) \neq 0$, then q_0 may be positive or negative. Note that the observer's measurement of q_0 from the

data does not depend on the observer's prior assumptions about spatial curvature, and so the following analysis of q_0 is sufficiently general and applies for arbitrary $k(r)$. If $a_1(t) = 0$, then the angular size distance is $R(r, t) = ra_0(t) + r^3 a_2(t) + \mathcal{O}(r^4)$, where r and t are evaluated along the path followed by a radially directed light ray. Evaluating the redshift for such a ray gives to lowest order $z = H_0 r + \mathcal{O}(r^2)$. Thus, the angular size distance is unaffected by density gradients up to terms of order z^3 . In other words, the standard expansion of the angular size distance $R \equiv D_A$ to order z^2 ,

$$H_0 D_A(z) = z - \frac{1}{2} z^2 (3 + q_0) + \mathcal{O}(z^3) , \quad (2.24)$$

is completely determined by the evolution of the uniformly dense core region of the expanding spherically-symmetric model, where the density is $\rho_0(t) = \rho_0(t_o)/a_0^3(t)$ from Eqs. (2.6) and (2.22), which is the density of dust expanding with scale factor $a_0(t)$. Therefore, the effective values of q_0 for such a model must lie in the same range as are found for exactly uniform, dust dominated FRW models: $q_0 \geq 0$.

We can gain further physical insight into the behavior of LTB models near $r = 0$ by expanding the field equations in r , assuming (see Eq. (2.21))

$$a(r, t) = a_0(t) + a_n(t)r^n + \dots , \quad (2.25)$$

and correspondingly

$$k(r) = k_0 + k_n r^n + \dots ; \quad (2.26)$$

we show in the next subsection that $a_1(t) = 0$ corresponds to having $k_1 = 0$ via a direct analysis of the LTB solutions. Thus, for non-singular models, $n = 2$ is the leading order correction to strict homogeneity near the center. The field equations are given in Bondi [20], and in our notation his Eq. (24) is

$$\frac{1}{2} \left(\frac{\partial R(r, t)}{\partial t} \right)^2 - \frac{4\pi G \rho_0(t_o) r^3}{3R(r, t)} = -\frac{1}{2} k(r) r^2 . \quad (2.27)$$

Substituting $R(r, t) = ra(r, t)$ we find

$$\left(\frac{\partial a(r, t)}{\partial t}\right)^2 = \frac{8\pi G\rho_0(t_o)}{3a(r, t)} - k(r). \quad (2.28)$$

Using the expansions (2.25) and (2.26) and equating like powers of r , we find

$$\begin{aligned} \dot{a}_0^2 &= \frac{8\pi G\rho_0(t_o)}{3a_0} - k_0 \equiv \frac{H_0^2\Omega_0}{a_0} + H_0^2(1 - \Omega_0) \\ 2\dot{a}_0\dot{a}_n &= -\frac{8\pi G\rho_0(t_o)a_n}{3a_0^2} - k_n = -\frac{H_0^2\Omega_0 a_n}{a_0^2} - k_n. \end{aligned} \quad (2.29)$$

The first of Eqs. (2.29) is exactly the same as the Friedmann equation for the scale factor $a_0(t)$ in a universe with arbitrary spatial curvature, subject to the single physical requirement $\Omega_0 \geq 0$. To solve the second equation, notice that $\ddot{a}_0 = -H_0^2\Omega_0/2a_0^2$, so rewrite it as

$$\dot{a}_0\dot{a}_n - \ddot{a}_0 a_n = \dot{a}_0^2 \frac{d}{dt} \left(\frac{a_n}{\dot{a}_0}\right) = -\frac{k_n}{2}, \quad (2.30)$$

which has the solution

$$a_n(t) = C\dot{a}_0 - \frac{k_n\dot{a}_0}{2} \int_0^t \frac{dt'}{\dot{a}_0^2(t')}, \quad (2.31)$$

where C is a constant. Let us define $\delta_n(t) = a_n(t)/a_0(t)$; then Eq. (2.31) becomes

$$\delta_n(t) = CH(t) - \frac{k_n H(t)}{2} \int_0^t \frac{dt'}{H^2(t')a_0^2(t')} = CH(t) - \frac{k_n H(t)}{2} \int_{a_0(0)}^{a_0(t)} \frac{da_0}{H^3(a_0)a_0^3}, \quad (2.32)$$

where

$$H \equiv \frac{\dot{a}_0}{a_0} = H_0 \sqrt{\frac{\Omega_0}{a_0^3} + \frac{1 - \Omega_0}{a_0^2}}. \quad (2.33)$$

Comparing with results in Peebles [33], we see that the first term of Eq. (2.32) is just the shrinking mode of linear theory, and the second is the growing mode. The amplitude C of the shrinking mode is related to the bang time function by $t_0(r) = -Cr^n + \dots$, and the growing mode amplitude k_n is related to the lowest

order energy perturbation $k_n r^n$. Note that this approximate solution holds for $a_n r^n \ll a_0(t)$, i.e. for $0 < r^n \ll 1/\delta_n$.

We have shown that for $n \geq 2$, the central value of q_0 is greater than or equal to zero. We now compare with the mildly singular case with $n = 1$. The evolutions of $a_0(t)$ and $a_1(t)$ are governed by Eqs. (2.29) and (2.31). For this case, the low z expansion of $D_A(z)$ depends on $a_1(t_o)$ and k_1 , and the effective value of q_0 near the origin becomes, from Eqs. (2.19), (2.24), and (2.25),

$$q_0 = \frac{1}{2}\Omega_0 - \frac{2a_1(t_0)}{H_0} + \frac{\dot{a}_1(t_0)}{H_0^2} = \frac{1}{2}\Omega_0 - \frac{a_1(t_0)}{H_0} \left(2 + \frac{\Omega_0}{2}\right) - \frac{k_1}{2H_0^2}. \quad (2.34)$$

This is no longer constrained to be positive.

2.2.3 Proof of $q_0 \geq 0$ Directly from LTB Solutions

We will now show directly from the solutions (2.2), (2.3), and (2.4) of the Einstein equations that LTB models without central singularities must have positive q_0 .

The zero energy solution $k(r) = 0$ has

$$a_1(t) \propto R''(r=0, t) = -\frac{4}{3} [6\pi G\rho_0(t_o)]^{1/3} t'_0(0) t^{-1/3}. \quad (2.35)$$

Thus, we see that the zero energy solution requires $t'_0(0) = 0$ in order to have no central singularity. More generally, for the $k(r) > 0$ solutions, we find

$$R''(0, t) = k'(0) \left[\frac{3F'(x_0)}{\sqrt{k_0}} t - \frac{8\pi G\rho_0(t_o) F(x_0)}{3k_0^2} \right] - t'_0(0) \left[2\sqrt{k_0} F'(x_0) \right] \quad (2.36)$$

where $k_0 \equiv k(r=0)$ and we have defined the function $F(x)$ by

$$1 - \cos u \equiv F(u - \sin u). \quad (2.37)$$

Here $x_0(t) = u_0 - \sin u_0$ is the value of x at the center $r = 0$ at time t :

$$x_0(t) = \frac{3k_0^{3/2}}{4\pi G\rho_0(t_0)} t. \quad (2.38)$$

Similarly, for the $k(r) < 0$ solutions we find

$$R''(0, t) = -k'(0) \left[\frac{3G'(x_0)}{\sqrt{-k_0}} t - \frac{8\pi G\rho_0(t_0) G(x_0)}{3k_0^2} \right] - t'_0(0) \left[2\sqrt{-k_0} G'(x_0) \right] \quad (2.39)$$

where we define the function $G(x)$ by

$$\cosh u - 1 \equiv G(\sinh u - u). \quad (2.40)$$

Since the bracketed expressions in Eqs. (2.36) and (2.39) are functions of time, $R''(r = 0, t)$ will vanish at arbitrary t only if $t'_0(0) = 0$ and $k'(0) = 0$, and only then can one avoid having a singularity at the symmetry center.

These conditions, $t'_0(0) = 0$ and $k'(0) = 0$, lead to the restriction that q_0 must be positive. C el erier [30] expands the luminosity distance for small redshift and finds the second order coefficient to be

$$D_L^{(2)} \equiv \frac{1}{2} \left[\frac{d^2 D_L}{dz^2} \right]_{r=0} = \frac{1}{2} \left[\frac{R'}{\dot{R}'} \left(1 + \frac{R' \ddot{R}'}{\dot{R}'^2} + \frac{R''}{R' \dot{R}'} - \frac{\dot{R}''}{\dot{R}'^2} \right) \right]_{r=0}, \quad (2.41)$$

where overdots again denote partial derivatives with respect to time. The deceleration parameter at $r = 0$ is therefore

$$q_0 = 1 - 2H_0 D_L^{(2)} = \left[-\frac{R' \ddot{R}'}{\dot{R}'^2} - \frac{R''}{R' \dot{R}'} + \frac{\dot{R}''}{\dot{R}'^2} \right]_{r=0}. \quad (2.42)$$

If $R''(0, t) = 0$ to avoid a singularity, we find that the last two terms in the above expression are also zero, and we obtain

$$q_0 = \left[-\frac{R' \ddot{R}'}{\dot{R}'^2} \right]_{r=0}. \quad (2.43)$$

Since $R'(r, t) > 0$ to prevent shell crossing, and \dot{R}^2 is obviously positive, we would need to have

$$\ddot{R}'(0, t) = \ddot{a}_0(t) > 0 \quad (2.44)$$

in order to have a negative q_0 . For the $k(r) = 0$ solution,

$$\ddot{R}'(0, t) = -\frac{2}{3} \left[\frac{2\pi G \rho_0(t_o)}{9} \right]^{1/3} t^{-4/3} < 0 ; \quad (2.45)$$

moreover, the $k(r) > 0$ solution has

$$\ddot{R}'(0, t) = -\frac{4\pi G \rho_0(t_o)}{3k_0} \left(\frac{du_0}{dt} \right)^2 < 0 , \quad (2.46)$$

and the $k(r) < 0$ solution has

$$\ddot{R}'(0, t) = \frac{4\pi G \rho_0(t_o)}{3k_0} \left(\frac{du_0}{dt} \right)^2 < 0 . \quad (2.47)$$

Therefore we can conclude that, in the absence of weak central singularities, all LTB solutions have positive q_0 since $\ddot{R}'(0, t)$ is always negative.

2.2.4 Models of Iguchi, Nakamura and Nakao

Here we verify explicitly that the models with $q_0 < 0$ studied by Iguchi *et al.* [31] contain weak singularities. For the first case in Iguchi *et al.*, the pure bang time inhomogeneity, there will be no singularity if $t'_0(0) = 0$, as shown from Eq. (2.35). If we expand $D_L(z)$ for this FRW model in a power series around $z = 0$, we can compare this term by term to the expansion of the luminosity distance for a zero energy LTB model to find [30]

$$\Omega_M = 1 + 5 \frac{t'_0(0)}{\alpha \beta^2} + \frac{29}{4} \frac{t_0''(0)}{\alpha^2 \beta^4} + \frac{5}{2} \frac{t_0'''(0)}{\alpha^2 \beta} \quad (2.48)$$

and

$$\Omega_\Lambda = -\frac{1}{2} \frac{t'_0(0)}{\alpha\beta^2} + \frac{29}{8} \frac{t_0'^2(0)}{\alpha^2\beta^4} + \frac{5}{4} \frac{t_0''(0)}{\alpha^2\beta}, \quad (2.49)$$

where $\alpha \equiv [6\pi G\rho_0(t_o)]^{1/3}$ and $\beta \equiv t^{1/3}$. Using the fact that $\Omega_M + \Omega_\Lambda = 1$, we combine Eqs. (2.48) and (2.49) to find

$$t'_0(0) = -\frac{1}{2}\alpha\beta^2\Omega_\Lambda. \quad (2.50)$$

A nonzero Ω_Λ requires that $t'_0(0)$ is also nonzero, and hence there will be a singularity in such models.

Iguchi *et al.* also look at models with $t_0(r) = 0$ and positive $E(r)$. By combining and rearranging Eqs. (6) and (39) from [30], we find that

$$\frac{3\Omega_\Lambda - 1}{2} = \frac{R'\ddot{R}'}{\dot{R}'^2} + \frac{R''}{R'\dot{R}'} - \frac{\dot{R}''}{\dot{R}'^2}. \quad (2.51)$$

Plugging into this the negative k solution for $R(r, t)$ and then setting $r = 0$, we can find an equation for $k'(0)$. Iguchi *et al.* make some simplifying definitions, wherein they set $H_0 = G = 1$ and then write everything else as a function of a parameter Ω_0 , which they vary between 0.1 and 1. They set $k_0 = \Omega_0 - 1$, $\rho_0(t_o) = 3\Omega_0/8\pi$,

$$u_0 = \ln \left[\frac{2 - \Omega_0}{\Omega_0} + \sqrt{\left(\frac{2 - \Omega_0}{\Omega_0}\right)^2 - 1} \right], \quad (2.52)$$

and

$$t(r = 0) = \frac{\Omega_0 (\sinh u_0 - u_0)}{2 (1 - \Omega_0)^{3/2}}, \quad (2.53)$$

where $t(r)$ is evaluated along radially inward-moving light rays. Plugging these in and then solving for $k'(0)$ yields

$$k'(0) = \frac{(1 - \Omega_0)^{3/2}}{6} \left[\frac{(3\Omega_\Lambda - 1) \sinh^2 u_0 (\cosh u_0 - 1) + 2 (\cosh u_0 - 1)^2}{3 \sinh u_0 - u_0 (\cosh u_0 + 2)} \right], \quad (2.54)$$

where it is assumed that $\Omega_\Lambda = 0.7$. This shows that $k'(0)$ is only zero if $\Omega_0 = 1$; we can see from their Fig. (4) that this corresponds to the uninteresting FRW dust solution $k(r) = 0$ for all r . All of the other choices for Ω_0 will correspond to models with $k'(0) \neq 0$ and a central singularity. Therefore, all of the non-trivial models computed in Ref. [31] have weak singularities at $r = 0$.

2.2.5 Achieving a Negative Apparent Deceleration Parameter at Nonzero Redshifts

Although models that have been previously analyzed contain central singularities, it is still possible to construct LTB models without such a singularity for which the effective deceleration parameter $q(z)$, as defined in Eq. (2.12), is negative for some nonzero redshifts. Here we explore a class of zero energy LTB models with a bang time function $t_0(r)$ that is quadratic near $r = 0$, and therefore non-singular there.

In a zero energy LTB model, we have

$$dt = -R'(r, t)dr \tag{2.55}$$

and therefore we can get the equation for $t(r)$ along light rays that we observe from supernovae. Also, z is a function of r via Eq. (2.8), specialized to $k(r) = 0$, and we get z as a function of r only by using our solution for $t(r)$ along the rays. The bang time function is chosen such that it will (i) approach a constant for large r , so as to have a uniform density for large redshifts, and (ii) have no terms linear in r , so as to avoid a singularity at the center. Thus we integrate Eqs. (2.8) and

(2.55) with the bang time function choice

$$t_0(r) = -\frac{\lambda r_c r^2}{r^2 + r_c^2 D^2} \quad (2.56)$$

where λ and D are dimensionless parameters, $r_c = [6\pi G\rho_0(t_o)]^{-1/2}$, and we choose units where $r_c = 1$. We choose the initial conditions at the center, $t(r = 0) = 1$ and $z(r = 0) = 0$, and we integrate from the center outward.

Figure 2.1 displays results for the effective $q(z)$ that we calculate from the above model using Eqs. (2.9), (2.11), and (2.12) for various values of λ and D , namely $(\lambda, D) = (0.094, 0.14)$, $(0.20, 0.29)$, $(0.46, 0.62)$, $(0.75, 0.91)$, and $(1.0, 1.2)$. We choose values of λ and D for which the minimum value of $q(z)$ that is attained is approximately -1 . As we can see, although all the models are forced to have $q(z = 0) = 1/2$, it is nevertheless possible for the deceleration parameter to become negative at nonzero redshifts, as we find a region of $q(z) < 0$ for $z \lesssim 1$.

In order to reproduce the current luminosity distance data, we want $q(z)$ to quickly fall to from $q(0) = 1/2$ to $q(z) \approx -1$ and then stay at that value until a redshift $z \sim 1$. In Fig. 2.2 we plot several quantities that encapsulate some of the characteristics of the functions $q(z)$, which are useful for assessing the feasibility of reproducing luminosity distance data. We define Δz_{neg} to be the width, in redshift, of the region where q is negative, and $\Delta z_{q<-1}$ to be the width of the region where q is below negative one. We also found that the large redshift behavior is unstable in these models: q blows up as we eventually approach the initial singularity. As an approximate measure of the location of this divergence, we define z_{max} to be the redshift at which $q(z)$ exceeds 3. Ideally, we want $\Delta z_{neg} \sim 1$, $\Delta z_{q<-1} = 0$, and $z_{max} \rightarrow \infty$. From Fig. 2.2, it does not appear as though this model can reproduce the data well, although it is conceivable that one could construct a model which

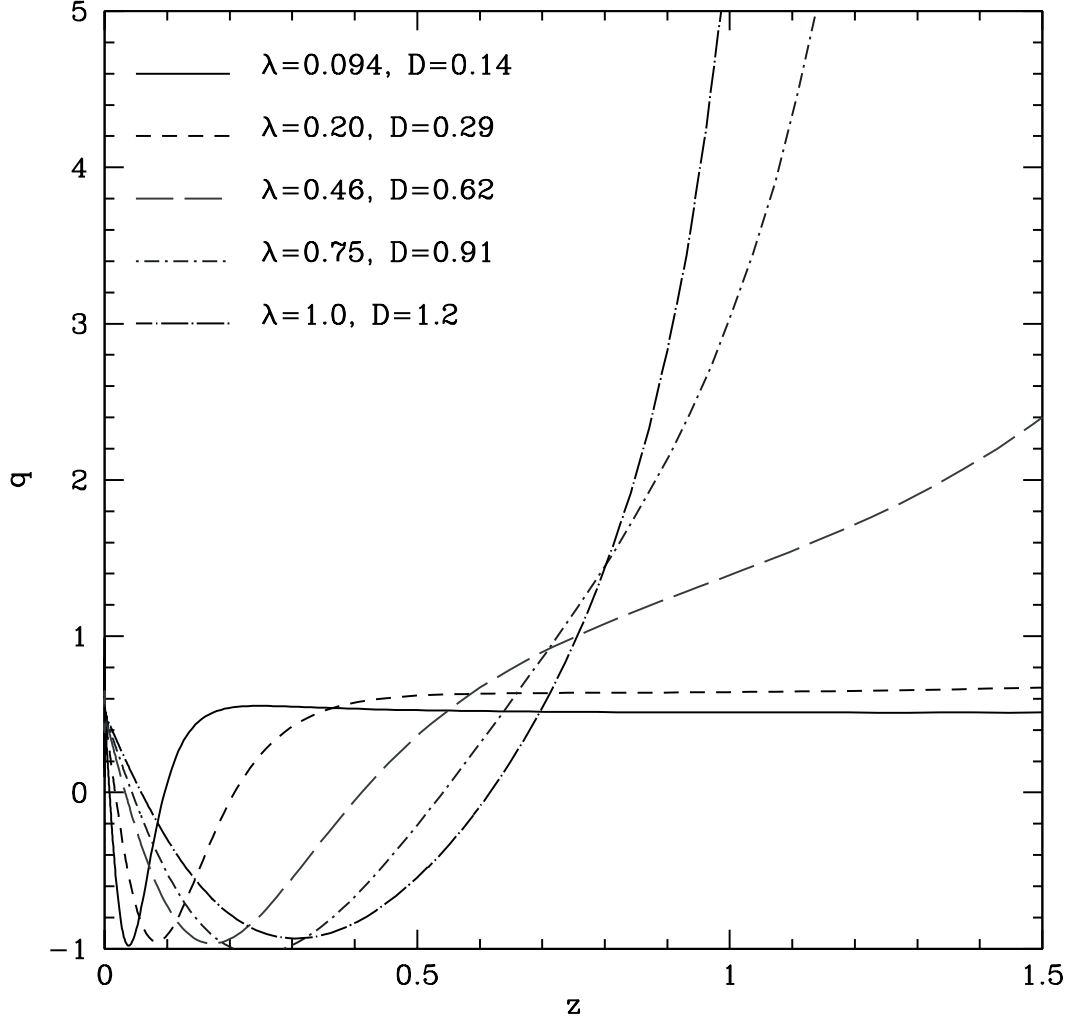


Figure 2.1: The effective deceleration parameter q versus redshift z for several quadratic bang time models which have a minimum q of approximately negative one. Plotted here are the data for models with $(\lambda, D) = (0.094, 0.14), (0.20, 0.29), (0.46, 0.62), (0.75, 0.91),$ and $(1.0, 1.2)$.

gives more realistic results. We see that by increasing D , we also increase the size of the region with negative $q(z)$, which makes the model more phenomenologically viable; however, by increasing D , we also decrease z_{max} and thus make the model less physically reasonable.

2.3 The Inverse Problem

Unfortunately, it is highly unlikely that one could guess a bang time function $t_0(r)$ that would yield the experimentally measured luminosity distance $D_L(z)$. A better approach would be to solve the inverse problem: given the appropriate $D_L(z)$, work backwards to try to find the corresponding $t_0(r)$, which may or may not exist. This approach has been taken before, but without avoiding the central singularity [31]. Models based on selected $D_L(z)$ generally break down at $z \sim 1$ upon encountering some pathology. We explore and clarify the possible pathologies below.

2.3.1 General Properties

In the LTB metric, the angular size distance is given by

$$D_A(r, t) = R(r, t) = rT^2(r, t) , \quad (2.57)$$

where $T \equiv [t - t_0(r)]^{1/3}$. Here we have specialized to units where $6\pi G\rho_0(t_o) = 1$.

We also define the equivalent FRW radial coordinate to be

$$r_{\text{FRW}}(z) \equiv (1 + z) D_A(z) , \quad (2.58)$$

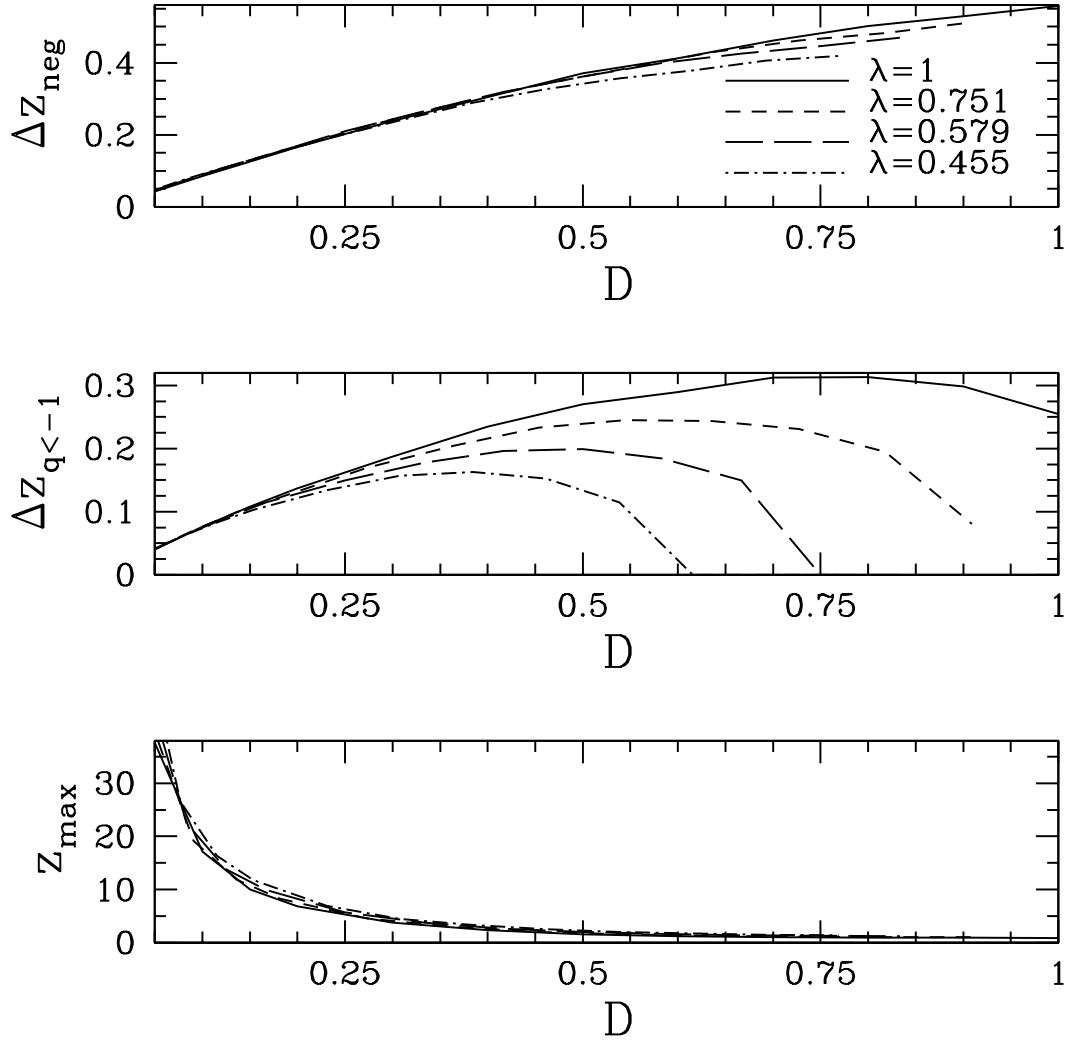


Figure 2.2: Several measures of the feasibility of quadratic bang time models, plotted versus D for $\lambda = 1, 0.751, 0.589,$ and 0.455 . From top to bottom, we have plotted $\Delta z_{\text{neg}}, \Delta z_{q < -1},$ and $z_{\text{max}},$ all versus D .

in terms of which we have

$$rT^2(1+z) = r_{\text{FRW}}(z) = \frac{D_L(z)}{1+z}. \quad (2.59)$$

Suppose we are given $r_{\text{FRW}}(z)$, and therefore $D_L(z)$ and $D_A(z)$, and from this we wish to find the corresponding zero energy LTB model.

The equations defining our flat LTB model with bang time function may be written in the form

$$\frac{dT}{dr} = -\frac{1}{3} + \frac{dt_0}{dr} \left(\frac{2r}{9T^3} - \frac{1}{3T^2} \right) \quad (2.60)$$

and

$$\frac{1}{(1+z)} \frac{dz}{dr} = \left(\frac{2}{3T} + \frac{2r}{9T^4} \frac{dt_0}{dr} \right). \quad (2.61)$$

Multiply Eq. (2.60) by $2/T$ and then add to Eq. (2.61) to find

$$\frac{dt_0}{dz} = \frac{3T}{2(1+z)(r/T-1)} \frac{d}{dz} [T^2(1+z)] ; \quad (2.62)$$

we can also combine Eqs. (2.60) and (2.61) such that we eliminate dt_0/dr altogether to find

$$\frac{r}{T} \frac{dT}{dz} + \left(\frac{r}{T} - 1 \right) \frac{dr}{dz} = \frac{1}{1+z} \left(r - \frac{3T}{2} \right). \quad (2.63)$$

Defining $X \equiv T^2(1+z)$, these equations can recast into

$$\frac{1}{X} \frac{dX}{dz} = \frac{(r_{\text{FRW}}\sqrt{1+z/X^{3/2}} - 1)}{r_{\text{FRW}}(3/2 - r_{\text{FRW}}\sqrt{1+z/X^{3/2}})} \left[\frac{3X^{3/2}}{2(1+z)^{3/2}} - \frac{dr_{\text{FRW}}}{dz} \right] \quad (2.64)$$

and

$$\frac{dt_0}{dz} = \frac{3X^{3/2}}{2r_{\text{FRW}}(1+z)^{3/2}(3/2 - r_{\text{FRW}}\sqrt{1+z/X^{3/2}})} \left[\frac{3X^{3/2}}{2(1+z)^{3/2}} - \frac{dr_{\text{FRW}}}{dz} \right]. \quad (2.65)$$

In the spatially flat, dust-dominated FRW model, $X = 1$ and $r_{\text{FRW}}(z) = 3[1 - 1/\sqrt{1+z}]$.

Given $r_{\text{FRW}}(z)$, Eq. (2.64) is a first order ordinary differential equation for $X(z)$.

It becomes singular when

$$\frac{r_{\text{FRW}}(z)\sqrt{1+z}}{X^{3/2}} = \frac{3}{2}; \quad (2.66)$$

for a flat, dust-dominated FRW model, this occurs when $z = 5/4$. Solutions $z = z_{\text{crit}}$ of Eq. (2.66), if these exist, are critical points of differential equation (2.64). Near the critical point,

$$\frac{1}{X} \frac{dX}{dz} \approx \frac{1}{2(3/2 - r_{\text{FRW}}\sqrt{1+z}/X^{3/2})} \left[\frac{1}{1+z} - \frac{d \ln r_{\text{FRW}}}{dz} \right] \quad (2.67)$$

and

$$\frac{dt_0}{dz} \approx \frac{r_{\text{FRW}}(z)}{(1+z)(3/2 - r_{\text{FRW}}\sqrt{1+z}/X^{3/2})} \left[\frac{1}{1+z} - \frac{d \ln r_{\text{FRW}}}{dz} \right]. \quad (2.68)$$

Transcritical solutions, which are non-singular at the critical point, are possible provided that $(1+z)d \ln r_{\text{FRW}}/dz = 1$ at the critical point. We discuss these solutions in more detail below. Clearly, the spatially-flat, dust-dominated FRW model is one special transcritical solution. For a general choice of $r_{\text{FRW}}(z)$, however, the conditions for passing smoothly through the critical point will not be generically satisfied, and both $d \ln X/dz$ and dt_0/dz will diverge there. This suggests that a flat LTB model with a bang time function can only mimic a generic $r_{\text{FRW}}(z)$ up to some limiting redshift below z_{crit} , where

$$K_{\text{FRW}}(z_{\text{crit}}) \equiv \frac{1}{1+z_{\text{crit}}} - \frac{d \ln r_{\text{FRW}}}{dz} \Big|_{z=z_{\text{crit}}} = 0. \quad (2.69)$$

We shall argue below that only the special class of transcritical solutions can extend to infinite redshift.

For exploring characteristics of the solutions, it proves useful to define the new variable

$$V \equiv 1 - \frac{2r_{\text{FRW}}\sqrt{1+z}}{3X^{3/2}}. \quad (2.70)$$

Substituting Eq. (2.70) into Eq. (2.64) gives, after some algebra,

$$\begin{aligned} \frac{dV}{dz} &= \frac{(1 - 4V + V^2)}{2V(1+z)} - \frac{(1-V)^2}{2V} \frac{d \ln r_{\text{FRW}}}{dz} \\ &= \frac{(1+V^2)}{2V} \left[\frac{1}{1+z} - \frac{d \ln r_{\text{FRW}}}{dz} \right] - \frac{2}{1+z} + \frac{d \ln r_{\text{FRW}}}{dz}. \end{aligned} \quad (2.71)$$

For a flat, dust-dominated FRW model, $V_{\text{FRW}} = 3 - 2\sqrt{1+z}$, and substituting this $V(z)$ into the right hand side of Eq. (2.71) yields $dV_{\text{FRW}}/dz = -1/\sqrt{1+z}$. Near $z = 0$, we have seen that flat LTB models resemble flat, dust-dominated FRW models, so

$$d \ln r_{\text{FRW}}/dz = z^{-1} \left[1 - \frac{1}{2}(1+q(0))z + \dots \right] = z^{-1}(1 - 3z/4 + \dots), \quad (2.72)$$

and therefore

$$V(z) \approx 1 - z + \frac{z^2}{4} - \frac{z^3}{8} + \dots \quad (2.73)$$

for $z \ll 1$. The first term in the small- z expansion of $V(z)$ that can deviate from Eq. (2.73) is of order z^4 .

At sufficiently small z , we expect $V(z)$ to decrease. There are three possible classes of solutions to Eq. (2.71): (i) solutions that decrease from $V(0) = 1$ to some constant $V_\infty < 1$ as $z \rightarrow \infty$, without crossing the critical point at $V = 0$; (ii) solutions that decrease until a redshift $z = z_0 < z_{\text{crit}}$, where they terminate; and (iii) transcritical solutions that pass through the critical point smoothly. We examine these three classes in turn. In our considerations, we keep $r_{\text{FRW}}(z)$ general, with the proviso that the model tends to $q = 1/2$ at both $z \rightarrow 0$ and $z \rightarrow \infty$. The former is dictated by the character of LTB models free of central singularities, whereas the latter must be true of any phenomenologically viable model. In particular, then, we assume that $H \approx \frac{2}{3}\Omega_{\text{FRW}}^{1/2}(1+z)^{3/2}$ at large z , where $\Omega_{\text{FRW}} < 1$. Therefore $r_{\text{FRW}}(z) \rightarrow r_{\text{FRW},\infty}$ as $z \rightarrow \infty$, where $r_{\text{FRW},\infty}$ is a constant.

Consider first solutions that decrease toward V_∞ asymptotically. At large values of z , Eq. (2.71) becomes

$$\begin{aligned} \frac{dV}{dz} &\approx \frac{1 - 4V_\infty + V_\infty^2}{2V_\infty(1+z)} - \frac{(1 - V_\infty)^2}{2V_\infty} \frac{d \ln r_{\text{FRW}}}{dz} \\ &\approx \frac{1 - 4V_\infty + V_\infty^2}{2V_\infty(1+z)} - \frac{3(1 - V_\infty)^2}{4V_\infty \Omega_{\text{FRW}}^{1/2} r_{\text{FRW},\infty} (1+z)^{3/2}}. \end{aligned} \quad (2.74)$$

The first term on the right hand side of Eq. (2.74) is negative as long as $V_\infty > V_0 \equiv 2 - \sqrt{3} \approx 0.27$, and it dominates the second term. But $V(z) \sim -\ln(1+z)$ in that case, and this diverges. Thus, we can only have $V_\infty = V_0$. In that case, we let $V(z) = V_0 + u(z)$ at large z , and find

$$\frac{du}{dz} \approx -\frac{u\sqrt{3}}{(2 - \sqrt{3})(1+z)} - \frac{3(\sqrt{3} - 1)^2}{4(2 - \sqrt{3})\Omega_{\text{FRW}}^{1/2} r_{\text{FRW},\infty} (1+z)^{3/2}}, \quad (2.75)$$

which has the general solution

$$u(z) = \frac{C}{(1+z)^{\sqrt{3}/(2-\sqrt{3})}} - \frac{3(\sqrt{3} - 1)^2}{2(3\sqrt{3} - 2)\Omega_{\text{FRW}}^{1/2} r_{\text{FRW},\infty} \sqrt{1+z}}, \quad (2.76)$$

where C is a constant. Although $u(z) \rightarrow 0$ as $z \rightarrow \infty$, it approaches zero from below, not from above, which contradicts our basic assumption. Thus, solutions that simply decrease toward constant $V(z) > 0$ asymptotically do not exist. Conceivably, there can be solutions that decrease to a minimum and then increase toward V_0 asymptotically. For these, however, $V(z)$ will be double valued. It then follows that $X = T^2(1+z)$ must be double valued, since $r_{\text{FRW}}\sqrt{1+z}$ is monotonically increasing, and such behavior could be pathological. More generally, we shall see below that solutions that avoid $V = 0$ must terminate at $z = z_{\text{crit}}$ in order to avoid other physical pathologies. Thus, a solution “on track” to a minimum value $V_{\text{min}} > 0$, and on to V_0 asymptotically, might end at finite redshift.

Next, consider solutions that reach $V = 0$ at $z = z_0 < z_{\text{crit}}$ and end there. Near

$V = 0$, Eq. (2.71) is approximately

$$\frac{dV}{dz} \approx \frac{K_{\text{FRW}}(z_0)}{2V}, \quad (2.77)$$

where $K_{\text{FRW}}(z) = (1+z)^{-1} - d \ln r_{\text{FRW}}/dz$, as in Eq. (2.69). Note that since $z_0 < z_{\text{crit}}$, $K_{\text{FRW}}(z_0) < 0$ as well. The solution to Eq. (2.77) is $V(z) \approx \sqrt{-K_{\text{FRW}}(z_0)(z_0 - z)}$, which terminates at $z = z_0$.

In order to reach the critical point, we must have

$$K_{\text{FRW}}(z) \leq 0 \quad (2.78)$$

all the way up to the critical point, with equality holding at $z = z_{\text{crit}}$ for the transcritical solution. For a transcritical solution to exist, we must be able to expand

$$K_{\text{FRW}}(z) = Q\Delta z + \mathcal{O}(\Delta z^2) \quad (2.79)$$

near the critical redshift, z_{crit} , where $\Delta z = z - z_{\text{crit}}$ and $Q > 0$. For a flat, dust-filled FRW model, we have $z_{\text{crit}} = 5/4$ and $Q = 8/27$. Using this linear approximation, we find from Eq. (2.71) that $V = k\Delta z + \mathcal{O}(\Delta z^2)$, where the slope $k < 0$ is the solution to

$$k^2 + \frac{k}{1 + z_{\text{crit}}} - \frac{Q}{2} = 0. \quad (2.80)$$

That is, we need the negative root

$$k = -\frac{1}{2(1 + z_{\text{crit}})} - \frac{1}{2} \sqrt{\left(\frac{1}{1 + z_{\text{crit}}}\right)^2 + 2Q}. \quad (2.81)$$

For a flat, dust-filled FRW model, we find $k = -2/3$. This is clearly a transcritical solution.

We can turn the above analysis into a test of whether a candidate for $r_{\text{FRW}}(z)$ that agrees with observations can be represented by a transcritical, zero energy

LTB model. First, for the candidate model, it is possible to find z_{crit} and Q algebraically; we can find z_{crit} using Eq. (2.69), by requiring that $K_{\text{FRW}}(z_{\text{crit}}) = 0$, and we can find $Q = dK_{\text{FRW}}/dz|_{z=z_{\text{crit}}}$, cf. Eq. (2.79). Next, find k given Q and z_{crit} from Eq. (2.81) and use this value of k to integrate Eq. (2.71) back toward $z = 0$. If the solution satisfies Eq. (2.73) as $z \rightarrow 0$, then it is an acceptable transcritical solution.

There are other disasters that may befall the solution for general $r_{\text{FRW}}(z)$, and some of these may even afflict transcritical solutions. Eq. (2.65) may be rewritten as

$$\frac{dt_0}{dz} = \frac{2r_{\text{FRW}}}{3(1+z)(1-V)} \left[\frac{1}{V} \left(\frac{1}{1+z} - \frac{d \ln r_{\text{FRW}}}{dz} \right) + \frac{1}{(1+z)(1-V)} \right]. \quad (2.82)$$

As we have noted before, dt_0/dz diverges at $V = 0$ for generic $r_{\text{FRW}}(z)$, but for transcritical solutions,

$$\frac{dt_0}{dz} = \frac{2r_{\text{FRW}}(z_{\text{crit}})}{3(1+z_{\text{crit}})} \left(\frac{Q}{k} + \frac{1}{1+z_{\text{crit}}} \right) + \mathcal{O}(\Delta z) \quad (2.83)$$

near the critical point, which is finite, so this potential disaster is avoided. In particular, for a flat, dust-filled FRW model with $Q = 8/27$ and $k = -2/3$ at $z_{\text{crit}} = 5/4$, we see that $Q/k + 1/(1+z_{\text{crit}}) = 0$, which is consistent with $t_0(z) = 0$ for all redshifts.

We must check for two other possible disasters, for solutions that are transcritical or not. As mentioned in the previous section, physical regions in any solution must have a positive, finite $R' = \partial R/\partial r$ and dr/dz . We find

$$\begin{aligned} \frac{\partial R}{\partial r} &= [3(1-V)]^{1/3} \left(\frac{2r_{\text{FRW}}}{1+z} \right)^{2/3} \left[\frac{(1+z)d \ln r_{\text{FRW}}/dz - 1}{(1-V)[(1+z)d \ln r_{\text{FRW}}/dz - 1] + 2V} \right] \\ \frac{dr}{dz} &= \left[\frac{2r_{\text{FRW}}}{3(1-V)(1+z)^4} \right]^{1/3} \left\{ \left(\frac{1-V}{2V} \right) \left[(1+z) \frac{d \ln r_{\text{FRW}}}{dz} - 1 \right] + 1 \right\}. \end{aligned} \quad (2.84)$$

Note that we have $\dot{R}' \propto (dr/dz)^{-1}$, and thus a finite, positive dr/dz implies that $\dot{R}' > 0$. These equations are evaluated along the path of a light ray directed radially inward. The requirement $\partial R/\partial r > 0$ along the light ray is a necessary but not sufficient condition for an acceptable model. The more general requirement is that $\partial R/\partial r > 0$ at all (r, t) , a global condition that is much harder to satisfy; but in general, from Eq. (2.2), this will be satisfied for models with $t_0(r)$ decreasing monotonically. From the first of Eqs. (2.84), we note that $\partial R/\partial r \rightarrow 0$ at $z = z_{\text{crit}}$ for solutions that are not transcritical. Solutions that terminate at $z_0 < z_{\text{crit}}$ would not encounter this pathology. Solutions of the first type described above, which decrease from $V(0) = 1$ but do not cross $V = 0$, would end at $z = z_{\text{crit}}$. For a transcritical solution,

$$\frac{\partial R}{\partial r} = 3^{1/3} \left(\frac{2r_{\text{FRW}}(z_{\text{crit}})}{1 + z_{\text{crit}}} \right)^{2/3} \left[\frac{Q(1 + z_{\text{crit}})}{Q(1 + z_{\text{crit}}) - 2k} \right] > 0 \quad (2.85)$$

at the critical point. Transcritical solutions therefore propagate right through the critical point with a positive, finite $\partial R/\partial r$. From the second of Eqs. (2.84), we see that dr/dz diverges for solutions that terminate at $V = 0$ and $z = z_0$. For transcritical solutions

$$\frac{dr}{dz} = \left[\frac{r_{\text{FRW}}(z_{\text{crit}})}{3(1 + z_{\text{crit}})} \right]^{1/3} \left(-\frac{Q}{k} + \frac{2}{1 + z_{\text{crit}}} \right) > 0 \quad (2.86)$$

at the critical point. Beyond the critical point, transcritical solutions have $V < 0$, and for reasonable $r_{\text{FRW}}(z)$ with decreasing $(1+z)d \ln r_{\text{FRW}}/dz$, it seems likely that dr/dz remains positive.

From these general considerations, we conclude that zero energy LTB models can only mimic a given, generic $r_{\text{FRW}}(z)$ – arranged, for example, to fit observations of Type Ia supernovae – for $0 \leq z \leq z_0 < z_{\text{crit}}$, where z_{crit} is the solution to Eq.

(2.69). There can be exceptional, transcritical models that extend to infinite z without any mathematical or physical pathologies. However, transcritical models are highly constrained mathematically, and may not exist for choices of $r_{\text{FRW}}(z)$ that conform to phenomenological requirements. The flat, dust-dominated FRW model is one transcritical solution, but it is ruled out by observations.

2.3.2 Manufacturing Transcritical Solutions

To manufacture transcritical solutions, we will specify $V(\tilde{r})$, where

$\tilde{r}(z) \equiv r_{\text{FRW}}(z)\sqrt{1+z}$, and find an equation for $\tilde{r}(z)$. From Eq. (2.71) we find

$$\frac{d\tilde{r}}{dz} = \frac{3 - 10V + 3V^2}{2(1+z)[2VV' + (1-V)^2/\tilde{r}]} \quad (2.87)$$

where $V'(\tilde{r}) \equiv dV(\tilde{r})/d\tilde{r}$. As long as $VV' \rightarrow 0$ near $V = 0$, Eq. (2.87) satisfies the transcriticality condition $K_{\text{FRW}} = 0$ when $V = 0$. As an example, suppose we assume that $V = 1 - k\tilde{r}$. Then we find $\tilde{r} = (2/k)(\sqrt{1+z} - 1)$ and we must choose $k = 2/3$ in order to have the proper behavior at small z . This solution is simply equivalent to the flat, dust-filled FRW solution.

Superficially, the prescription is simple: specify a $V(\tilde{r})$, make sure that $VV' \rightarrow 0$ when $V = 0$, and then find the corresponding $\tilde{r}(z)$ by integrating Eq. (2.87). However, we know that acceptable solutions must have $d\tilde{r}/dz \geq 0$ and finite; these conditions are not so easy to guarantee.

Let us assume $V(\tilde{r}) = 1 - \frac{2}{3}\tilde{r}f(\tilde{r})$; then Eq. (2.87) becomes

$$\frac{d\tilde{r}}{dz} = \frac{(\tilde{r}f - 1)(\tilde{r}f + 3)}{2(1+z)[f(\tilde{r}f - 1) - (1 - 2\tilde{r}f/3)\tilde{r}f']} \quad (2.88)$$

The numerator of Eq. (2.88) is zero when $\tilde{r}f(\tilde{r}) = 1$, or $V = 1/3$. If the denominator of Eq. (2.87) is nonzero at this point, then $d\tilde{r}/dz$ goes to zero, and changes sign upon crossing it. Thus, we also want the denominator to vanish for an acceptable solution. In other words, $V = 1/3$ must be a critical point of Eq. (2.87): we have only succeeded in hiding the critical nature of the problem, rather than eliminating it. Eq. (2.88) shows that to pass through this critical point we must require that $\tilde{r}f' = 0$ when $\tilde{r}f = 1$. Clearly, the spatially flat, dust-filled FRW model, for which $f(\tilde{r}) = 1$, is one possibility.

It is also possible that the denominator of Eq. (2.88) vanishes, so $d\tilde{r}/dz \rightarrow \infty$ before $\tilde{r}f \rightarrow 1$. This happens when

$$f' = \frac{f(\tilde{r}f - 1)}{\tilde{r}(1 - 2\tilde{r}f/3)}. \quad (2.89)$$

If $f' < 0$ at small values of \tilde{r} , it is possible that infinite $d\tilde{r}/dz$ occurs before $\tilde{r}f \rightarrow 1$. Since we also want $f(0) = 1$ for nonsingular models, and $f(\infty) = \text{constant}$ for models that approximate a flat FRW model with $\Omega_M < 1$ at sufficiently large redshift, we have several requirements on $f(\tilde{r})$ that must be met simultaneously for a model that is acceptable mathematically. Moreover, physically acceptable models must also have $\partial R/\partial r > 0$ and $\dot{R}' > 0$. Only a subset of such models – if any – will also be acceptable phenomenologically.

To examine the phenomenological properties of a candidate transcritical solution, first define the effective Hubble parameter $H_{\text{eff}}(z)$ via

$$\frac{dr_{\text{FRW}}}{dz} = \frac{1}{H_{\text{eff}}(z)}. \quad (2.90)$$

It is straightforward to show that, normalizing so that $H_{\text{eff}}(0) = 1$,

$$h(z) \equiv \frac{H_{\text{eff}}(z)}{(1+z)^{3/2}} = \frac{3}{2} \left[(1+z) \frac{d\tilde{r}}{dz} - \frac{\tilde{r}}{2} \right]^{-1} = \frac{3[f(\tilde{r}f-1) - (1-2\tilde{r}f/3)\tilde{r}f']}{3(\tilde{r}f-1) + (1-2\tilde{r}f/3)\tilde{r}^2f'}. \quad (2.91)$$

We can also calculate the effective value of the equation of state parameter

$$\begin{aligned} w_{\text{eff}} &= \frac{2(1+z)}{3} \frac{d \ln h}{dz} \\ &= \frac{(\tilde{r}f+3)(\tilde{r}f-1)}{3[f(\tilde{r}f-1) - (1-\frac{2}{3}\tilde{r}f)\tilde{r}f']^2 [3(\tilde{r}f-1) + (1-\frac{2}{3}\tilde{r}f)\tilde{r}^2f']} \\ &\quad \times \left\{ f' \left[\frac{4(\tilde{r}f)^3}{3} + 2(\tilde{r}f)^2 - 8\tilde{r}f + 6 \right] + (\tilde{r}f')^2 \left[-\frac{2(\tilde{r}f)^2}{9} + \frac{2\tilde{r}f}{3} + 1 \right] \right. \\ &\quad \left. - \tilde{r}f''(\tilde{r}f-1)(\tilde{r}f+3) \left(1 - \frac{2\tilde{r}f}{3} \right) \right\}. \quad (2.92) \end{aligned}$$

$H_{\text{eff}}(z)$ is the Hubble parameter that would be measured by an observer who assumes her observations are described by a spatially flat FRW model, and $w_{\text{eff}}(z)$ is the associated equation of state parameter. (A less dogmatic observer would allow for the possibility of spatial curvature.) Note that Eq. (2.91) implies that for $f' = 0$, $H_{\text{eff}}/(1+z)^{3/2} = f = \text{constant}$. If we are interested in using LTB models to mimic a spatially flat FRW model with a mixture of dust plus cosmological constant, we shall want $f \rightarrow \sqrt{\Omega_M} = \sqrt{1 - \Omega_V}$ at large redshift, where Ω_M and Ω_V are the present density parameters in nonrelativistic matter and cosmological constant, respectively. Moreover, $f \rightarrow 1$ as $z \rightarrow 0$; thus f must decrease from 1 to $\sqrt{1 - \Omega_V}$ as redshift increases to mimic observations in an FRW model of this sort.

For any choice of $f(\tilde{r})$ tailored to pass smoothly through both $V = 0$ and $\tilde{r}f(\tilde{r}) = 1$, we can integrate Eq. (2.88) to find a transcritical solution. However, such a solution still must pass the tests outlined in the previous section to extend

to arbitrarily large redshifts. In terms of \tilde{r} and $f(\tilde{r})$,

$$\begin{aligned} \frac{dt_0}{dz} &= \frac{3(h-f)}{2(1+z)^{5/2}f^2h\tilde{r}(1-2\tilde{r}f/3)} \\ (1+z)\frac{\partial R}{\partial r} &= \frac{f^{1/3}(3-2h\tilde{r})}{f+2h-2f\tilde{r}} \\ \frac{3\dot{R}'}{2(1+z)^{1/2}} &= \frac{3f^{1/3}(1-2\tilde{r}f/3)}{2+f/h-2\tilde{r}f} . \end{aligned} \quad (2.93)$$

We reject any transcritical solution for which dt_0/dz is ever positive, or $\partial R/\partial r$ or \dot{R}' change sign.³ Moreover, even if a transcritical solution is found that possesses none of the pathologies discussed above, it may not conform to observational constraints. Thus, if there are any nonsingular, non-pathological LTB solutions that can also mimic the observations, they must be very exceptional indeed.

Designing nonsingular, non-pathological transcritical solutions is a formidable challenge. Suppose that at small values of \tilde{r} , we expand $f(\tilde{r}) = 1 + f_n\tilde{r}^n + \dots$. Then we find that $h \approx 1 + f_n(1+n)\tilde{r}^n + \dots$ and $w_{\text{eff}} = f_n n(n+1)\tilde{r}^{n-1} + \dots$ near the origin, where $\tilde{r} \approx \frac{3}{2}z$. Also

$$\begin{aligned} \frac{dt_0}{dz} &\approx \frac{3(h-f)}{2\tilde{r}} \approx \frac{3}{2}f_n n\tilde{r}^{n-1} \\ (1+z)\frac{\partial R}{\partial r} &\approx 1 - \frac{2(h-1)}{3} \\ \frac{3\dot{R}'}{2(1+z)^{1/2}} &\approx 1 + \frac{1}{3}(h-1) . \end{aligned} \quad (2.94)$$

We wish to tailor $f(\tilde{r})$ to maintain positive values of both $\partial R/\partial r$ and \dot{R}' , but already near the origin $\partial R/\partial r$ and \dot{R}' deviate from their flat, dust-filled FRW relationships in opposite senses. Notice that to avoid the weak singularity near

³For LTB with bang time perturbations only, $(\partial R/\partial r)_t = [t - t_0(r)]^{-1/3}[t - t_0(r) - \frac{2}{3}rdt_0/dr]$, which is only zero for a shell at coordinate radius r when $t - t_0(r) = \frac{2}{3}rdt_0/dr$. If $dt_0(r)/dr < 0$, this occurs before $t_0(r)$ and is therefore irrelevant. As long as $dt_0(z)/dz < 0$ and $\dot{R}' > 0$ along the light ray path, $dt_0(r)/dr < 0$ and $(\partial R/\partial r)_t$ is never zero.

the origin, we need to have $n \geq 2$. Moreover, we want to make sure that $t_0(z)$ is monotonically decreasing to avoid shell crossing. Near the origin, decreasing $t_0(z)$ implies $f_n < 0$.

To illustrate how difficult it is to manufacture non-pathological transcritical solutions from Eq. (2.88), we have considered

$$f(\tilde{r}) = \frac{1}{\tilde{r}_1} \left[1 + K \left(\frac{\tilde{r}_1^n - \tilde{r}^n}{\tilde{r}_2^n + \tilde{r}^n} \right)^p \right]. \quad (2.95)$$

The model has four parameters: K , \tilde{r}_1 , n , and p ; the remaining parameter \tilde{r}_2 will be determined in terms of these four. To be sure that h and w_{eff} are finite near $\tilde{r}f = 1$, we want either $p \equiv 2$ or $p \geq 3$. Expanding near the origin, we find

$$f(\tilde{r}) = \frac{1 + K(\tilde{r}_1/\tilde{r}_2)^n}{\tilde{r}_1} - \frac{Kp}{\tilde{r}_1} \left(\frac{\tilde{r}_1}{\tilde{r}_2} \right)^{np} \left(\frac{1}{\tilde{r}_2^n} + \frac{1}{\tilde{r}_1^n} \right) \tilde{r}^n + \dots; \quad (2.96)$$

requiring $f(0) = 1$ implies

$$\tilde{r}_2^n = \tilde{r}_1^n \left(\frac{K}{\tilde{r}_1 - 1} \right)^{1/p}, \quad (2.97)$$

and so we can rewrite the expansion in the form $f(\tilde{r}) = 1 + f_n \tilde{r}^n + \dots$ with

$$f_n = -\frac{Kp}{\tilde{r}_1} \left(\frac{\tilde{r}_1}{\tilde{r}_2} \right)^{np} \left(\frac{1}{\tilde{r}_2^n} + \frac{1}{\tilde{r}_1^n} \right) = -\frac{p(\tilde{r}_1 - 1)}{\tilde{r}_1^{n+1}} \left[1 + \left(\frac{\tilde{r}_1 - 1}{K} \right)^{1/p} \right]. \quad (2.98)$$

Thus, we want $\tilde{r}_1 - 1 > 0$ and therefore $K > 0$ for $f_n < 0$ and real \tilde{r}_2 . At large values of \tilde{r} , $f(\tilde{r}) \rightarrow \tilde{r}_1^{-1}[1 + (-1)^p K]$. Thus, we expect models that can mimic decelerating FRW models successfully to have $\tilde{r}_1^{-1}[1 + (-1)^p K] < 1$, suggesting either large \tilde{r}_1 or odd p , or both. Empirically, we have been unable to find any non-pathological models based on Eq. (2.95) with these properties.

Figure 2.3 shows an example of a transcritical solution with $K = 1$, $\tilde{r}_1 = 1.05$, $n = 3$, and $p = 2$. Although the figure only displays $z < 1000$, we have integrated

this model out to $z = 10^6$ to verify that it asymptotes smoothly to a high redshift FRW model, with constant t_0 . The left panel shows $r_{\text{FRW}}(z)/r_{\text{FRW}}^{(0)}(z)$ (dotted line), where $r_{\text{FRW}}^{(0)}(z)$ is computed for a flat Λ CDM FRW reference cosmology with $\Omega_M = 0.27$ and $\Omega_\Lambda = 0.73$, $h(z)$ (short dashed line), and $w_{\text{eff}}(z)$ (solid line). Since $h \rightarrow 2/1.05 = 1.905$ at high z for this model, inevitably there must be regions with $w_{\text{eff}} > 0$; this is in the range $0.75 \lesssim z \lesssim 3.9$, with a peak value $w_{\text{eff}} \approx 2.13$. There are two regions of negative w_{eff} : (i) one at $0 < z \lesssim 0.75$, with minimum value $w_{\text{eff}} \approx -0.98$; and (ii) an extensive region at $z \gtrsim 3.9$, with a minimum value $w_{\text{eff}} \approx -0.292$. The right panel verifies the transcritical nature of the solution: it shows V (short dashed line), $1 - d \ln r_{\text{FRW}} / d \ln(1 + z)$ (dotted line), and t_0 (solid line), and the long dashed line is at 0. The first two cross zero simultaneously, as they must for a transcritical solution, and at large redshifts, V is approximately proportional to $\sqrt{1 + z}$ while $1 - d \ln r_{\text{FRW}} / d \ln(1 + z)$ tends toward one. For this model, $t_0(z) \leq 0$ at all z , and we have also verified that it decreases monotonically. In addition, we can verify that the model behaves as predicted at small redshifts: $t_0(z) \approx -0.34z^3$ and $w_{\text{eff}} \approx -2.7z^2$.

Figure 2.4 compares the relative distance moduli

$$\Delta m = 5.0 \log_{10}[r_{\text{FRW}}(z)/r_{\text{FRW}}^{(0)}(z)] \quad (2.99)$$

for models with $K = 1$ and $(n, p) = (3, 2)$ (solid line), $(n, p) = (3, 4)$ (dotted line), $(n, p) = (2, 2)$ (dashed line), and $(n, p) = (2, 4)$ (dash-dot line), with $\tilde{r}_1 = 1.05$ in the lower set of curves and $\tilde{r}_1 = 1.5$ in the upper set; there is no solid line in the upper set for $(n, p) = (3, 2)$ because the model is pathological. For the lower set, luminous objects would appear systematically brighter than they would in the standard Λ CDM model. As \tilde{r}_1 is increased, a period of substantial acceleration is

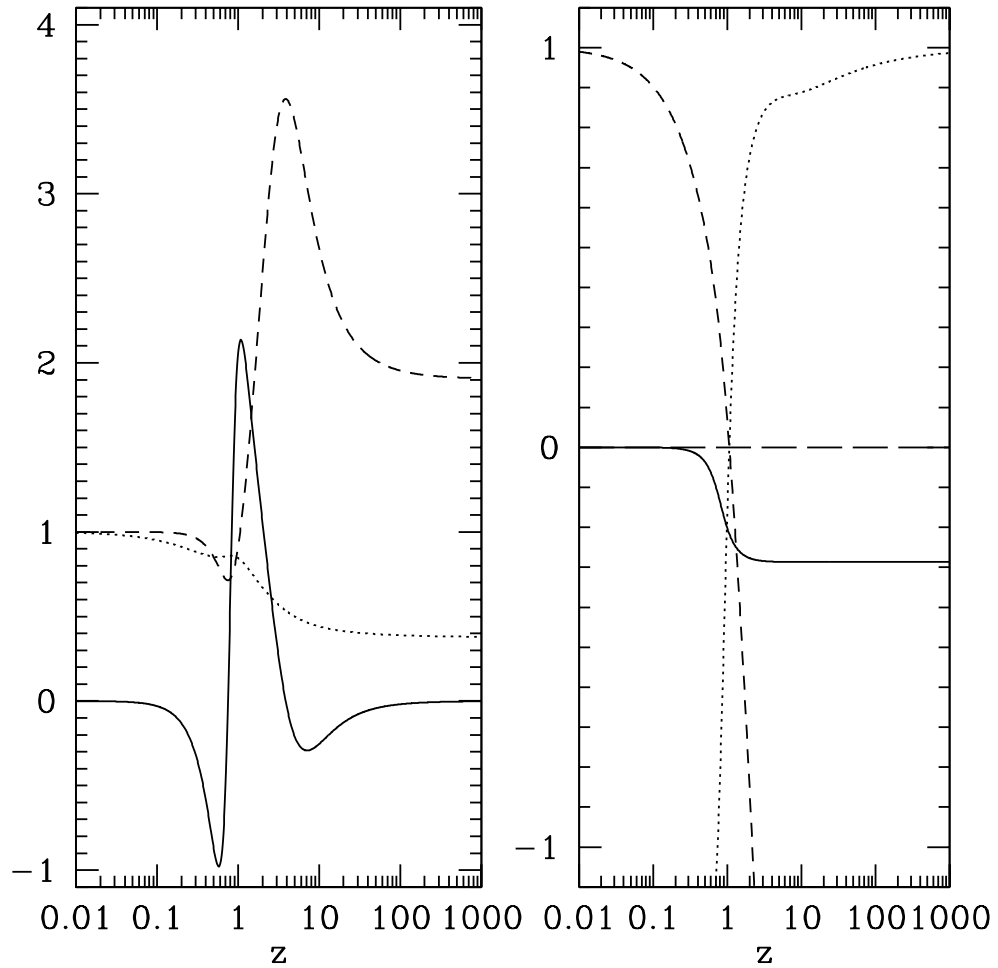


Figure 2.3: Results for our candidate transcritical model with $K = 1$, $p = 2$, $n = 3$, and $\tilde{r}_1 = 1.05$, out to $z = 1000$. The left panel shows $r_{\text{FRW}}(z)/r_{\text{FRW}}^{(0)}(z)$ (dotted), $h(z) \equiv H(z)/[H_0(1+z)^{3/2}]$ (short dashed), and $w_{\text{eff}}(z)$ (solid). The reference model corresponding to $r_{\text{FRW}}^{(0)}(z)$ is the spatially flat Λ CDM model with $\Omega_M = 0.27$. The right panel shows V (short dashed), $1 - d \ln r_{\text{FRW}} / d \ln(1+z)$ (dotted), and t_0 (solid).

seen in the models below $z \sim 1$, leading to the systematic brightening relative to Λ CDM as seen in the upper set of curves. In either case, the luminosity differences would be easy to discern observationally.

These few models illustrate several important qualitative points. First, it is possible to construct non-pathological transcritical solutions that also avoid any central weak singularities. Second, the model has a complicated “effective equation of state”, including regions where $w_{\text{eff}} < 0$, but also regions where $w_{\text{eff}} > 0$. In this case, we found a range of values $-1 \lesssim w_{\text{eff}} \lesssim 2$. Finally, although it is possible to construct models that are well-behaved mathematically, these models do not generally conform to observational constraints. We have not, however, excluded the possibility that transcritical models in agreement with observations may exist.

2.4 Conclusions

Some have tried to use the spherically-symmetric LTB cosmological models to explain the seemingly anomalous supernova data, as introducing a large degree of inhomogeneity can significantly distort the dependence of luminosity distance on redshift. We have shown that one must take care in using these models, as they will contain a weak singularity at the symmetry center unless certain very restrictive conditions are met. Realistic LTB solutions require that the first derivative of the bang time function vanish at the center, $t'_0(0) = 0$, and also that $k'(0) = 0$, where $2E(r) \equiv -k(r)r^2$. Otherwise there are physical parameters, such as the density and Ricci scalar, which are not differentiable at the origin.

We have also shown that any LTB models without a central singularity will nec-

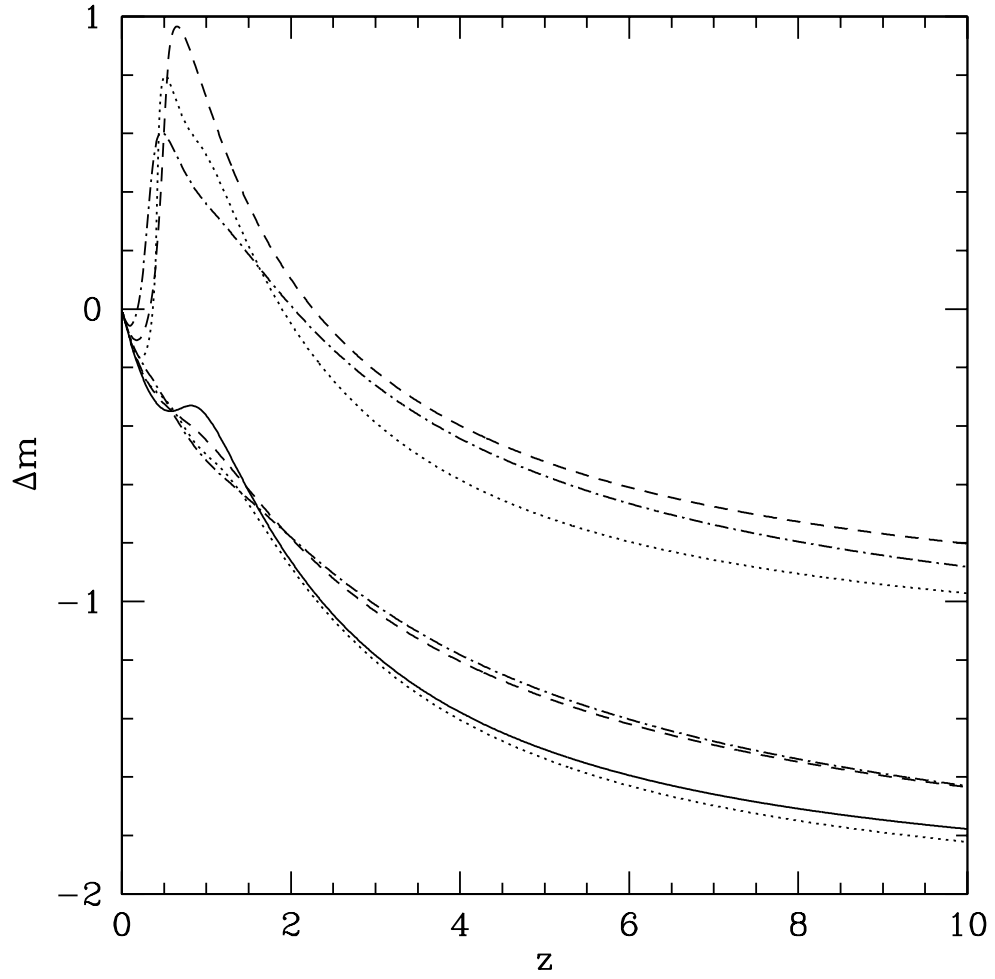


Figure 2.4: Distance moduli relative to spatially flat Λ CDM with $\Omega_M = 0.27$ for models with $K = 1$ and $(n, p) = (3, 2)$ (solid), $(n, p) = (3, 4)$ (dotted), $(n, p) = (2, 2)$ (dashed), and $(n, p) = (2, 4)$ (dash-dot), with $\tilde{r}_1 = 1.05$ for the lower set of curves, and $\tilde{r}_1 = 1.5$ for the upper set.

essarily have a positive central deceleration parameter q_0 , and thus all previously considered LTB models with $q_0 < 0$ are singular at the origin. However, it is still possible to obtain a negative effective deceleration parameter for nonzero redshifts, which we have shown using as an example the model with zero energy and with the bang time function (2.56), that is quadratic at small r . These models have regions of apparent acceleration, where $q(z)$ is negative. If our goal is to reproduce luminosity distance data with a non-singular LTB model, we can try to smooth out the center appropriately and tailor the model to fit the data at modest redshifts, say $z \geq 0.01$. This is not an easy task because there are other singular behaviors that generally occur when trying to represent a given luminosity distance function $D_L(z)$ with a zero energy LTB model.

Our detailed examination of the “inverse problem” elucidates how difficult it is to match zero energy LTB models to observed luminosity distance data. We have shown that the underlying differential equations generically become singular at a critical point. We have also shown that some exceptional choices of $r_{\text{FRW}} = D_L(z)/(1+z)$ admit transcritical solutions which are smooth at the critical point $z = z_{\text{crit}}$, and may extend to arbitrarily high redshift, given that they do not encounter other pathologies along the way. All other solutions terminate at some redshift $z_0 < z_{\text{crit}}$. We have shown how transcritical solutions can be constructed via a simple procedure. Although these solutions show both enhanced deceleration, seen as regions with $w_{\text{eff}}(z) > 0$, and acceleration, seen as regions with $w_{\text{eff}}(z) < 0$, none that we have constructed explicitly conform to observations. Here we have only studied the effects of a bang time function, and did not consider the case of a non-zero energy function $E(r)$. We expect generic solutions with $E(r) \neq 0$ to share the basic characteristics of the models studied here, namely the critical points and

other singularities that we have discussed. However, we cannot say for sure that there are no transcritical and nonsingular solutions with non-zero $t_0(r)$ and $E(r)$ that agree with observational data on $r_{FRW}(z)$, although it does not appear to be likely, as is evident from previous unsuccessful attempts to find such solutions [31].

Even if it were possible to reproduce determinations of $D_L(z)$ from supernova data in a LTB model without dark energy, we would still be left with the task of matching all of the other cosmological data with such a model. First, the Wilkinson Microwave Anisotropy Probe is one of our most important sources of information about the Universe, via CMB data; Alnes *et al.* [34] try to reproduce the first peak of the angular power spectrum with LTB models, and Schneider and C el erier [35] claim to be able to account for the apparent anisotropy in the dipole and quadrupole moments with an off center observer. There are further constraints on inhomogeneous models from the kinetic Sunyaev-Zel'dovich effect, which constrains radial velocities relative to the CMB [36]. However, observations of large scale structure formation may be the most difficult to reconcile. These data strongly disfavor a currently dust dominated universe, as density perturbations would have grown too much without dark energy present to speed up the cosmic expansion rate and consequently retard the growth of fluctuations.

Chapter 3

Systematic Effects of Cosmological Voids and Sheets

3.1 Introduction

Studies of the spherically-symmetric LTB models have shown that it is in principle possible to construct a matter dominated cosmological model that will appear to be accelerating, if the luminosity distance-redshift relation of Type Ia supernovae is interpreted within the framework of a homogeneous FRW universe. However, it is highly unlikely that we would live so close to the center of a spherically-symmetric universe with such severe large scale inhomogeneities, and so we should study this effect within the context of more realistic models of structure formation.

On very large scales, the matter in the Universe is arranged in a web of filaments and sheets of matter, with large ~ 50 Mpc voids in between [37]. The aim of this chapter is to develop a simple analytic model for this scenario, so that we can explore how such structures systematically affect supernova data. In the work that follows, we will construct a model wherein we take the standard matter-dominated FRW model and cut out spherical voids in a random arrangement. In Section 3.2, we will find that such a scenario will only be a valid solution of general relativity if each void is bounded by a thin shell of matter that contains all of the mass that is missing from the void. Hence, this model incorporates the voids and sheets of matter that we see in large scale structure surveys and simulations. This is a

variant of the “Swiss cheese” cosmological models [38, 39, 40].

Light propagation through a single void has already been studied in detail Ref. [41]. This in contrast to our goal in this chapter, which is to find the systematic effects of voids on the luminosity distance-redshift relation, and this requires the statistical study of light propagation through many voids. It was discovered during the preparation of this manuscript that a similar study was done previously [42], and subsequently another study appeared [43].

The organization of this chapter is as follows. In Section 3.2, we use the Israel junction conditions [44] to find the dynamics of our model, and in Section 3.3 we compute the motion of a single light ray through a void, to second order in the ratio of the void size to the Hubble length. We find that there is no net redshift change, but there is an impact parameter dependent deflection. Then, in Section 3.4, we compute the effect that this would have on the luminosity distances of supernovae. We find that there is no mean amplification of supernova images, but there is an induced error. This error is several orders of magnitude smaller than the intrinsic error in measuring supernova luminosities, and therefore we find that the effect is negligible.

3.2 Model Dynamics

Our model for cosmological voids consists of an FRW universe which contains spherical empty regions. The construction of such a situation implies the joining of two metrics: the external FRW metric and the internal vacuum metric. Joining these involves satisfying the Israel junction conditions, and we will eventually find

that these conditions will only be satisfied if each empty region is surrounded by a thin mass compensating shell.

In order to find the proper junction conditions for shells surrounding the voids, it is convenient to first consider just one such void, centered at the origin of a spherically-symmetric coordinate system. Inside the shell, the boundary of which we will call Σ , we will have vacuum with the coordinates x^α and the line element

$$ds^2 = -d\tau^2 + d\chi^2 + \chi^2 d\Omega^2 , \quad (3.1)$$

where $d\Omega^2 \equiv d\theta^2 + \sin^2\theta d\phi^2$. Outside Σ , we will have the standard FRW line element

$$ds^2 = -dt^2 + a^2(t) \left[\frac{dr^2}{1 - kr^2} + r^2 d\Omega^2 \right] . \quad (3.2)$$

Let us also refer to the region outside Σ as \mathcal{V}^+ and the region inside Σ as \mathcal{V}^- . If we choose the coordinates on the hypersurface describing Σ to be $y^a = (t, \theta, \phi)$, and if we assume that this surface will be comoving with the FRW flow, then Σ is described by

$$r = R = \text{constant} \quad (3.3)$$

as seen from \mathcal{V}^+ , and by $\chi = X(t)$ and $\tau = T(t)$ as seen from \mathcal{V}^- .

The first junction condition states that the induced metric h_{ab} on the hypersurface Σ has to be the same on both sides. From the outside, we have

$$ds_{\Sigma+}^2 = -dt^2 + a^2(t) R^2 d\Omega^2 \quad (3.4)$$

and from the inside, we have

$$ds_{\Sigma-}^2 = \left(-\dot{T}^2 + \dot{X}^2 \right) dt^2 + X^2 d\Omega^2 . \quad (3.5)$$

Since $ds_{\Sigma_+}^2 = ds_{\Sigma_-}^2$, this means that $X(t) = a(t)R$ and

$$\dot{X}^2 + 1 = \dot{T}^2 . \quad (3.6)$$

Thus, $X(t)$ is the physical size of a void with comoving size R at a time t . The solution for $a(t)$ can be obtained from the Einstein equations for the FRW exterior with uniform dust density ρ , namely

$$\dot{a}^2 + k = \frac{8\pi}{3}\rho a^2 . \quad (3.7)$$

So we can easily find the solutions for $X(t)$ and $T(t)$ using the above relations.

The second junction condition says that the jump in extrinsic curvature tells us the surface stress energy S_{ab} of the shell, where the shell's stress energy tensor is given by

$$T_{\Sigma}^{\alpha\beta} = \delta(l)S^{ab}e_a^\alpha e_b^\beta . \quad (3.8)$$

Here $l = 0$ at Σ , l measures proper length in the direction perpendicular to Σ , and $e_a^\alpha = \partial x^\alpha / \partial y^a$. Given the extrinsic curvature K_{ab}^\pm on each side (with a plus or a minus to tell us which side) and the traces $K_\pm = h^{ab}K_{ab}^\pm$, the surface stress energy tensor on Σ is

$$S_{ab} = -\frac{1}{8\pi} [(K_{ab}^+ - K_{ab}^-) - (K_+ - K_-)h_{ab}] . \quad (3.9)$$

The extrinsic curvature is

$$K_{ab} = n_{\alpha;\beta}e_a^\alpha e_b^\beta , \quad (3.10)$$

where we define the unit normal vector n_α such that $n^\alpha n_\alpha = 1$ and

$$n_\alpha = \frac{\Phi_{,\alpha}}{|g^{\mu\nu}\Phi_{,\mu}\Phi_{,\nu}|^{1/2}} , \quad (3.11)$$

and where Σ is described above as being a condition on the coordinates: $\Phi(x^\alpha) = 0$.

As seen from \mathcal{V}^+ , $\Phi^+ = r - R = 0$. This means that $n_t = n_\theta = n_\phi = 0$ and

$$n_r = \frac{a}{\sqrt{1 - kr^2}} . \quad (3.12)$$

Using this, we find that

$$K_{tt}^+ = n_{t,t} = n_{t,t} - \Gamma_{tt}^r n_r = 0 ; \quad (3.13)$$

both terms of this are zero, since $n_t = 0$ and $\Gamma_{tt}^r = 0$ for the FRW metric. Working in a similar fashion, we also find that

$$K_{+\theta}^\theta = K_{+\phi}^\phi = \frac{\sqrt{1 - kR^2}}{aR} \quad (3.14)$$

at the surface.

As seen from \mathcal{V}^- , $\Phi^- = \chi - X(t) = 0$ and $\tau = T(t)$. Therefore $n_\theta = n_\phi = 0$, $n_\chi = \dot{T}$, and $n_\tau = -\dot{X}$. Also,

$$e_t^\tau \equiv u^\tau = \dot{T} \quad (3.15)$$

and

$$e_t^\chi \equiv u^\chi = \dot{X} . \quad (3.16)$$

Working as we did before, we now find that

$$K_{-\theta}^\theta = K_{-\phi}^\phi = \frac{\dot{T}}{X} . \quad (3.17)$$

As in Ref. [45], we can find the time-time term of K most easily by noting that

$$K_{tt}^- = n_{\alpha;\beta} u^\alpha u^\beta = -n_\alpha u_{;\beta}^\alpha u^\beta = -a^\alpha n_\alpha , \quad (3.18)$$

where a^α is the acceleration of an observer comoving with the surface

$$a^\alpha = u^\beta u_{;\beta}^\alpha . \quad (3.19)$$

This means that

$$K_{tt}^- = -n_\alpha u^\beta \partial_\beta u^\alpha - \Gamma_{\mu\beta}^\alpha n_\alpha u^\beta u^\mu \quad (3.20)$$

where the second term is zero for our vacuum, since all of the needed connection coefficients vanish. The remaining term gives us

$$K_{-t}^t = n_\alpha u^\beta \partial_\beta u^\alpha = n_\alpha \frac{\partial}{\partial t} u^\alpha = \dot{T}\ddot{X} - \dot{X}\ddot{T} . \quad (3.21)$$

Therefore the two traces are

$$\begin{aligned} K_+ &= \frac{2\sqrt{1-kR^2}}{aR} \\ K_- &= \dot{T}\ddot{X} - \dot{X}\ddot{T} + \frac{2\dot{T}}{X} . \end{aligned} \quad (3.22)$$

Now we can calculate the surface stress-energy tensor of the shell at Σ . Given the symmetries of the problem, S_{ab} may be written in the form

$$S_{ab} = (\sigma + \mu) u_a u_b + \mu h_{ab} \quad (3.23)$$

where σ and μ are the 2-dimensional analogues of density and pressure, respectively. This means that $S^t_t = -\sigma$ and $S^\theta_\theta = \mu$. Using these relations, along with Eq. (3.9) and our computed extrinsic curvatures, we find

$$\begin{aligned} \sigma &= \frac{1}{4\pi} \left(\frac{\dot{T}}{X} - \frac{\sqrt{1-kR^2}}{aR} \right) \\ &= \frac{\sqrt{1+R^2\dot{a}^2} - \sqrt{1-kR^2}}{4\pi aR} \end{aligned} \quad (3.24)$$

and

$$\begin{aligned} \mu &= \frac{1}{8\pi} \left(\frac{\sqrt{1-kR^2}}{aR} - \frac{\dot{T}}{X} + \dot{X}\ddot{T} - \dot{T}\ddot{X} \right) \\ &= -\frac{\sigma}{2} + \frac{1}{8\pi} \left(\dot{X}\ddot{T} - \dot{T}\ddot{X} \right) . \end{aligned} \quad (3.25)$$

From this second relation, we can define an equation of state parameter

$$w \equiv \frac{\mu}{\sigma} = -\frac{1}{2} \left(1 + \frac{X\ddot{X}}{1 + \dot{X}^2 - \sqrt{1 + \dot{X}^2}\sqrt{1 - kR^2}} \right) \quad (3.26)$$

where we have used Eq. (3.6) to get everything in terms of $X(t)$ and its derivatives.

Things simplify if we assume that the void is much smaller than the horizon scale,

$$\dot{X}^2 = R^2\dot{a}^2 = R^2(Ha)^2 \ll 1, \quad (3.27)$$

such that, to lowest order,

$$\sqrt{1 + R^2\dot{a}^2} \approx 1 + \frac{1}{2}R^2\dot{a}^2 \quad (3.28)$$

and

$$\sqrt{1 - kR^2} \approx 1 - \frac{1}{2}kR^2. \quad (3.29)$$

Therefore, using this approximation in conjunction with the FRW relation, Eq.

(3.7), we find that

$$\sigma \approx \frac{R}{8\pi a} (\dot{a}^2 + k) = \frac{m}{4\pi a^2 R^2} \quad (3.30)$$

where we have defined the mass of the shell

$$m \equiv \frac{4\pi}{3} a^3 R^3 \rho = \text{constant} \quad (3.31)$$

which is the mass of an equivalent volume of the FRW exterior. Using the above

“small void approximation” and Eq. (3.7), the equation of state parameter be-

comes

$$w \approx -\frac{1}{2} \left(1 + \frac{2X\ddot{X}}{\dot{X}^2 + kR^2} \right) = -\frac{1}{2} \left(1 + \frac{2a\ddot{a}}{\dot{a}^2 + k} \right) = 0, \quad (3.32)$$

which means that the pressure μ is approximately zero. Therefore, if we take

uniform FRW dust and cut out a comoving sphere which is significantly smaller

than the horizon scale, then the resulting universe is a solution of general relativity

if all of the mass that was removed is smeared out in a thin shell of pressureless dust at the boundary of the sphere. This same property has been independently discovered by [42] and [43].

3.3 Motion of a Single Light Ray

In order to solve the geodesic equations, we define a cartesian coordinate system outside the shell, (t, x, y, z) , and one inside the shell, $(\tau, \bar{x}, \bar{y}, \bar{z})$, such that $z = r \cos \theta$, $x = r \sin \theta$, $\bar{z} = \chi \cos \theta$, and $\bar{x} = \chi \sin \theta$. The unit vectors in these coordinate systems are related to the aforementioned spherical polar coordinate systems' unit vectors thusly (hats denote unit vectors, and by symmetry we can restrict ourselves to the $x - z$ plane):

$$\hat{z} = \cos \theta \hat{r} - \frac{1}{r} \sin \theta \hat{\theta} , \quad (3.33)$$

$$\hat{x} = \sin \theta \hat{r} + \frac{1}{r} \cos \theta \hat{\theta} , \quad (3.34)$$

$$\hat{z} = \cos \theta \hat{\chi} - \frac{1}{\chi} \sin \theta \hat{\theta} , \quad (3.35)$$

and

$$\hat{x} = \sin \theta \hat{\chi} + \frac{1}{\chi} \cos \theta \hat{\theta} , \quad (3.36)$$

and we can reverse these relations to revert back to polar coordinates.

The metrics in the two regions match at the shell, and so we can relate the coordinates (t, r, θ, ϕ) outside to the coordinates $(\tau, \chi, \theta, \phi)$ inside by requiring that the unit normals \vec{n} and four-velocities \vec{u} also match at the shell. Outside the shell, $\vec{n} = \hat{r}/a$ and $\vec{u} = \hat{t}$, and inside, $\vec{n} = \dot{X}\hat{r} + \dot{T}\hat{\chi}$ and $\vec{u} = \dot{T}\hat{r} + \dot{X}\hat{\chi}$. Therefore

$$\hat{r} = a\dot{X}\hat{r} + a\dot{T}\hat{\chi} \quad (3.37)$$

and

$$\hat{t} = \dot{T}\hat{\tau} + \dot{X}\hat{\chi} . \quad (3.38)$$

The procedure for this calculation is basically a series of coordinate changes. We start with the incident ray, which we will choose to be traveling in the negative z direction,

$$\vec{k}_i = k_0 \left(\hat{t} - \frac{1}{a_1} \hat{z} \right) , \quad (3.39)$$

where a subscript “1” denotes quantities that are evaluated at the initial time of impact of the light ray with the shell, t_1 . We then transform to spherical polar coordinates (t, r, θ, ϕ) , calling the angle of initial encounter θ_1 . The void is centered at $r = 0$ and ϕ is set to zero for the entire calculation. Then, we propagate the ray through the shell by keeping \vec{k} constant and transforming to the inside polar coordinates $(\tau, \chi, \theta, \phi)$, and then we transform to the cartesian coordinates $(\tau, \bar{x}, \bar{y}, \bar{z})$ to make the null geodesic equation trivial: $\vec{k} = \text{constant}$. At the second shell encounter, we transform back to polar coordinates $(\tau, \chi, \theta, \phi)$, where now the time is t_2 , the scale factor is a_2 and the angle of this second shell impact is θ_2 , which will not in general equal $\pi - \theta_1$. A subscript “2” denotes quantities that are evaluated at the time t_2 . The light ray then crosses the shell again and we transform back $(\tau, \chi, \theta, \phi) \rightarrow (t, r, \theta, \phi)$. Finally, we convert back to cartesian coordinates (t, x, y, z) and compare the result with the unperturbed ray, what we would have if the ray had just gone through FRW instead of the shell and void:

$$\vec{k}_{FRW} = \frac{a_1 k_0}{a_2} \left(\hat{t} - \frac{1}{a_2} \hat{z} \right) , \quad (3.40)$$

and find the redshift and deflection angle.

After the first half of the trip, we find the 4-momentum inside the void to be

$$\vec{k} = k_0 (A_1 \hat{t} + B_1 \hat{x} + C_1 \hat{z}) \quad (3.41)$$

where

$$A_1 = \dot{T}_1 - \cos \theta_1 \dot{X}_1, \quad (3.42)$$

$$B_1 = \dot{X}_1 \sin \theta_1 - \dot{T}_1 \sin \theta_1 \cos \theta_1 + \sin \theta_1 \cos \theta_1, \quad (3.43)$$

and

$$C_1 = \dot{X}_1 \cos \theta_1 - \dot{T}_1 \cos^2 \theta_1 - \sin^2 \theta_1. \quad (3.44)$$

For the second half of the trip, if we start with \vec{k} in the form of Eq. (3.41), we find the final 4-momentum to be

$$\vec{k}_e = k_0 (A_2 \hat{t} + B_2 \hat{x} + C_2 \hat{z}) \quad (3.45)$$

where

$$A_2 = A_1 \dot{T}_2 - \dot{X}_2 (B_1 \sin \theta_2 + C_1 \cos \theta_2), \quad (3.46)$$

$$B_2 = \frac{1}{a_2} \left[-A_1 \dot{X}_2 \sin \theta_2 + B_1 \left(\dot{T}_2 \sin^2 \theta_2 + \cos^2 \theta_2 \right) + C_1 \sin \theta_2 \cos \theta_2 \left(\dot{T}_2 - 1 \right) \right], \quad (3.47)$$

and

$$C_2 = \frac{1}{a_2} \left[-A_1 \dot{X}_2 \cos \theta_2 + B_1 \sin \theta_2 \cos \theta_2 \left(\dot{T}_2 - 1 \right) + C_1 \left(\dot{T}_2 \cos^2 \theta_2 + \sin^2 \theta_2 \right) \right]. \quad (3.48)$$

This is the exact result, which we will approximate in the following subsections by expanding in powers of aHR .

3.3.1 First Order Results

To first order in aHR , the equations above for A_2 , B_2 , and C_2 simplify to give the exiting ray 4-momentum

$$\begin{aligned} \vec{k}_e = & k_0 \left[\left(1 - \dot{X}_1 \cos \theta_1 + \dot{X}_2 \cos \theta_2 \right) \hat{t} + \frac{1}{a_2} \left(\dot{X}_1 \sin \theta_1 - \dot{X}_2 \sin \theta_2 \right) \hat{x} \right. \\ & \left. - \frac{1}{a_2} \left(1 - \dot{X}_1 \cos \theta_1 + \dot{X}_2 \cos \theta_2 \right) \hat{z} \right] + \mathcal{O} \left(\dot{X}^2 \right) . \end{aligned} \quad (3.49)$$

We would like to get our answer in Eq. (3.45) in terms of only k_0 , θ_1 , and $a_1 H_1 R$.

First, we can Taylor expand $X(t)$ around t_1 :

$$X(t) = X_1 + \dot{X}_1 \delta t + \mathcal{O} \left(\dot{X}_1^2 \right) , \quad (3.50)$$

where $\delta t \equiv t_2 - t_1$, and so $\dot{X}_1 = \dot{X}_2$ in Eq. (3.49) to the desired accuracy. Second, in the “outside cartesian” coordinates (t, x, y, z) , the distance traveled during the journey described above in the x and z directions are

$$\Delta x = R \sin \theta_2 - R \sin \theta_1 \quad (3.51)$$

and

$$\Delta z = R \cos \theta_2 - R \cos \theta_1 , \quad (3.52)$$

respectively. Inside the void, the path is a straight line, and so we can say that

$$\frac{\Delta x}{\Delta z} = \frac{dx}{dz} = \frac{dx/d\lambda}{dz/d\lambda} = \frac{(dx/d\bar{x}) k^{\bar{x}}}{(dz/d\bar{z}) k^{\bar{z}}} = \frac{k^{\bar{x}}}{k^{\bar{z}}} \quad (3.53)$$

where λ is an affine parameter describing the ray in the void, and $dx/d\bar{x} = dz/d\bar{z}$ due to symmetry. Plugging in the results of Eqs. (3.41) through (3.44), we find

$$\frac{\Delta x}{\Delta z} = \frac{\dot{X}_1 \sin \theta_1}{\dot{X}_1 \cos \theta_1 - 1} = -\dot{X}_1 \sin \theta_1 + \mathcal{O} \left(\dot{X}_1^2 \right) \quad (3.54)$$

and so, to first order,

$$\frac{\sin \theta_2 - \sin \theta_1}{\cos \theta_1 - \cos \theta_2} = \dot{X}_1 \sin \theta_1 . \quad (3.55)$$

Defining $\epsilon \equiv \dot{X}_1 \approx \dot{X}_2$ and $\Delta \equiv \cos \theta_1 - \cos \theta_2$, and taking everything to first order in ϵ , the exiting ray four-momentum is

$$\vec{k}_e = k_0 \left[(1 - \epsilon \Delta) \hat{t} + \mathcal{O}(\epsilon^2 \Delta) \hat{x} - \frac{1}{a_2} (1 - \epsilon \Delta) \hat{z} \right] + \mathcal{O}(\epsilon^2) \quad (3.56)$$

and so, since Δ is of order one (we will find Δ in the next paragraph), a net direction change of the ray does not happen at first order.

Equation (3.55) is most easily approximated if θ_2 is expanded like so

$$\theta_2 = (\pi - \theta_1) - \delta\theta \quad (3.57)$$

where $\delta\theta = 0$ if there is no Hubble expansion. Then,

$$\cos \theta_2 = -\cos \theta_1 \cos \delta\theta + \sin \theta_1 \sin \delta\theta \quad (3.58)$$

and

$$\sin \theta_2 = \sin \theta_1 \cos \delta\theta + \cos \theta_1 \sin \delta\theta , \quad (3.59)$$

so that

$$\Delta = \cos \theta_1 + \cos \theta_1 \cos \delta\theta - \sin \theta_1 \sin \delta\theta = 2 \cos \theta_1 + \mathcal{O}(\delta\theta) . \quad (3.60)$$

Plugging all of this information into Eq. (3.55), we find that

$$\delta\theta = 2\epsilon \sin \theta_1 + \mathcal{O}(\epsilon^2) , \quad (3.61)$$

$$\Delta = 2 \cos \theta_1 + \mathcal{O}(\epsilon) , \quad (3.62)$$

and therefore,

$$\vec{k}_e = k_0 \left[(1 - 2\epsilon \cos \theta_1) \hat{t} - \frac{1}{a_2} (1 - 2\epsilon \cos \theta_1) \hat{z} \right] + \mathcal{O}(\epsilon^2) . \quad (3.63)$$

This should be compared with the four-momentum of the unperturbed ray that we find from Eq. (3.40), noting that

$$\delta t = 2X_1 \cos \theta_1 + \mathcal{O}(X_1 \epsilon) \quad (3.64)$$

and so

$$\frac{a_1}{a_2} = \frac{X_1}{X_2} \approx \frac{X_1}{X_1 + \dot{X}_1 \delta t} \approx 1 - 2\epsilon \cos \theta_1 + \mathcal{O}(\epsilon^2) . \quad (3.65)$$

So at first order there is no effect on the frequency, with respect to what would happen in an FRW model, and there is no net direction change, as $\vec{k}_e = \vec{k}_{FRW}$.

3.3.2 Second Order Results

To second order in $\dot{X} = aHR$, we find the exiting ray to have the 4-momentum

$$\begin{aligned} \frac{\vec{k}_e}{k_0} = & \left[1 - \dot{X}_1 \cos \theta_1 + \dot{X}_2 \cos \theta_2 + \frac{1}{2} (\dot{X}_1^2 + \dot{X}_2^2) \right. \\ & \left. - \dot{X}_1 \dot{X}_2 (\cos \theta_1 \cos \theta_2 + \sin \theta_1 \sin \theta_2) \right] \hat{t} \\ & + \frac{1}{a_2} \left[\dot{X}_1 \sin \theta_1 - \dot{X}_2 \sin \theta_2 - \frac{1}{2} (\dot{X}_1^2 \sin \theta_1 \cos \theta_1 + \dot{X}_2^2 \sin \theta_2 \cos \theta_2) \right. \\ & \left. + \dot{X}_1 \dot{X}_2 \cos \theta_1 \sin \theta_2 \right] \hat{x} \\ & + \frac{1}{a_2} \left[-1 + \dot{X}_1 \cos \theta_1 - \dot{X}_2 \cos \theta_2 - \frac{1}{2} (\dot{X}_2^2 \cos^2 \theta_2 + \dot{X}_1^2 \cos^2 \theta_1) \right. \\ & \left. + \dot{X}_1 \dot{X}_2 \cos \theta_1 \cos \theta_2 \right] \hat{z} + \mathcal{O}(\epsilon^3) . \quad (3.66) \end{aligned}$$

We can phase this in terms of $\epsilon = \dot{X}_1 = a_1 H_1 R$ and θ_1 by first expanding \dot{X}_2 around t_1 , as before. Assuming a flat external cosmology ($k = 0$) and then noting that $\ddot{a}_1 = -\dot{a}_1^2/2a$, we find

$$\dot{X}_2 = \dot{X}_1 + \ddot{X}_1 \delta t + \mathcal{O}(\dot{X}_1^3) = \dot{X}_1 - \dot{X}_1^2 \frac{\delta t}{2X_1} = \dot{X} - \dot{X}_1^2 \cos \theta_1 + \mathcal{O}(\epsilon^3) . \quad (3.67)$$

We also need to find $\cos \theta_2$ and $\sin \theta_2$ in terms of θ_1 , using Eqs. (3.58), (3.59), and (3.61):

$$\cos \theta_2 = -\cos \theta_1 + 2\epsilon \sin^2 \theta_1 + \mathcal{O}(\epsilon^2) \quad (3.68)$$

and

$$\sin \theta_2 = \sin \theta_1 + 2\epsilon \sin \theta_1 \cos \theta_1 + \mathcal{O}(\epsilon^2) . \quad (3.69)$$

Then we find that the x -component k^x is still zero, and

$$\begin{aligned} \vec{k}_e = k_0 & \left\{ [1 - 2\epsilon \cos \theta_1 + \epsilon^2 (\cos^2 \theta_1 + 2)] \hat{t} \right. \\ & \left. - \frac{1}{a_2} [1 - 2\epsilon \cos \theta_1 + \epsilon^2 (\cos^2 \theta_1 + 2)] \hat{z} \right\} \\ & + \mathcal{O}(\epsilon^3) \end{aligned} \quad (3.70)$$

which is also equal to \vec{k}_{FRW} , since

$$\frac{a_1}{a_2} \approx \frac{X_1}{X_1 + \dot{X}_1 \delta t + \ddot{X}_1 \delta t^2 / 2} \approx 1 - 2\epsilon \cos \theta_1 + \epsilon^2 (\cos^2 \theta_1 + 2) , \quad (3.71)$$

where we have used the expansion

$$\delta t = X_1 [2 \cos \theta_1 + \epsilon (\sin^2 \theta_1 - \cos^2 \theta_1) + \mathcal{O}(\epsilon^2)] \quad (3.72)$$

that came from integrating

$$\int_{t_1}^{t_2} \frac{dt}{a} = \int_{z_1}^{z_2} dz \sqrt{1 + \left(\frac{\Delta x}{\Delta z}\right)^2} = \Delta z \sqrt{1 + \left(\frac{k^{\bar{x}}}{k^{\bar{z}}}\right)^2} . \quad (3.73)$$

As such, we find that there is still no difference between the exiting ray four-momentum and that of an unperturbed ray at second order, and thus the redshifts will be the same.

The second order effects on \vec{k} that we would expect are a possible gravitational redshift, and the first and second order Doppler shift. Firstly, the Newtonian

potential at a time t outside a mass m shell, i.e. for $r > R$, is

$$\phi(r, t) = -\frac{Gm(t)}{a(t)r} = -\frac{4\pi G a^3(t) R^3 \rho(t)/3}{ar} = -\frac{R}{2r} \dot{X}^2 . \quad (3.74)$$

But since $\dot{X}_1^2 = \dot{X}_2^2$ at this order, this means that ϕ is not a function of time, i.e. it is a static potential well. Therefore, when a photon falls into the well and then climbs back out, it receives no net frequency shift from it. So the only effect is the Doppler shift, which, to second order, accounts for the answer that we found in Eq. (3.70).

At this order, we would expect to have an extra focusing, due to the x direction shift of the photon trajectory:

$$x \rightarrow x' = x + \Delta x = x [1 + 2\epsilon \cos \theta_1] = x \left[1 + 2\epsilon \sqrt{1 - \frac{x^2}{R^2}} \right] . \quad (3.75)$$

More generally, if a photon travels to the void along the z direction, then the impact parameter \vec{b} will be in the $x - y$ plane, and the resulting deflection (in units of horizon size $(aH)^{-1}$) will be

$$\vec{\alpha} = 2\epsilon^2 \vec{u} \sqrt{1 - u^2} , \quad (3.76)$$

where we have defined the rescaled impact parameter $\vec{u} \equiv \vec{b}/R$ and $u \equiv |\vec{u}|$.

3.4 Effect on the Luminosity Distance

In this section we will only look at the effects of these voids and sheets up to second order in ϵ , where $\epsilon \sim 10^{-2}$. Since the exiting 4-momentum is the same as we would have for an FRW model, the redshift of sources is unaltered and we only have to worry about any extra focusing that might occur.

Given the deflection from Eq. (3.76), we can use the procedure outlined in [46] to find the magnification tensor μ to be

$$\mu_{ij} = \delta_{ij} + \frac{\partial \alpha_i}{\partial u_j} . \quad (3.77)$$

Then the magnification M is the absolute value of the determinant of this, namely

$$M(u) = 1 + 2\epsilon^2 \left(\frac{2 - 3u^2}{\sqrt{1 - u^2}} \right) . \quad (3.78)$$

This means that the apparent luminosity is changed by a factor of M .

3.4.1 Mean Effect

The average of M over impact parameters is

$$\langle M \rangle = \int_0^1 M(u) u du = 1 \quad (3.79)$$

and so there is no focusing on average. Indeed, it is already known that the average amplification due to weak lensing is zero [47, 48, 49, 50]. We can understand this result by way of a few simple arguments.

First, consider a spherically-symmetric matter distribution with a total radius R , a total mass M , and a radius-dependent density $\rho(r)$. Let us further say that a small beam comes in from the z direction and then encounters this sphere with an impact parameter b , which will then be in the $x - y$ plane. The convergence of the beam is proportional to the integrated column density along the beam's unperturbed path, which is defined to be

$$\Sigma \equiv \int_{path} \rho[r(\lambda)] d\lambda \quad (3.80)$$

(not to be confused with our earlier use of Σ), where the path depends on b , and λ is the affine parameter of a central ray. Since we are using the unperturbed path for this, it is clear that we do the above integral along a straight line, parallel to the z axis. Then the total mass of the spherical distribution comes from integrating Σ over the remaining two spatial axes, the x and the y :

$$\begin{aligned}\mathcal{M} &= \int_{all\ space} \rho(r) dV = \int_{all\ space} \rho(r) dx dy dz \\ &= \int_{x-y\ plane} \Sigma [b(x, y)] dx dy = \int_0^R \Sigma(r) 2\pi r dr\end{aligned}\quad (3.81)$$

The average focusing is proportional to the average of the integrated column density over impact parameters,

$$\begin{aligned}\langle \Sigma \rangle &= \frac{1}{R^2} \int_0^R \Sigma(b) \times b db = \frac{1}{R^2} \int_0^R \Sigma(r) r dr \\ &= \frac{1}{R^2} \left(\frac{\mathcal{M}}{2\pi} \right) = \frac{\mathcal{M}}{2\pi R^2}\end{aligned}\quad (3.82)$$

which only depends on total mass and size, and not on how the mass is distributed.

For example, a delta-function shell of mass \mathcal{M} and a radius R has

$$\Sigma \equiv \Sigma_B = \langle \Sigma_B \rangle = \left(\frac{\mathcal{M}}{4\pi R^2} \right) \times 2 = \frac{\mathcal{M}}{2\pi R^2}\quad (3.83)$$

and a ball of the FRW exterior with the same mass and total size has

$$\Sigma \equiv \Sigma_{FRW} = \frac{\mathcal{M}}{4\pi R^3/3} \times 2R \sqrt{1 - \frac{b^2}{R^2}}\quad (3.84)$$

where the average of $\sqrt{1 - b^2/R^2}$ is $1/3$, and therefore

$$\langle \Sigma_{FRW} \rangle = \frac{\mathcal{M}}{2\pi R^2}.\quad (3.85)$$

Thus we see that removing a sphere of FRW and replacing it with a mass-compensating shell, as we did above in our void model, will not affect focusing on average.

This claim that there is no systematic magnification offset holds not just for spherically-symmetric lenses, but in fact it is true whenever the lensing can be considered “weak”, i.e. in the Newtonian limit. Again, in the weak lensing formalism, the convergence κ depends on the surface density Σ

$$\kappa \propto \Sigma = \int_{-\infty}^{\infty} \rho dz \quad (3.86)$$

and if we average this over viewing angles, we find

$$\langle \kappa \rangle \propto \left\langle \int_{-\infty}^{\infty} \rho dz \right\rangle = \int_{-\infty}^{\infty} \langle \rho \rangle dz . \quad (3.87)$$

This is the same as the FRW result.

3.4.2 Variance Estimate

Now we will find the variance in the magnification M . Assuming a very large sample size, this is

$$\begin{aligned} \sigma_M^2 &= \langle (M - \langle M \rangle)^2 \rangle = 4\epsilon^4 \left\langle \left(\frac{2 - 3u^2}{\sqrt{1 - u^2}} \right)^2 \right\rangle \\ &= 4\epsilon^4 \int_0^1 \left(\frac{2 - 3u^2}{\sqrt{1 - u^2}} \right)^2 u du , \end{aligned} \quad (3.88)$$

which diverges logarithmically as $u \rightarrow 1$. This will not be a problem in practice, as an impact parameter of exactly $u = 1$ will never naturally occur. We can impose a cutoff to our integral,

$$I(\delta) = \int_0^{1-\delta} \left(\frac{2 - 3u^2}{\sqrt{1 - u^2}} \right)^2 u du = \frac{1}{4} \left[\ln \left(\frac{1}{4\delta^2} \right) - 3 \right] , \quad (3.89)$$

where δ corresponds to the ratio of the shell thickness to the void size, and $\delta \ll 1$.

If $\delta = 0.01$, then $I \approx 1.3$, and if $\delta = 10^{-4}$, then $I \approx 3.5$. Therefore, for $\epsilon \sim 10^{-2}$,

we can make the order of magnitude estimate

$$\sigma_M^2 = 4\epsilon^4 \times (\text{a few}) \sim 10^{-7} \quad (3.90)$$

and the standard deviation is the square root of this:

$$\sigma_M \sim 3 \times 10^{-4} . \quad (3.91)$$

This corresponds to an error σ_m in the apparent magnitude:

$$\sigma_m \approx (1.086 \text{ mag}) \sigma_M \sim 3 \times 10^{-4} \text{ mag} , \quad (3.92)$$

which is several orders of magnitude smaller than the intrinsic spread in the magnitudes of Type Ia supernovae, $\sigma \approx 0.2 \text{ mag}$.

3.5 Conclusions

We have constructed a model for cosmological voids and sheets by removing spherical regions of matter from a matter dominated FRW universe, and then spreading this matter into a thin shell at the void-FRW interface. In Section 3.2, we demonstrated that this model is a valid solution to general relativity.

In this model, we have found that a single light ray experiences no net redshift change with respect to what it would experience in an FRW model. However, there is a net deflection which leads to an impact parameter dependent amplification, given by Eq. (3.78). Averaging this magnification over impact parameters, we found that on average there is no effect on measured apparent luminosities. This means that, in the limit of very large sample sizes, the luminosity distance-redshift relation will be the same in this model as it would be in the corresponding homogeneous model. We have also computed the variance in the magnification due to

these inhomogeneities: $\sigma_M^2 \sim 10^{-7}$. This leads to an extra error in the apparent magnitude, which we found to be $\sigma_m \sim 3 \times 10^{-4}$ mag. This is much smaller than the intrinsic error in the observed magnitudes of Type Ia supernovae, $\sigma \approx 0.2$ mag. Therefore, within the confines of this model, the effect of inhomogeneity on supernova data is negligible.

Chapter 4

Systematic Effects in General Three

Dimensional Models[†]

4.1 Introduction

Our goal in this chapter is to calculate the lowest order fitting effect by calculating the cosmological constant density Ω_Λ that one would deduce from a perturbed luminosity distance-redshift relation $D_L(z)$, in full three dimensional generality. If we treat cosmological fluctuations perturbatively and as a random process as suggested by the “fair sample hypothesis” [33], then this fitting effect should be fundamentally nonlinear in the density contrast $\delta = (\rho - \langle\rho\rangle)/\langle\rho\rangle$, requiring that we work to at least second order in δ . This is because the ensemble averages of first order quantities vanish. We model observations out to some moderate redshift $z_{max} \sim 0.1 \ll 1$. Within the corresponding comoving spherical region, the Hubble flow velocity v_H is bounded above by

$$\frac{v_H}{c} \lesssim z_{max} \sim 0.1 , \quad (4.1)$$

allowing us to use post-Newtonian expansions. There are two different velocity scales that occur, the Hubble flow velocity v_H and the peculiar velocity v_p . The corresponding dimensionless small parameters are

$$\varepsilon_H = \frac{v_H}{c} \sim \frac{H_0 r}{c} \lesssim z_{max} \sim 0.1 \quad (4.2)$$

[†]This chapter is published in Vanderveld, Flanagan, and Wasserman (2007).

and

$$\varepsilon_p = \frac{v_p}{c} \sim \delta \left(\frac{H_0 \lambda_c}{c} \right), \quad (4.3)$$

where $\lambda_c \sim 10$ Mpc is the wavelength of the dominant perturbation mode. In our computation, we will treat both of these parameters as being of formally the same order, and we will denote both by “ ε ” for book keeping purposes. At the end of our computation we can identify terms that scale as $\varepsilon_H^n \varepsilon_p^m$ for different values of m and n . As mentioned above, we also expand separately in the fractional density perturbation δ . We will compute redshifts $z(\lambda)$ and luminosity distances $H_0 D_L(\lambda)$ as functions of the affine parameter λ to third order in ε and to second order in δ . Combining these results to eliminate λ will yield D_L as a function of z .

Using this expansion method, we find that the lowest order inhomogeneity-induced correction to the luminosity distance scales as $|\Delta D_L|/D_L \sim \delta^2 (H_0 \lambda_c / c) \sim 10^{-5}$. We then fit this relation to what one would expect from a homogeneous cosmological model which contains dust with a density Ω_M and a cosmological constant with a density Ω_Λ ,

$$D_L(z) = \frac{1+z}{H_0 \sqrt{|1-\Omega_M-\Omega_\Lambda|}} \mathcal{F} \left[H_0 \sqrt{|1-\Omega_M-\Omega_\Lambda|} \int_0^z \frac{dz'}{H(z')} \right], \quad (4.4)$$

where

$$H(z) = H_0 \sqrt{\Omega_M (1+z')^3 + (1-\Omega_M-\Omega_\Lambda) (1+z')^2 + \Omega_\Lambda}, \quad (4.5)$$

by maximizing a likelihood function. Here $\mathcal{F}(u) = u$ for a flat universe, $\mathcal{F}(u) = \sinh(u)$ for an open universe, and $\mathcal{F}(u) = \sin(u)$ for a closed universe. We find that the result for the cosmological constant density is dependent on the size of the redshift range for which we have supernova data. These results are summarized in Figure 4.1. For data from $z_{min} = 0.02$ out to a limiting redshift $z_{max} = 0.15$, we find that the best-fit cosmological constant density is $\Omega_\Lambda \approx 0.004$, and Ω_Λ tends to get

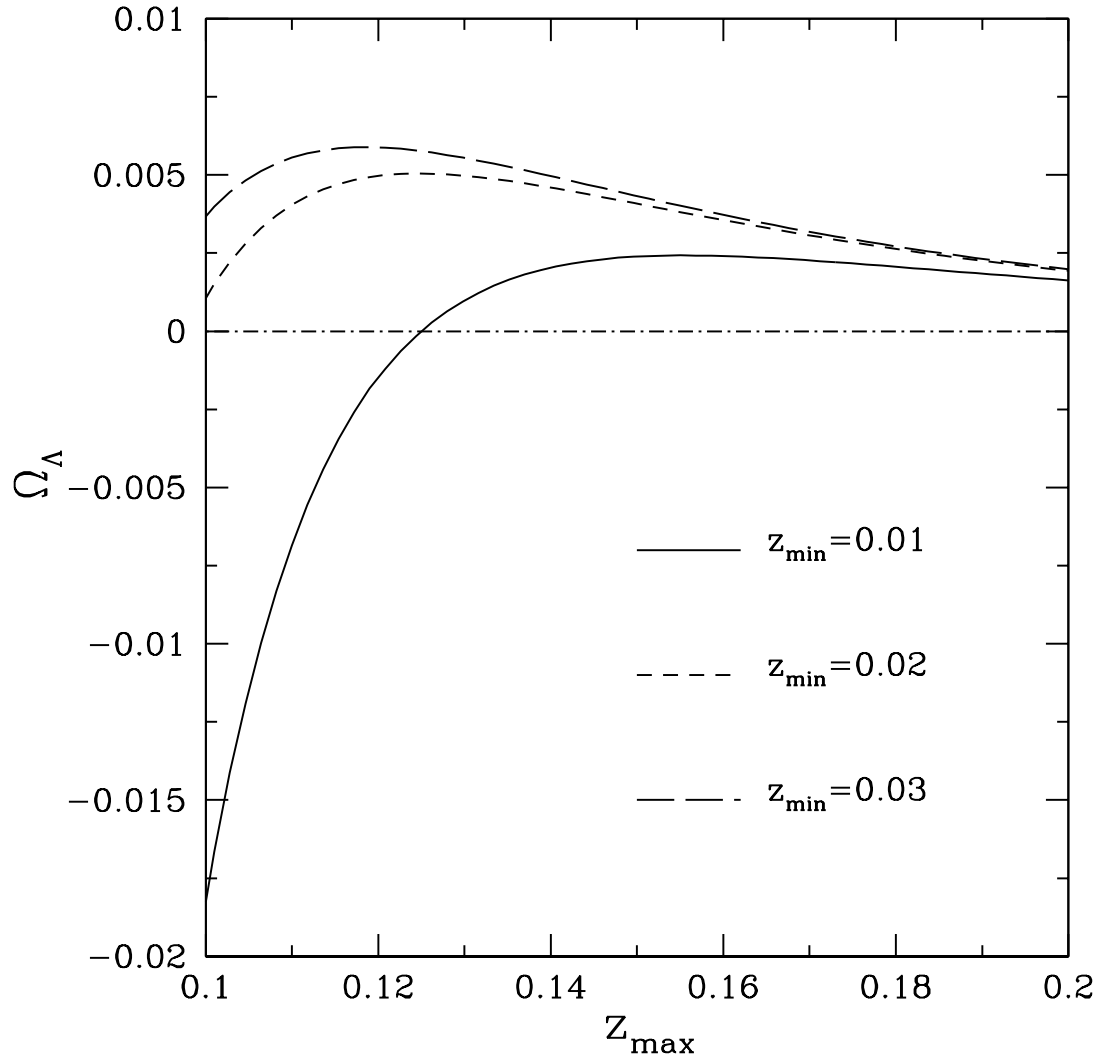


Figure 4.1: The best-fit cosmological constant density Ω_{Λ} plotted as a function of the maximum redshift z_{\max} , for the choices $z_{\min} = 0.01, 0.02,$ and 0.03 . The horizontal dash-dot line shows the actual model value $\Omega_{\Lambda} = 0$.

larger as z_{max} gets smaller. The best-fit $|\Omega_\Lambda|$ also becomes larger as z_{min} becomes smaller, since $|\Delta D_L|/D_L$ becomes large on small scales. Although this ensemble averaged result is still quite small, we find that the variance can be $\sigma_\Lambda^2 \sim 1$ for a sample of 100 supernovae out to a redshift $z_{max} \sim 0.2$. One implication of these results is that precision measurements of the cosmological constant from nearby supernova data require that we measure $D_L(z)$ over a large enough redshift range, with a large enough sample. One could also try to correct for some of the effects of inhomogeneity, using available information about large scale structure and about our own peculiar velocity [51, 52].

The analysis presented here is more realistic than similar analyses within the context of simplified models of structure formation, such as the spherically symmetric Lemaître-Tolman-Bondi (LTB) models [20, 30, 31, 53], Swiss cheese models [40] and their variants [54, 55, 56, 57]. This is because we look at the full three dimensional problem, and assume that there are no bulk flows on cosmological length scales. There have also been analyses of the perturbations to the luminosity distance-redshift relation that go to Newtonian order [49, 50, 58], that only consider superhorizon perturbation modes [26, 27], and that use Taylor expansions of the luminosity distance [59], which are most appropriate for long-wavelength perturbations. In contrast, we go to post-Newtonian order, we only consider subhorizon modes, and we fit to FRW models, so that we may fully address the “fitting problem”.

Our analysis is also fundamentally different from those in Refs. [10, 11, 13, 14, 60, 61], as we choose a different method for obtaining averaged expansion parameters. These authors average the expansion rate over a constant time slice, whereas

we choose to calculate only observable quantities, namely the luminosity distance and the redshift, along the past light cone of the observer. We then combine these expressions into $D_L(z, \theta, \phi)$, average over viewing angles and ensemble average, and then fit the results to what one would expect in a homogeneous model containing dust and a cosmological constant to find the best-fit value for Ω_Λ . This approach better simulates the process of gathering and analyzing supernova data, and it leads to a different result with a stable perturbative expansion.

Refs. [10, 11, 13, 14] base their characterization of the expansion rate of the Universe on quantities that are not related to how observers have deduced the existence of dark energy. In these papers, perturbations are spatially averaged over a constant time slice. Such a spatial average is somewhat arbitrary, as it is dependent on the choice of spatial hypersurface. This is in contrast to the observable significance of $D_L(z)$. Refs. [10, 11, 14] also use the synchronous gauge for their calculations, wherein there are metric perturbations of order δ . Since $\delta \gtrsim 1$ on small scales, this gauge is particularly ill suited to perturbation theory. In contrast, in Newtonian-type gauges the metric perturbation is of order $\delta(H_0\lambda_c/c)^2 \ll \delta$. We explore this difference in Section 4.6.

The organization of this chapter is as follows: In Section 4.2 below, we introduce our coordinate choice, wherein we recast the Friedmann-Robertson-Walker (FRW) metric as an expansion around flat space, and in Section 4.3 we present the fundamental post-Newtonian optics equations that we will need for this calculation. We then explain our method of computation and calculate the necessary unperturbed quantities in Section 4.4. Here we also compute the luminosity distances and redshifts for a perturbed matter dominated universe, finding z and

$H_0 D_L$ to second order in δ and to third order in ε , and we find that we may write the lowest order correction to $D_L(z)$ in terms of the peculiar velocity field. We then fit to a homogeneous model in Section 4.5 to find the best-fit Ω_Λ and its variance. The detailed redshift and luminosity distance equations are in Appendix A.1, the necessary results of second order perturbation theory are reviewed in Appendix A.2, and the averaging is discussed in Appendix A.3. Then, in Section 4.6 we discuss the previous results in the synchronous gauge and show that one can choose coordinates and a definition of “acceleration” such that it appears as though there could be a larger fitting effect. We argue that such a result would be unphysical. A detailed discussion of transforming to synchronous coordinates is given in Appendix A.4. Finally, in Section 4.7 we make our concluding remarks. As usual, Greek indices will be summed over all four spacetime dimensions while Latin indices will be summed only over the three spatial dimensions. We will also write 3-vectors in boldface and put arrows over 4-vectors.

4.2 Post-Newtonian Expansion of the Local FRW Metric

In general, certain coordinate choices allow us to conveniently recast the local metric as an expansion around flat space, as was first emphasized for the FRW metric by Peebles [62]. We will take advantage of such an expansion so that we may use the standard post-Newtonian formalism for this calculation. Starting with the usual FRW metric with $c = G = 1$,

$$ds^2 = -d\tau^2 + a^2(\tau) (d\chi^2 + \chi^2 d\Omega^2) , \quad (4.6)$$

we can define the new radial coordinate

$$\tilde{r} = a(\tau)\chi \quad (4.7)$$

so that the line element becomes

$$ds^2 = - (1 - H^2\tilde{r}^2) d\tau^2 - 2H\tilde{r}d\tau d\tilde{r} + d\tilde{r}^2 + \tilde{r}^2 d\Omega^2, \quad (4.8)$$

where the Hubble parameter of a flat and dust-dominated FRW universe is $H(\tau) = (1/a)(da/d\tau) = 2/3\tau$; we will specialize to this case for the remainder of this chapter. Now we change coordinates to the standard post-Newtonian gauge. In this gauge, the metric to first post-Newtonian order can be written as

$$ds^2 = g_{\mu\nu}dx^\mu dx^\nu = - (1 + 2\Phi + 2\Phi^2) dt^2 + 2\zeta_i dx^i dt + (1 - 2\Phi) \gamma_{ij} dx^i dx^j, \quad (4.9)$$

where γ_{ij} is a flat spatial metric, the potential Φ contains both Newtonian and post-Newtonian pieces, ζ_i is the usual gravitomagnetic potential, and

$$3\dot{\Phi} + \nabla \cdot \zeta = 0 \quad (4.10)$$

is the gauge condition. Achieving this form for the metric entails transforming from τ and \tilde{r} to t and r , defined by

$$\tau = t \left[1 - \frac{r^2}{3t^2} - \frac{r^4}{30t^4} + O\left(\frac{r^6}{t^6}\right) \right] \quad (4.11)$$

and

$$\tilde{r} = r \left[1 - \frac{r^2}{9t^2} + O\left(\frac{r^4}{t^4}\right) \right]. \quad (4.12)$$

Then the line element becomes

$$\begin{aligned} ds^2 = & - \left[1 + \frac{2r^2}{9t^2} + \frac{46r^4}{405t^4} + O\left(\frac{r^6}{t^6}\right) \right] dt^2 + \left[\frac{4r^3}{15t^3} + O\left(\frac{r^5}{t^5}\right) \right] dr dt \\ & + \left[1 - \frac{2r^2}{9t^2} + O\left(\frac{r^4}{t^4}\right) \right] (dr^2 + r^2 d\Omega^2) \end{aligned} \quad (4.13)$$

to the necessary order in r . This metric is of the post-Newtonian form (4.9) if we define

$$\Phi_{(0)} = \frac{r^2}{9t^2} + \frac{2r^4}{45t^4} \quad (4.14)$$

and

$$\zeta_{r(0)} = \frac{2r^3}{15t^3} . \quad (4.15)$$

Here subscripts “(0)” denote unperturbed, background quantities; we will add cosmological perturbations in subsequent sections. The unperturbed density in the new coordinates is

$$\rho_{(0)} = \frac{1}{6\pi t^2} \left[1 + \frac{2r^2}{3t^2} + O\left(\frac{r^4}{t^4}\right) \right] , \quad (4.16)$$

and the continuity equation tells us that the unperturbed 3-velocity must be of the form $\mathbf{v}_{(0)} = v_{(0)}\partial/\partial r$, where

$$v_{(0)} = \frac{2r}{3t} \left[1 + \frac{r^2}{9t^2} + O\left(\frac{r^4}{t^4}\right) \right] , \quad (4.17)$$

and where $v_{(0)} = dr/dt$. Thus, we see that counting orders of $\varepsilon \sim v/c$ is equivalent to counting orders of r/t in these coordinates. Our coordinate choice and expansion method also have the consequence that the analysis of this chapter is only valid for small redshifts.

In general in the standard post-Newtonian gauge, the connection coefficients are

$$\Gamma_{tt}^t = \dot{\Phi} , \quad (4.18)$$

$$\Gamma_{ti}^t = \Phi_{,i} , \quad (4.19)$$

$$\Gamma_{ij}^t = -\dot{\Phi}\gamma_{ij} - \zeta_{(i|j)} , \quad (4.20)$$

$$\Gamma_{tt}^i = \gamma^{ij}\Phi_{,j} , \quad (4.21)$$

$$\Gamma_{tj}^i = -\dot{\Phi}\delta_j^i + \gamma^{ik}\zeta_{[k|j]} , \quad (4.22)$$

and

$$\Gamma_{jk}^i = \tilde{\Gamma}_{jk}^i - \Phi_{,k}\delta_j^i - \Phi_{,j}\delta_k^i + \Phi_{,l}\gamma^{il}\gamma_{jk} , \quad (4.23)$$

to the necessary order in ε , where $\tilde{\Gamma}_{jk}^i$ is the connection associated with the flat spatial metric γ_{ij} , which we will choose to be that of standard spherical coordinates (r, θ, ϕ) , as in Ref. [63]. Vertical bars represent covariant derivatives with respect to γ_{ij} . We will also need the Ricci tensor components

$$R_{tt} = \nabla^2\Phi \quad (4.24)$$

and

$$R_{ij} = \nabla^2\Phi\delta_{ij} . \quad (4.25)$$

Furthermore, the first post-Newtonian hydrodynamic and Einstein equations are

$$\frac{\partial}{\partial t} \left[\rho \left(1 + \frac{v^2}{2} - 3\Phi \right) \right] + \nabla \cdot \left[\rho \left(1 + \frac{v^2}{2} - 3\Phi \right) \mathbf{v} \right] = 0 , \quad (4.26)$$

$$\begin{aligned} \frac{\partial \vec{v}}{\partial t} + \left(\vec{v} \cdot \vec{\nabla} \right) \vec{v} &= -\vec{\nabla} (\Phi + 2\Phi^2) - \dot{\zeta} - \left(\vec{\zeta} \times \vec{\nabla} \right) \times \vec{v} + 3\dot{\Phi}\vec{v} \\ &\quad + 4\vec{v} \left(\vec{v} \cdot \vec{\nabla} \right) \Phi - v^2 \vec{\nabla} \Phi , \end{aligned} \quad (4.27)$$

$$\nabla^2\Phi = 4\pi\rho (1 + 2v^2 - 2\Phi) , \quad (4.28)$$

and

$$\nabla^2\zeta = 16\pi\rho\mathbf{v} + \nabla\dot{\Phi} , \quad (4.29)$$

in this gauge. The 3-velocity \mathbf{v} is related to the 4-velocity \vec{u} of the fluid by

$$\vec{u} = (u^t, u^i) \equiv \gamma (1, v^i) , \quad (4.30)$$

where demanding that $\vec{u} \cdot \vec{u} = -1$ yields

$$\gamma^2 = 1 + v^2 - 2\Phi + 2\Phi^2 - 6\Phi v^2 + v^4 + 2\zeta \cdot \mathbf{v} . \quad (4.31)$$

4.3 Computation of Luminosity Distance and Redshift

4.3.1 Computing $D_L(z)$ in a General Spacetime

In this section we will review how to compute luminosity distances and redshifts in a general spacetime, as in Refs. [63, 64]. Our analysis is initially similar to that of Ref. [59], although they eventually rely on Taylor expansions around the observer's location. Such expansions are sensible for long-wavelength perturbations, but not for the short-wavelength perturbations that we consider here. We focus attention on a particular observer at some event \mathcal{P} . In our application to perturbed FRW spacetimes, this observer will be at $r = 0$ and at $t = t_0$ for some fixed t_0 . We consider the congruence of geodesics forming this observer's past light cone. Given the connection, we then find ray trajectories $x^\alpha(\lambda)$ by noting that the 4-momentum is $k^\alpha = dx^\alpha/d\lambda$, and by using the geodesic equation

$$\frac{dk^\alpha}{d\lambda} = k^\beta \partial_\beta k^\alpha = -\Gamma_{\mu\nu}^\alpha k^\mu k^\nu, \quad (4.32)$$

where we have defined $d/d\lambda = k^\alpha \partial_\alpha$. Here the affine parameter λ is chosen such that $\lambda = 0$ at the observer and $\lambda = \lambda_s < 0$ at the source. We also note that the 4-momentum is null.

The expansion θ of the congruence of null rays is related to the area $\mathcal{A}(\lambda)$ of a bundle of rays by

$$\theta = \frac{1}{\mathcal{A}} \frac{d\mathcal{A}(\lambda)}{d\lambda}. \quad (4.33)$$

We can find θ by using the Raychadhuri equation

$$\frac{d\theta}{d\lambda} = -R_{\mu\nu} k^\mu k^\nu - \frac{1}{2}\theta^2 - 2|\sigma|^2, \quad (4.34)$$

where we have defined the shear of the congruence

$$|\sigma|^2 = \frac{1}{2} \left[k_{\alpha;\beta} k^{\alpha;\beta} - \frac{1}{2} \theta^2 \right] , \quad (4.35)$$

and where we require $\theta \sim 2/\lambda$ as $\lambda \rightarrow 0$, so that the area of the beam goes to zero at $\lambda = 0$. The shear $\sigma \equiv \sqrt{|\sigma|^2}$ is given by the differential equation

$$\frac{d\sigma}{d\lambda} = -\sigma\theta + C_{\alpha\beta\mu\nu} k^\alpha k^\nu \bar{t}^\mu \bar{t}^\beta , \quad (4.36)$$

where $C_{\alpha\beta\mu\nu}$ is the Weyl tensor, and we have defined a null Newman-Penrose tetrad composed of the real 4-vectors k^μ and m^μ , and the complex conjugate 4-vectors t^μ and \bar{t}^μ . These satisfy the orthogonality conditions

$$k^\mu m_\mu = \bar{t}^\mu t_\mu = 1 \quad (4.37)$$

and

$$k^\mu k_\mu = m^\mu m_\mu = t^\mu t_\mu = k^\mu t_\mu = m^\mu t_\mu = 0 , \quad (4.38)$$

as in [59]. They are chosen at the observer and then extended along each geodesic in the congruence by parallel transport. We also choose the initial condition $\sigma = 0$ at $\lambda = 0$.

Once we find θ , we then find the luminosity distance as a function of the affine parameter at the source,

$$\begin{aligned} D_L(\lambda_s) &= \lim_{\Delta\lambda \rightarrow 0} \left[-\Delta\lambda (1+z)^2 \exp \left(\frac{1}{2} \int_{\Delta\lambda}^{\lambda_s} \theta d\lambda \right) \right] \\ &= -\lambda_s (1+z)^2 \exp \left[\frac{1}{2} \int_0^{\lambda_s} \left(\theta - \frac{2}{\lambda} \right) d\lambda \right] \end{aligned} \quad (4.39)$$

where $\Delta\lambda$ corresponds to the size of the observer's telescope, which we set to zero. The right hand side of Eq. (4.39) has a well defined, finite, limit as $\Delta\lambda \rightarrow 0$ due to the aforementioned initial condition placed on θ . Note also that the right hand

side has an overall minus sign due to our convention that the affine parameter is negative.

The redshift observed at $\lambda = 0$, of the light emitted from the source at λ_s , is

$$1 + z(\lambda_s) = \frac{(u_\alpha k^\alpha)_s}{(u_\beta k^\beta)_o}, \quad (4.40)$$

where

$$u_\alpha k^\alpha = \gamma (g_{tt}k^t + g_{ti}k^i + g_{it}v^i k^t + g_{ij}v^i k^j), \quad (4.41)$$

and where the subscript “s” will in general denote quantities evaluated at the source at the emission time and the subscript “o” will denote quantities evaluated at the observer at the observation time. By combining Eqs. (4.39) and (4.40) we can, in principle, compute D_L as a function of z in a general spacetime.

4.3.2 Computing $D_L(z)$ to First Post-Newtonian Order

Now we specialize the results of the preceding subsection to a perturbed FRW metric in the post-Newtonian gauge (4.9). Our goal is to find both $H_0 D_L$ and z to order ε^3 . At the observer, we have chosen $r = 0$ and $t = t_0$ and we have normalized the 4-momentum such that $k^r = -1$. This implies that $\lambda \approx -r$ and $r/t \sim -\lambda/t \sim \varepsilon$ to lowest order. We will thus need to find the right hand side of Eq. (4.39) to order $\lambda\varepsilon^2$ so that we may find $H_0 D_L$ to order ε^3 . Because of this, we see that we will need the integral in the exponential to order ε^2 , and therefore we will need to find $\lambda\theta$ to order ε^2 . Similarly, inspection of Eq. (4.40) tells us to what post-Newtonian order we will need to compute the components of k^α . To lowest order, $g_{tt} \sim 1$, $g_{ti} = g_{it} \sim \varepsilon^3$, $g_{ij} \sim 1$, $\gamma \sim 1$, and $v^i \sim \varepsilon$, and therefore we will need k^t to order ε^3 and we will need the spatial components k^i to order ε^2 .

The post-Newtonian pieces of k^α must be as small or smaller than order ε^2 , as can be seen by noting that $\lambda\Gamma_{\mu\nu}^\alpha \sim \varepsilon^2$ in the null geodesic equation (4.32). Given this assumption and the normalization of k^α , Eq. (4.32) reduces to

$$\frac{dk^\alpha}{d\lambda} = \frac{\partial k^\alpha}{\partial t} - \frac{\partial k^\alpha}{\partial r} + O\left(\frac{\varepsilon^4}{\lambda}\right) = -\Gamma_{tt}^\alpha + 2\Gamma_{tr}^\alpha - \Gamma_{rr}^\alpha + O\left(\frac{\varepsilon^4}{\lambda}\right) . \quad (4.42)$$

Plugging in the connection coefficients from Eq. (4.18)-(4.23), we find

$$\frac{dk^t}{d\lambda} = 2\Phi_{,r} + \zeta_{r,r} + O\left(\frac{\varepsilon^4}{\lambda}\right) , \quad (4.43)$$

$$\frac{dk^r}{d\lambda} = O\left(\frac{\varepsilon^3}{\lambda}\right) , \quad (4.44)$$

$$\frac{d}{d\lambda} (rk^\theta) = -\frac{2}{r}\Phi_{,\theta} + O\left(\frac{\varepsilon^3}{\lambda}\right) , \quad (4.45)$$

and

$$\frac{d}{d\lambda} (rk^\phi) = -\frac{2}{r\sin^2\theta}\Phi_{,\phi} + O\left(\frac{\varepsilon^3}{\lambda}\right) . \quad (4.46)$$

Using the specified initial conditions, the solutions to these equations are

$$k^t = 1 - 2\Phi - \zeta_r - 2 \int_0^r \dot{\Phi} dr' + O(\varepsilon^4) , \quad (4.47)$$

$$k^r = -1 + O(\varepsilon^3) , \quad (4.48)$$

$$k^\theta = \frac{2}{r} \int_0^r \frac{dr'}{r'} \Phi_{,\theta} + O(\varepsilon^3) , \quad (4.49)$$

and

$$k^\phi = \frac{2}{r\sin^2\theta} \int_0^r \frac{dr'}{r'} \Phi_{,\phi} + O(\varepsilon^3) ; \quad (4.50)$$

the integrals above are performed along the unperturbed ray, where $t(\lambda) = t_0 + \lambda$ and $r(\lambda) = -\lambda$. We can then find the perturbed ray trajectory by integrating Eqs. (4.47)-(4.50) with respect to λ . Most notably, Eq. (4.48) leads to $\lambda = -r + O(\lambda\varepsilon^3)$. This means that we can easily rewrite Eq. (4.39) in terms of the radial coordinate r of the source:

$$D_L = r(1+z)^2 \exp\left[-\frac{1}{2} \int_0^r \left(\theta + \frac{2}{r'}\right) dr'\right] + O(r\varepsilon^3) . \quad (4.51)$$

In order to find the expansion θ , we first need to find the shear, given by Eq. (4.36). The solution to this equation is

$$\sigma = \frac{1}{\lambda^2} \int_0^\lambda (\lambda')^2 C_{\alpha\beta\mu\nu} k^\alpha k^\nu \bar{t}^\mu \bar{t}^\beta d\lambda' ; \quad (4.52)$$

since $|k| \sim |\bar{t}| \sim 1$, it turns out that the lowest order shear is $\sigma \sim \varepsilon^2/\lambda$. Inserting $|\sigma|^2 \sim \varepsilon^4/\lambda^2$ into the Raychaudhuri equation (4.34) gives a contribution of order ε^4/λ to the expansion θ . However, we already know that we only need θ to order ε^2/λ , and so this contribution is negligible for our purposes here. Neglecting shear and defining $\delta\theta = \theta - 2/\lambda$, we rewrite Eq. (4.34) as

$$\begin{aligned} \frac{d(\delta\theta)}{d\lambda} &= -R_{tt} - R_{rr} - \frac{2}{\lambda}(\delta\theta) + O\left(\frac{\varepsilon^3}{\lambda^2}\right) \\ &= -2\nabla^2\Phi - \frac{2}{\lambda}(\delta\theta) + O\left(\frac{\varepsilon^3}{\lambda^2}\right) . \end{aligned} \quad (4.53)$$

The solution to this is

$$\delta\theta = \frac{2}{r^2} \int_0^r (r')^2 \nabla^2\Phi dr' + O\left(\frac{\varepsilon^3}{\lambda}\right) , \quad (4.54)$$

where we are using $\lambda = -r + O(\lambda\varepsilon^3)$. Using this result in Eq. (4.51) yields our final result for the post-Newtonian luminosity distance

$$D_L = r(1+z)^2 \left[1 - \int_0^r \frac{dr'}{r'^2} \int_0^{r'} (r'')^2 \nabla^2\Phi dr'' \right] + O(r\varepsilon^3) . \quad (4.55)$$

We now turn to evaluating the redshift z as a function of the affine parameter λ . Equation (4.40) is the general expression for the redshift, and it depends on $u_\alpha k^\alpha$ at the source and at the observer. To order ε^3 , using Eqs. (4.9), (4.31), and our solutions for k^α , we obtain

$$\begin{aligned} u_\alpha k^\alpha &= g_{\alpha\beta} u^\alpha k^\beta \\ &= -1 - v^r - \frac{1}{2}v^2 + \Phi + 3v^r\Phi - \frac{1}{2}v^r v^2 + 2 \int_0^r \dot{\Phi} dr' \\ &\quad + v_\theta k^\theta + v_\phi k^\phi + O(\varepsilon^4) \end{aligned} \quad (4.56)$$

where k^θ and k^ϕ are given by Eqs. (4.49) and (4.50), respectively. Therefore, the post-Newtonian redshift is

$$\begin{aligned}
1 + z &= \frac{(u_\alpha k^\alpha)_s}{(u_\beta k^\beta)_o} \\
&= 1 + v_s^r - v_o^r + \Phi_o - \Phi_s + \frac{1}{2} (v_s^2 - v_o^2) + (v_o^r)^2 - v_o^r v_s^r - 2 \int_0^r \dot{\Phi} dr' \\
&\quad + (v_\theta k^\theta + v_\phi k^\phi)_o - (v_\theta k^\theta + v_\phi k^\phi)_s + \Phi_o v_o^r + \Phi_s v_o^r + \Phi_o v_s^r - 3\Phi_s v_s^r \\
&\quad - \frac{1}{2} v_o^2 (v_s^r - v_o^r) + (v_o^r)^2 (v_s^r - v_o^r) + \frac{1}{2} v_s^2 (v_s^r - v_o^r) + O(\varepsilon^4) . \quad (4.57)
\end{aligned}$$

In Eqs. (4.55) and (4.57), the right hand sides are evaluated at $r = -\lambda$ and $t = t_0 + \lambda$. Recall that subscripts “o” denote quantities evaluated at the observer where $r = 0$ and $t = t_0$, while subscripts “s” denote quantities evaluated at the source $(t(\lambda), r(\lambda), \theta, \phi)$.

4.4 Adding Density Perturbations

4.4.1 Basic Method

In this section we apply the formalism of Section 4.3 to a spherical region in a perturbed FRW spacetime. We will describe that region using the post-Newtonian metric (4.9). We expand the metric functions Φ and ζ^i and the fluid 3-velocity v^i in powers of the density contrast δ as

$$\Phi = \Phi_{(0)} + \Phi_{(1)} + \Phi_{(2)} + O(\delta^3) , \quad (4.58)$$

$$\zeta_i = \zeta_{i(0)} + \zeta_{i(1)} + \zeta_{i(2)} + O(\delta^3) , \quad (4.59)$$

and

$$v^i = v_{(0)}^i + v_{(1)}^i + v_{(2)}^i + O(\delta^3) , \quad (4.60)$$

respectively. We also expand the null geodesic x^α and 4-momentum $k^\alpha = dx^\alpha/d\lambda$ as

$$x^\alpha = x_{(0)}^\alpha + x_{(1)}^\alpha + x_{(2)}^\alpha + O(\delta^3) \quad (4.61)$$

and

$$k^\alpha = k_{(0)}^\alpha + k_{(1)}^\alpha + k_{(2)}^\alpha + O(\delta^3) \quad , \quad (4.62)$$

respectively. For the remainder of the chapter, quantities that are zeroth order in δ will be denoted by a subscript “(0)”, first order by a subscript “(1)”, and second order by a subscript “(2)”. Also henceforth “first order” and “second order” will always refer to orders in δ , not ε , unless otherwise specified.

In the perturbed spacetime, we will calculate the redshift z and luminosity distance D_L as functions of the observation time t_0 , of the affine parameter λ along the past-directed null geodesic, and of the 4-momentum \vec{k} of photons at $r = 0$ and $t = t_0$. We parameterize this future-directed null vector \vec{k} in terms of angles θ and ϕ , in such a way that $k^r = -1$ and \vec{k} is in the direction (θ, ϕ) at $r = 0$. We can thus express D_L and z as functions of λ , θ , and ϕ at fixed t_0 , and by eliminating the affine parameter λ we can compute $D_L(z, \theta, \phi)$.

We can then take an average over angles to find $D_L(z)$, where we must take some care since there are two sets of relevant angles. There are the angles $(\tilde{\theta}, \tilde{\phi})$ which parameterize the direction of \vec{k} in the observer’s rest frame, and then there are the coordinate angles (θ, ϕ) . We will need to average over $(\tilde{\theta}, \tilde{\phi})$. This means that we will need to know the relationship between the related infinitesimal solid angles $d\Omega^2$ and $d\tilde{\Omega}^2$. We define Cartesian coordinates (x^1, x^2, x^3) in terms of the polar coordinates (r, θ, ϕ) in the standard way. An orthonormal set of basis vectors for the observer’s local Lorentz frame can be obtained by renormalizing the coordinate

basis vectors $\partial/\partial t$ and $\partial/\partial x^i$ and boosting. The result is

$$\vec{e}_i = \left[1 + \frac{1}{2}v_o^2 - \Phi_o + O(\varepsilon^3) \right] \frac{\partial}{\partial t} + [v_o^i + O(\varepsilon^3)] \frac{\partial}{\partial x^i} \quad (4.63)$$

and

$$\vec{e}_i = [v_o^i + O(\varepsilon^3)] \frac{\partial}{\partial t} + \left[\delta_{ij} (1 + \Phi_o) + \frac{1}{2}v_o^i v_o^j + O(\varepsilon^3) \right] \frac{\partial}{\partial x^j} . \quad (4.64)$$

The angles (θ, ϕ) are defined by

$$\vec{k} = k^t \frac{\partial}{\partial t} - n^i \frac{\partial}{\partial x^i} , \quad (4.65)$$

with

$$\mathbf{n} = (\sin \theta \cos \phi, \sin \theta \sin \phi, \cos \theta) , \quad (4.66)$$

while the observer's angles $(\tilde{\theta}, \tilde{\phi})$ are defined by

$$\vec{k} \propto \vec{e}_t - \tilde{n}^i \vec{e}_i , \quad (4.67)$$

with

$$\tilde{\mathbf{n}} = \left(\sin \tilde{\theta} \cos \tilde{\phi}, \sin \tilde{\theta} \sin \tilde{\phi}, \cos \tilde{\theta} \right) . \quad (4.68)$$

By inserting (4.63) and (4.64) into (4.67) and then comparing with (4.65), we find

$$\mathbf{n} \propto \tilde{\mathbf{n}} + \Phi_o \tilde{\mathbf{n}} - \mathbf{v}_o + \frac{1}{2} (\mathbf{v}_o \cdot \tilde{\mathbf{n}}) \mathbf{v}_o + O(\varepsilon^3) . \quad (4.69)$$

This gives

$$d^2 \tilde{\Omega} = d^2 \Omega [1 - 2(\mathbf{v}_o \cdot \mathbf{n}) + O(\varepsilon^2)] . \quad (4.70)$$

After averaging over viewing angles, we find the expected value of $D_L(z)$ by taking an ensemble average, wherein we treat the density perturbation δ at any fixed time as a homogeneous random process. Once we have the averaged $D_L(z)$, we can then analyze these data in terms of a homogeneous universe to see if we

would find an apparent acceleration. Assuming Gaussian uncertainties, we perform a chi-squared fit to an FRW model with a matter density Ω_M and a cosmological constant density Ω_Λ .

4.4.2 Unperturbed Quantities

In the unperturbed background, everything is spherically symmetric, and the line element in our coordinates is given by Eq. (4.13). The background four-momentum k_0^α is purely in the $t - r$ plane, and is given by Eqs. (4.47) and (4.48) to be

$$k_{(0)}^t(r, t) = 1 - \frac{2r^2}{9t^2} + \frac{2r^3}{135t^3} + O\left(\frac{r^4}{t^4}\right) \quad (4.71)$$

and

$$k_{(0)}^r(r, t) = -1 - \frac{4r^3}{27t^3} + O\left(\frac{r^4}{t^4}\right). \quad (4.72)$$

Since $k_{(0)}^t = dt/d\lambda$ and $k_{(0)}^r = dr/d\lambda$, we can integrate and invert these equations to find the unperturbed ray trajectory; keeping in mind the conditions that $r = \lambda = 0$ and $t = t_0$ at the observer, we find

$$t(\lambda) = t_0 + \lambda \left[1 - \frac{2\lambda^2}{27t_0^2} + O\left(\frac{\lambda^3}{t_0^3}\right) \right] \quad (4.73)$$

and

$$r(\lambda) = -\lambda \left[1 + O\left(\frac{\lambda^3}{t_0^3}\right) \right] \quad (4.74)$$

in the unperturbed background.

Using this, we can use the solution (4.54) to the Raychaudhuri equation to find the background expansion $\theta_{(0)}$,

$$\theta_{(0)}(\lambda) = \frac{2}{\lambda} - \frac{4}{9t_0^2}\lambda + O\left(\frac{\lambda^2}{t_0^3}\right). \quad (4.75)$$

Then the zeroth-order luminosity distance is given by Eq. (4.55) to be

$$\begin{aligned} D_{L(0)} &= (1+z)^2 r \left(1 - \frac{r^2}{9t^2} \right) + O\left(\frac{r^4}{t^3}\right) \\ &= \frac{2}{3H_0} (1+z)^2 \frac{r}{t} \left[1 - \frac{r}{t} + \frac{8r^2}{9t^2} + O\left(\frac{r^3}{t^3}\right) \right], \end{aligned} \quad (4.76)$$

where we have defined $H_0 = 2/3t_0$. The zeroth-order redshift is found from Eq. (4.57),

$$z_{(0)} = \frac{2r}{3t} + \frac{r^2}{9t^2} + \frac{4r^3}{27t^3} + O\left(\frac{r^4}{t^4}\right), \quad (4.77)$$

and we eventually find the expected $D_{L(0)}(z)$ by inverting Eq. (4.77) and plugging the result into Eq. (4.76):

$$D_{L(0)}(z) = \frac{z}{H_0} \left[1 + \frac{1}{4}z - \frac{1}{8}z^2 + O(z^3) \right]. \quad (4.78)$$

Thus, for the background, the best-fit cosmological constant density is $\Omega_\Lambda = 0$ and the deceleration parameter is $q_0 = 1/2$.

4.4.3 Second Order Perturbed Optics

The perturbed post-1-Newtonian line element is, from Eq. (4.9),

$$\begin{aligned} ds^2 \approx & - \left(1 + 2\Phi_{(0)} + 2\Phi_{(0)}^2 + 2\Phi_{(1)} + 4\Phi_{(0)}\Phi_{(1)} + 2\Phi_{(2)} + 2\Phi_{(1)}^2 + 4\Phi_{(0)}\Phi_{(2)} \right) dt^2 \\ & + 2 \left(\zeta_{i(0)} + \zeta_{i(1)} + \zeta_{i(2)} \right) dx^i dt \\ & + \left(1 - 2\Phi_{(0)} - 2\Phi_{(1)} - 2\Phi_{(2)} \right) \gamma_{ij} dx^i dx^j \end{aligned} \quad (4.79)$$

and the perturbed luminosity distance (4.55) is defined to be

$$D_L = (1+z)^2 E_L, \quad (4.80)$$

where

$$\begin{aligned}
E_L(r, \theta, \phi) &= E_{L(0)}(r, \theta, \phi) + E_{L(1)}(r, \theta, \phi) + E_{L(2)}(r, \theta, \phi) + O(\delta^3) \\
&= r \left[1 - \int_0^r \frac{dr'}{r'^2} \int_0^{r'} (r'')^2 \nabla^2 (\Phi_{(0)} + \Phi_{(1)} + \Phi_{(2)}) dr'' \right] \\
&\quad + O(\delta^3) , \tag{4.81}
\end{aligned}$$

and where we have pulled out the factor of $(1+z)^2$ for simplicity. We then find that the order δ perturbation is

$$E_{L(1)} = -\frac{2}{3H_0} \frac{r}{t_0} \int_0^r \frac{dr'}{r'^2} \int_0^{r'} (r'')^2 \nabla^2 \Phi_{(1)} dr'' , \tag{4.82}$$

and the order δ^2 perturbation is

$$E_{L(2)} = -\frac{2}{3H_0} \frac{r}{t_0} \int_0^r \frac{dr'}{r'^2} \int_0^{r'} (r'')^2 \nabla^2 \Phi_{(2)} dr'' , \tag{4.83}$$

where $H_0 = 2/3t_0$. In general, all of the terms involving potentials and velocities in these equations, and in those that follow, are evaluated along the zeroth-order, unperturbed, geodesic.

We can now calculate the perturbed redshift

$$z(r, \theta, \phi) = z_{(0)}(r, \theta, \phi) + z_{(1)}(r, \theta, \phi) + z_{(2)}(r, \theta, \phi) + O(\delta^3) \tag{4.84}$$

from Eq. (4.57), using our knowledge of the zeroth-order quantities, to find

$$\begin{aligned}
z_{(1)} &= v_{s(1)}^r - v_{o(1)}^r + \Phi_{o(1)} - \Phi_{s(1)} + \frac{2r}{3t} (v_{s(1)}^r - v_{o(1)}^r) - 2 \int_0^r \dot{\Phi}_{(1)} dr' \\
&\quad + \frac{2r}{3t} \Phi_{o(1)} - \frac{2r}{t} \Phi_{s(1)} - \frac{r^2}{9t^2} v_{o(1)}^r + \frac{r^2}{3t^2} v_{s(1)}^r + O(\delta\varepsilon^4) \tag{4.85}
\end{aligned}$$

and

$$\begin{aligned}
z_{(2)} = & v_{s(2)}^r - v_{o(2)}^r + \Phi_{o(2)} - \Phi_{s(2)} + \frac{2r}{3t} (v_{s(2)}^r - v_{o(2)}^r) + \frac{1}{2} (v_{s(1)}^2 - v_{o(1)}^2) \\
& + (v_{o(1)}^r)^2 - v_{o(1)}^r v_{s(1)}^r - 2 \int_0^r \dot{\Phi}_{(2)} dr' + \left(v_{\theta(1)} k_{(1)}^\theta + v_{\phi(1)} k_{(1)}^\phi \right)_o \\
& - \left(v_{\theta(1)} k_{(1)}^\theta + v_{\phi(1)} k_{(1)}^\phi \right)_s + \frac{2r}{3t} \Phi_{o(2)} - \frac{2r}{t} \Phi_{s(2)} - \frac{r^2}{9t^2} v_{o(2)}^r + \frac{r^2}{3t^2} v_{s(2)}^r \\
& + \frac{r}{3t} [v_{s(1)}^2 - v_{o(1)}^2] + \frac{2r}{3t} \left[(v_{s(1)}^r)^2 + (v_{o(1)}^r)^2 - v_{s(1)}^r v_{o(1)}^r \right] \\
& + \Phi_{o(1)} v_{o(1)}^r + \Phi_{s(1)} v_{o(1)}^r + \Phi_{o(1)} v_{s(1)}^r - 3\Phi_{s(1)} v_{s(1)}^r + x_{(1)}^i v_{s(1),i}^r \\
& + O(\delta^2 \varepsilon^4) , \tag{4.86}
\end{aligned}$$

where the first order perturbation to the null geodesic is

$$x_{(1)}^i = - \int_0^r k_{(1)}^i dr' . \tag{4.87}$$

All of the quantities above are evaluated along the zeroth-order geodesic, and the integrals are performed along an unperturbed central ray where $r(\lambda) = -\lambda$ and $t(\lambda) = t_0 + \lambda$.

Now we have found the redshift z and luminosity distance $H_0 D_L$ as functions of affine parameter λ and initial 4-momentum \vec{k}_o , to second order in δ and to third order in ε . Adding the redshift equations (4.77), (4.85), and (4.86) yields $z(\lambda, \theta, \phi)$. Similarly, the luminosity distance $D_L(\lambda, \theta, \phi)$ is found from adding Eqs. (4.78), (4.82), and (4.83), after replacing the factors of $(1+z)^2$. Inverting $z(\lambda, \theta, \phi)$ perturbatively, in terms of either δ or ε , gives us λ as a function of z . Plugging this into $D_L(\lambda, \theta, \phi)$ yields an expression for $D_L(z, \theta, \phi)$. We then angle average this and then ensemble average, assuming that density fluctuations at a given cosmic time are a homogeneous random process. Details of this full procedure are given in Appendices A, B, and C, and the result is

$$D_L(z) = \frac{z}{H_0} \left(1 + \frac{1}{4}z - \frac{1}{8}z^2 \right) + \Delta D_L(z) , \tag{4.88}$$

where $\Delta D_L(z)$ depends on the two point correlation function. We will only need the lowest order piece of this, which is

$$\Delta D_L(z) = -\frac{1}{3H_0^2} f' \left(\frac{z}{H_0} \right) \langle v_{o(1)}^2 \rangle + O \left(\frac{f \varepsilon^2 \delta^2}{H_0} \right), \quad (4.89)$$

using $z \approx H_0 r$ to lowest order. The function f is related to the velocity two point correlation function (see Appendix A.3):

$$f(r) = \frac{3 \langle \mathbf{n} \cdot \mathbf{v}(\mathbf{r}_0, t) \mathbf{n} \cdot \mathbf{v}(\mathbf{r}_0 + r \mathbf{n}, t) \rangle}{\langle |\mathbf{v}(\mathbf{r}_0, t)|^2 \rangle} - 1, \quad (4.90)$$

where \mathbf{n} is a unit vector that defines the viewing direction and \mathbf{r}_0 is an arbitrary location in space. Note that $f(r)$ is independent of time, even though $\langle \mathbf{v}(\mathbf{r}_0, t)^2 \rangle$ does depend on time. This is because the time dependences of the numerator and denominator cancel.

The perturbation to the luminosity distance is proportional to

$$\langle v_{o(1)}^2 \rangle = \frac{4}{9H_0^2} \langle (\nabla \Phi_{o(1)})^2 \rangle; \quad (4.91)$$

this qualitative scaling has been argued for in Refs. [65] and [66]. We can Fourier transform $\Phi_{(1)}$, in terms of a wavevector k^i (not to be confused with the previously-defined 4-momentum) [10],

$$\Phi_{(1)} = \int \frac{d^3 k}{(2\pi)^3} \Phi_{\mathbf{k}} e^{i\mathbf{k} \cdot \mathbf{r}} \quad (4.92)$$

so that we may write the average of $(\nabla \Phi_{(1)})^2$ as a sum over modes:

$$\langle (\nabla \Phi_{(1)})^2 \rangle = \frac{9}{4} H_0^4 \int_0^\infty \frac{dk}{k^3} \Delta^2(k), \quad (4.93)$$

where $\Delta(k)$ is the dimensionless power spectrum of matter density fluctuations at the present time, defined by

$$\langle \delta^2 \rangle = \int_{-\infty}^{\infty} d(\ln k) \Delta(k)^2. \quad (4.94)$$

We adopt the following power spectrum

$$\Delta^2(k) = C^2 \left(\frac{k}{H_0} \right)^4 T^2 \left(\frac{k}{k_{eq}} \right), \quad (4.95)$$

where the factor of $(k/H_0)^4$ reflects a Harrison-Zel'dovich flat spectrum, the amplitude $C = 1.9 \times 10^{-5}$ is set by observations, and $T(y)$ is the transfer function. The BBKS transfer function [67] is a good fit for T in the absence of dark energy,

$$T(y) = \frac{\ln(1 + 2.34y)}{2.34y} [1 + 3.89y + (16.1y)^2 + (5.46y)^3 + (6.71y)^4]^{-1/4}, \quad (4.96)$$

where

$$y = \frac{k}{k_{eq}} = \frac{k\theta^{1/2}}{\Omega_X h^2 \text{Mpc}^{-1}}. \quad (4.97)$$

Here we show the most general form of the transfer function, where $\theta = \rho_{ER}/1.68\rho_\gamma$ (not to be confused with the expansion θ) is the density of relativistic particles divided by the density of photons, Ω_X is the density of cold dark matter, and $h = H_0/(100 \text{ km s}^{-1} \text{ Mpc}^{-1})$. We choose $\Omega_X = 1$ for our analysis.

Using this spectrum,

$$\langle (\nabla \Phi_{o(1)})^2 \rangle = \frac{9C^2 k_{eq}^2}{4} \int_0^\infty y dy T^2(y), \quad (4.98)$$

where $k_{eq} = 1/\lambda_c = \Omega_X h^2 \theta^{-1/2} \text{Mpc}^{-1} \approx 3000 \Omega_X h \theta^{-1/2} H_0$ and the integral is approximately 2.31×10^{-2} , using the transfer function in Eq. (4.96). So we finally find

$$\langle (\nabla \Phi_{o(1)})^2 \rangle \approx 9 \times 10^{-6} H_0^2 \left[\left(\frac{\Omega_X}{0.27} \right) \left(\frac{h}{0.7} \right) \right]^2 \theta^{-1} \quad (4.99)$$

and therefore

$$\langle v_{o(1)}^2 \rangle \approx 3 \times 10^{-6} \left[\left(\frac{\Omega_X}{0.27} \right) \left(\frac{h}{0.7} \right) \right]^2 \theta^{-1}. \quad (4.100)$$

Using the power spectrum (4.95) we also find

$$\begin{aligned} \langle \mathbf{n} \cdot \mathbf{v}(\mathbf{r}_0, t) \mathbf{n} \cdot \mathbf{v}(\mathbf{r}_0 + r\mathbf{n}, t) \rangle = \\ \frac{C^2 k_{eq}^2}{H_0^2} \int_0^\infty y dy T^2(y) \left[\frac{1}{3} j_0 \left(\frac{k_{eq} z y}{H_0} \right) - \frac{2}{3} j_2 \left(\frac{k_{eq} z y}{H_0} \right) \right], \end{aligned} \quad (4.101)$$

where j_0 and j_2 are spherical Bessel functions of the first kind, defined in Eqs. (A.28) and (A.29) of Appendix A.3. We plot $1 + f(r)$, found by combining Eqs. (4.90) and (4.101), in Figure 4.2. Note that this becomes negative for $k_{eq} r \gtrsim 10$. Note also that we have not used any truncation of the power on scales that are nonlinear. If we instead were to impose a high- k cutoff, so as not to include the effects of any modes that have $\Delta^2(k) > 1$, then this would lead to differences of a factor of about two. A different approach would be to include the quasi-linear regime, with the power spectrum given from N-body simulations [68].

We will specialize to $k_{eq}/H_0 = 1000$ for the rest of this chapter, which yields

$$\langle v_{o(1)}^2 \rangle \approx 8.34 \times 10^{-6}. \quad (4.102)$$

In Figure 4.3, we show how the perturbation $\Delta D_L(z)$ scales relative to the unperturbed luminosity distance $D_{L(0)}(z)$, for the choice $k_{eq}/H_0 = 10^3$. Note that we are plotting the logarithm of the absolute value, as the perturbation changes sign from positive to negative as one looks at larger distances. By inspection, it becomes clear that $\Delta D_L(z)$ is not actually a perturbation for very small redshifts, i.e. for where $|\Delta D_L|/D_{L(0)} \sim 1$, and thus our computation of ΔD_L is no longer valid in that regime. Indeed, it is well known that the peculiar velocities of objects within the Local Supercluster are not small when compared to their redshifts. However, this will not be a problem in practice, as Type Ia supernovae at such small redshifts are typically not used for cosmological parameter fitting. We will

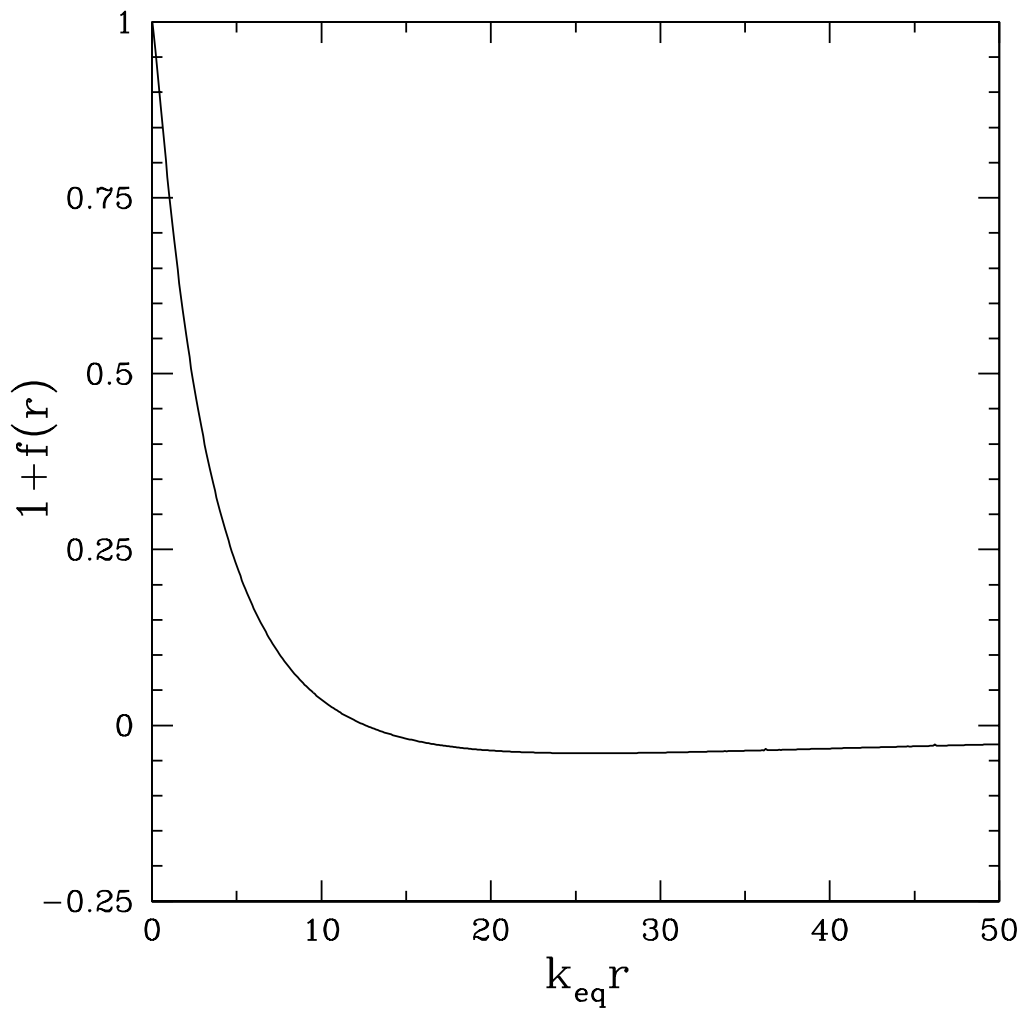


Figure 4.2: The function $1 + f(r)$ plotted versus $k_{eq}r$, where k_{eq} is the wavenumber of the dominant perturbation mode.

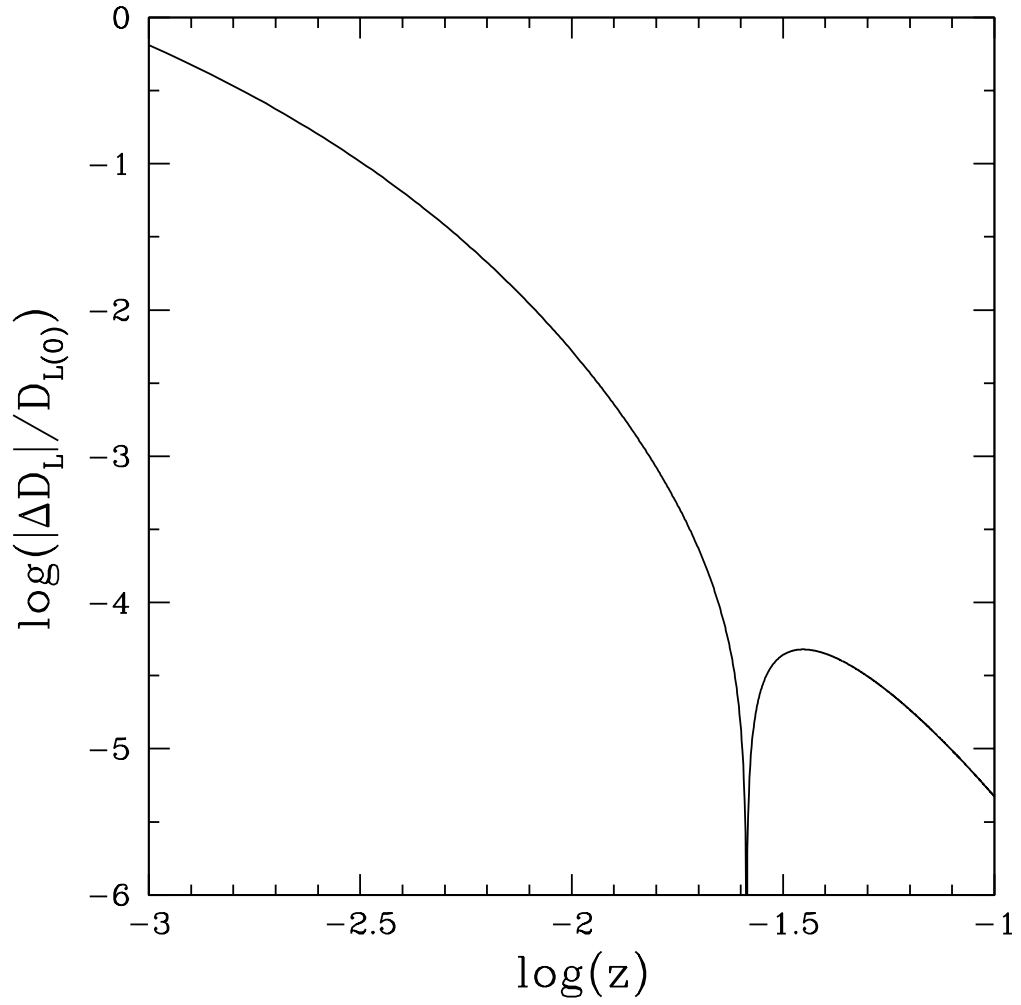


Figure 4.3: The relative size of the perturbation $\log[|\Delta D_L(z)|/D_{L(0)}(z)]$ plotted versus $\log(z)$, assuming that the dominant perturbation wavelength is 10^3 times smaller than the Hubble scale: $k_{eq}/H_0 = 10^3$.

eventually take this breakdown of perturbation theory into account by imposing a lower cutoff z_{min} when we fit our data to a theoretical model. By eye, we see that it should be safe to choose $z_{min} \sim 0.01$.

4.5 The Perturbation to the Inferred Cosmological Constant

4.5.1 Finding the Best-Fit FRW Model

We may now find the inferred cosmological constant and deceleration parameter by analyzing Eq. (4.88) within the context of what one would expect in a homogeneous model. The lowest order perturbation to the luminosity distance depends on the difference between the peculiar velocities at the source and at the observer, and so the question that we now ask is: How do peculiar velocities and their correlations affect inferences drawn from data about cosmological models? We cannot simply Taylor expand Eq. (4.88) around the observer to find q_0 . This is because f varies on short lengthscales of order $k_{eq}^{-1} \sim 10$ Mpc, so that a Taylor series expansion would effectively mean computing q_0 from $D_L(z)$ within this unrealistically short lengthscale. A good alternative then is to fit the perturbed luminosity distance over a finite range of redshifts to what one would expect in a homogeneous model with matter and a cosmological constant.

Suppose that the observer can measure redshifts $\{z_i\}$ for a set of distant objects arbitrarily well. From the distance determinations $\{D_{Li}\}$, the observer can compute $\{r_i = D_{Li}/(1 + z_i)\}$, and we can therefore take $\{z_i, r_i\}$ to be the data

gathered by the observer. Suppose also that in actuality the Universe is spatially flat with Hubble parameter H_0 and matter only. Let

$$r_i = H_0^{-1} [F(z_i) + \Delta_i(z_i)] \quad (4.103)$$

be the physical value of r_i , where for a flat matter-only cosmology

$$F(z_i) = \int_0^{z_i} \frac{dz}{(1+z)^{3/2}} = 2 \left[1 - \frac{1}{\sqrt{1+z_i}} \right] \quad (4.104)$$

and $\Delta_i(z_i)$ (not to be confused with the matter perturbation power spectrum) is the non-FRW contribution to r_i , from fluctuations via velocity differences. From Eq. (4.89), we find the ensemble averaged perturbation

$$\begin{aligned} \Delta_i(z_i) \approx \frac{C^2 k_{eq}^3}{H_0^3} \int_0^\infty dy T^2(y) & \left[\frac{y \cos(k_{eq} z_i y / H_0)}{k_{eq} z_i / H_0} - 3 \frac{\sin(k_{eq} z_i y / H_0)}{(k_{eq} z_i / H_0)^2} - 6 \frac{\cos(k_{eq} z_i y / H_0)}{(k_{eq} z_i / H_0)^3 y} \right. \\ & \left. + 6 \frac{\sin(k_{eq} z_i y / H_0)}{(k_{eq} z_i / H_0)^4 y^2} \right]. \end{aligned} \quad (4.105)$$

The observer fits the data to an FRW model that is slightly curved and has a small cosmological constant. The fitted model is then

$$r_i^{fit} = \int_0^{z_i} \frac{dz}{H(z)} - \frac{k}{6} \left(\int_0^{z_i} \frac{dz}{H(z)} \right)^3, \quad (4.106)$$

where $k = (\Omega_M + \Omega_\Lambda - 1) H_{fit}^2$ and

$$\begin{aligned} H^2(z) &= H_{fit}^2 \left[\Omega_M (1+z)^3 + (1 - \Omega_M - \Omega_\Lambda) (1+z)^2 + \Omega_\Lambda \right] \\ &= H_{fit}^2 (1+z)^3 \left[1 - \frac{(1 - \Omega_M)z}{1+z} - \frac{\Omega_\Lambda z(2+z)}{(1+z)^3} \right]; \end{aligned} \quad (4.107)$$

here H_{fit} is the fitted Hubble parameter, and Ω_M and Ω_Λ are the density parameters for matter and for the cosmological constant, respectively. Let us work to first order in $1 - \Omega_M$ and Ω_Λ , a simplification which ought to suffice as long as $\Delta_i \ll 1$.

Thus, the fitted model is

$$\begin{aligned} r_i^{fit} &= H_{fit}^{-1} [F(z_i) + (1 - \Omega_M)G(z_i) + \Omega_\Lambda I(z_i)] \\ &\equiv H_{fit}^{-1} [F(z_i) + \epsilon_M G(z_i) + \epsilon_\Lambda I(z_i)] , \end{aligned} \quad (4.108)$$

where $F(z_i)$ is the same as before, and we have defined

$$G(z) = \frac{1}{2} \int_0^z \frac{dz z}{(1+z)^{5/2}} + \frac{1}{6} [F(z)]^3 \quad (4.109)$$

and

$$I(z) = \frac{1}{2} \int_0^z \frac{dz z(2+z)}{(1+z)^{9/2}} - \frac{1}{6} [F(z)]^3 . \quad (4.110)$$

There are three fitting parameters: H_{fit} , $\epsilon_M = 1 - \Omega_M$ and $\epsilon_\Lambda = \Omega_\Lambda$.

From the data and our model we can compute a likelihood function. Assuming Gaussian uncertainties this will be the exponential of

$$\begin{aligned} \tilde{\chi}^2 &= -\frac{1}{2} \sum_i \frac{[r_i - r_i^{fit}(z_i)]^2}{\sigma_i^2} \\ &= -\frac{1}{2} \sum_i \frac{[(H_0^{-1} - H_{fit}^{-1}) F_i + H_0^{-1} \Delta_i - H_{fit}^{-1}(\epsilon_M G_i + \epsilon_\Lambda I_i)]^2}{\sigma_i^2} , \end{aligned} \quad (4.111)$$

where σ_i is the estimated uncertainty in the value of r_i inferred from observations and $Q_i \equiv Q(z_i)$ for $Q = F, G, I$.

The next step is to maximize $\tilde{\chi}^2$ with respect to the parameters of the fit, which will lead to a set of coupled nonlinear equations. To simplify, let us linearize in the small parameters ϵ_M , ϵ_Λ , $\{\Delta_i\}$ and $h = H_{fit}/H_0 - 1$. The resulting equations are

$$\langle \Delta_i F_i \rangle = \epsilon_M \langle G_i F_i \rangle + \epsilon_\Lambda \langle I_i F_i \rangle - h \langle F_i^2 \rangle , \quad (4.112)$$

$$\langle \Delta_i G_i \rangle = \epsilon_M \langle G_i^2 \rangle + \epsilon_\Lambda \langle I_i G_i \rangle - h \langle G_i F_i \rangle , \quad (4.113)$$

and

$$\langle \Delta_i I_i \rangle = \epsilon_M \langle I_i G_i \rangle + \epsilon_\Lambda \langle I_i^2 \rangle - h \langle I_i F_i \rangle , \quad (4.114)$$

where we have defined the average $\langle Q_i \rangle \equiv \sum_i Q_i / (N \sigma_i^2)$. Solving for the parameters of the fit, we get

$$\begin{aligned} \epsilon_\Lambda = D^{-1} & \left[\langle \Delta_i F_i \rangle (\langle I_i F_i \rangle \langle G_i^2 \rangle - \langle I_i G_i \rangle \langle G_i F_i \rangle) \right. \\ & + \langle \Delta_i G_i \rangle (\langle I_i G_i \rangle \langle F_i^2 \rangle - \langle I_i F_i \rangle \langle G_i F_i \rangle) \\ & \left. + \langle \Delta_i I_i \rangle (\langle G_i F_i \rangle^2 - \langle G_i^2 \rangle \langle F_i^2 \rangle) \right] , \quad (4.115) \end{aligned}$$

$$\begin{aligned} \epsilon_M = D^{-1} & \left[\langle \Delta_i F_i \rangle (\langle G_i F_i \rangle \langle I_i^2 \rangle - \langle I_i F_i \rangle \langle I_i G_i \rangle) \right. \\ & + \langle \Delta_i G_i \rangle (\langle I_i F_i \rangle^2 - \langle I_i^2 \rangle \langle F_i^2 \rangle) \\ & \left. + \langle \Delta_i I_i \rangle (\langle I_i G_i \rangle \langle F_i^2 \rangle - \langle G_i F_i \rangle \langle I_i F_i \rangle) \right] , \quad (4.116) \end{aligned}$$

and

$$\begin{aligned} h = -D^{-1} & \left[\langle \Delta_i F_i \rangle (\langle I_i G_i \rangle^2 - \langle I_i^2 \rangle \langle G_i^2 \rangle) \right. \\ & + \langle \Delta_i G_i \rangle (\langle G_i F_i \rangle \langle I_i^2 \rangle - \langle I_i G_i \rangle \langle I_i F_i \rangle) \\ & \left. + \langle \Delta_i I_i \rangle (\langle I_i F_i \rangle \langle G_i^2 \rangle - \langle G_i F_i \rangle \langle I_i G_i \rangle) \right] , \quad (4.117) \end{aligned}$$

where

$$\begin{aligned} D = & \langle I_i G_i \rangle^2 \langle F_i^2 \rangle - 2 \langle I_i F_i \rangle \langle I_i G_i \rangle \langle G_i F_i \rangle - \langle I_i^2 \rangle \langle F_i^2 \rangle \langle G_i^2 \rangle \\ & + \langle I_i^2 \rangle \langle G_i F_i \rangle^2 + \langle I_i F_i \rangle^2 \langle G_i^2 \rangle . \quad (4.118) \end{aligned}$$

These are fairly general for small Δ_i , and show that there may be contributions to ϵ_Λ , ϵ_M , and h from velocity fluctuations.

Next, we need to compute the averages. To do this, we recall that F corresponds to comoving radial coordinate, modulo a factor of H_0^{-1} . To the order of

approximation underlying our calculations, we can take the comoving source density to be uniform. Moreover, we do not need to worry about Malmquist bias, at least for Type Ia supernovae, which are very bright. Let us also assume that all of the $\{\sigma_i^2\}$ are the same, to keep the problem as simple as possible. Then σ_i^2 drops out of our expressions for ϵ_M , ϵ_Λ , and h , although it remains in their uncertainties. We suppose that our source catalog extends to some maximum value F_{max} , with a corresponding maximum redshift z_{max} . It is worth remembering that $F < 2$ is an absolute upper bound, and that for $z < 1$, $F < 2 - \sqrt{2} \approx 0.6$, so we will be dealing with relatively small values of F typically. Moreover, as we have already noted in Figure 4.3, our small Δ_i assumption breaks down below a minimum redshift $z_{min} \lesssim 0.01$, but this is not a problem as no supernovae below this redshift have ever been used for cosmological model fitting [1, 2]. So we will assume a lower cutoff for all of our sums of F_{min} . Then, for example,

$$\langle F_i^2 \rangle = \frac{3}{F_{max}^3 - F_{min}^3} \int_{F_{min}}^{F_{max}} dF F^2 F^2 , \quad (4.119)$$

and Eqs. (4.104), (4.109), (4.110), and (4.118) give the lowest order result, assuming that $F_{max}^3 \gg F_{min}^3$,

$$\mathcal{D} \approx -\frac{1}{5268480} F_{max}^{12} . \quad (4.120)$$

Keeping only lowest order terms in F_{max} in the numerators of Eqs. (4.115), (4.116), and (4.117) as well, we get

$$\epsilon_\Lambda \approx -\frac{5268480}{16} \left[\frac{3\langle \Delta_i F_i \rangle}{784 F_{max}^4} - \frac{3\langle \Delta_i F_i^2 \rangle}{280 F_{max}^5} + \frac{\langle \Delta_i F_i^3 \rangle}{140 F_{max}^6} \right] , \quad (4.121)$$

$$\epsilon_M \approx -2\epsilon_\Lambda , \quad (4.122)$$

and

$$h \approx -\frac{5268480}{16} \left[\frac{\langle \Delta_i F_i \rangle}{448 F_{max}^2} - \frac{\langle \Delta_i F_i^2 \rangle}{168 F_{max}^3} + \frac{3\langle \Delta_i F_i^3 \rangle}{784 F_{max}^4} \right] . \quad (4.123)$$

We see that if $\Delta_i \propto F_i$, then ϵ_Λ is zero, because the three terms in Eq. (4.121) cancel. This means that if Δ_i arises from velocity correlations, it is only the correlation function of velocities at two separated points that matters, not the RMS velocity at a point. Also note that, for this fitting procedure, the deceleration parameter is still $q_0 = 1/2$, since

$$\begin{aligned} \Delta q_0 &= q_0 - \frac{1}{2} = -\frac{1}{2} - (\ddot{a}a/H^2)_0 \\ &= \frac{1}{2}(\Omega_M - 1 - 2\Omega_\Lambda) = \frac{1}{2}(-\epsilon_M - 2\epsilon_\Lambda) = \frac{1}{2}(2\epsilon_\Lambda - 2\epsilon_\Lambda) = 0 \end{aligned} \quad (4.124)$$

from Eq. (4.122), in agreement with Refs. [26], [27], and [69].

The perturbation Δ_i , given in Eq. (4.105), depends on the correlation function $f(r)$, and so it does contribute to ϵ_Λ . For $z_{min} = 0.02$ and $z_{max} = 0.15$, we numerically integrate to find that the best-fit cosmological constant density is $\Omega_\Lambda \approx 0.004$. Table 4.1 gives a few more results for the best-fit values for ϵ_Λ , ϵ_M , and h as a function of the two limiting redshifts z_{min} and z_{max} in the continuum limit, where we have made the assumption that the number of sources N is very large: $N \rightarrow \infty$. In this limit, $\Delta_i(z_i) \rightarrow \Delta(z)$ and

$$\epsilon_\Lambda = \int_{F_{min}}^{F_{max}} dF w(F) \Delta(F), \quad (4.125)$$

where we have the weighting function

$$w(F) \equiv -\frac{5268480}{16} \left(\frac{3F}{784F_{max}^4} - \frac{3F^2}{280F_{max}^5} + \frac{F^3}{140F_{max}^6} \right). \quad (4.126)$$

We also plot these results in Figure 4.1, in the Introduction. Note that Ω_Λ may be positive or negative, depending on the redshift range, since ΔD_L changes sign in the region of interest.

In order to test the robustness of these continuum limit calculations, we have

Table 4.1: Best-fit parameters in the continuum limit for a few values of the source catalog limiting redshifts z_{min} and z_{max} , also for the choice that the dominant perturbation wavelength is 10^3 times smaller than the Hubble scale: $k_{eq}/H_0 = 10^3$.

z_{min}	z_{max}	Ω_Λ	$1 - \Omega_M$	$H_{fit}/H_0 - 1$
0.01	0.1	-0.018	0.036	-4.3×10^{-5}
	0.2	0.0016	-0.0032	4.0×10^{-5}
0.03	0.1	0.0037	-0.0074	7.1×10^{-5}
	0.2	0.0020	-0.0040	4.7×10^{-5}

also applied our fitting procedure to randomly-generated catalogs of synthetic redshift data. To generate a data point F_i for such a catalog, we assume that the quantity $(F_i^3 - F_{min}^3)/(F_{max}^3 - F_{min}^3)$ is distributed uniformly between 0 and 1. In this way, we create catalogs of $N = 100$ data points, wherein each data point is a value of F_i for a source with a random location. For each data point, we use the ensemble averaged formula for $\Delta D_L(z)$ to find Δ_i . We then fit these data to a homogeneous model as outlined above, using sums instead of integrals. Using 20 randomly-generated catalogs, the average best-fit values for Ω_Λ are summarized in Table 4.2, along with their standard deviations. We also found the best-fit cosmological constant with 50 catalogs for $z_{min} = 0.02$ and $z_{max} = 0.15$, to find $\Omega_\Lambda = 0.005 \pm 0.001$.

4.5.2 Variance

Although the best-fit values for Ω_Λ of the previous subsection are very small, we must keep in mind that they are derived from the ensemble averaged perturbation

Table 4.2: Best-fit parameters for 20 catalogs of N=100 samples each, for a few values of the source catalog limiting redshifts z_{min} and z_{max} . We have also made the choice that the dominant perturbation wavelength is 10^3 times smaller than the Hubble scale: $k_{eq}/H_0 = 10^3$.

z_{min}	z_{max}	Ω_Λ
0.01	0.1	-0.020 ± 0.002
	0.2	0.002 ± 0.001
0.03	0.1	0.014 ± 0.001
	0.2	0.0025 ± 0.0004

to the luminosity distance. For a given source, this ensemble averaged perturbation will be far smaller than the leading order perturbation, which depends linearly on the peculiar velocity. This linear perturbation will be the main source of the variance in the best-fit parameters, and this variance should overwhelm the systematic error for typical supernova sample sizes. This complication was pointed out by Ref. [70] and it was shown to cause errors of $\Delta\Omega_\Lambda \approx -0.04$ for a sample of actual nearby supernovae in Ref. [51].

Consider our expression for the best-fit Ω_Λ , in terms of N discrete sources, rewritten as a weighted sum,

$$\Omega_\Lambda = \frac{1}{N} \sum_i w(F_i) \Delta_i . \quad (4.127)$$

What we have computed is the ensemble average of this,

$$\langle \Omega_\Lambda \rangle = \frac{1}{N} \sum_i w(F_i) \langle \Delta_i \rangle . \quad (4.128)$$

The variance is then

$$\begin{aligned}\sigma_\Lambda^2 &= \langle (\Omega_\Lambda - \langle \Omega_\Lambda \rangle)^2 \rangle = \langle \Omega_\Lambda^2 \rangle + O(\delta^3) \\ &= \frac{1}{N^2} \sum_{i,j} w(F_i)w(F_j) \langle \Delta_i \Delta_j \rangle ,\end{aligned}\quad (4.129)$$

which has two types of terms contributing: those with $i = j$ and those with $i \neq j$.

Separating these, we have $\sigma_\Lambda^2 = \sigma_1^2 + \sigma_2^2$, where

$$\sigma_1^2 \equiv \frac{1}{N^2} \sum_i w^2(F_i) \langle \Delta_i^2 \rangle \quad (4.130)$$

and

$$\sigma_2^2 \equiv \frac{1}{N^2} \sum_{i \neq j} w(F_i)w(F_j) \langle \Delta_i \Delta_j \rangle . \quad (4.131)$$

In the continuum limit $N \rightarrow \infty$, the first piece of the variance becomes

$$\sigma_1^2 \approx \frac{1}{N} \frac{3}{F_{max}^3} \int_0^{F_{max}} F^2 dF w^2(F) \langle \Delta^2(F) \rangle \quad (4.132)$$

where, from Eq. (4.105),

$$\langle \Delta^2(F) \rangle = \langle \Delta^2(H_0 r) \rangle = \langle \mathbf{n} \cdot [\mathbf{v}(\mathbf{r}) - \mathbf{v}(0)] \mathbf{n} \cdot [\mathbf{v}(\mathbf{r}) - \mathbf{v}(0)] \rangle \sim \langle v_o^2 \rangle . \quad (4.133)$$

The integrand in Eq. (4.132) is integrable as $F \rightarrow 0$, and so the quantity σ_1 is to a good approximation independent of z_{min} for small z_{min} . Thus we can for simplicity take $z_{min} = 0$. After integrating, we find

$$\sigma_1^2 \sim \frac{100}{N} \left(\frac{\langle v_o^2 \rangle}{8 \times 10^{-6}} \right) \left(\frac{z_{max}}{0.2} \right)^{-6} . \quad (4.134)$$

For a source catalog of 100 sources out to a limiting redshift $z_{max} = 0.2$, we find that this variance is significant: $\sigma_1^2 \sim 1$.

The second piece (4.131) of the variance does not depend on the sample size, although it does depend on F_{max} . In the continuum limit,

$$\sigma_2^2 \approx \frac{9}{F_{max}^6} \int_0^{F_{max}} F^2 dF w(F) \int_0^{F_{max}} (F')^2 dF' w(F') \langle \Delta(F) \Delta(F') \rangle \quad (4.135)$$

where

$$\langle \Delta(F)\Delta(F') \rangle = \frac{1}{3} \langle v_{o(1)}^2 \rangle \left[f \left(\frac{F}{H_0} - \frac{F'}{H_0} \right) - f \left(\frac{F}{H_0} \right) - f \left(\frac{F'}{H_0} \right) \right]. \quad (4.136)$$

Plugging Eq. (4.136) into Eq. (4.135), then using Eqs. (4.90) and (4.101), and then finally doing some rearranging, we find

$$\sigma_2^2 \approx \left(\frac{246960CH_0}{F_{max}^5 k_{eq}} \right)^2 \int_0^y \frac{dy}{y^3} T^2(y) \left[I \left(\frac{2k_{eq}F_{max}}{H_0} y \right) \right]^2 \quad (4.137)$$

where

$$I(q) \equiv \int_0^1 dx \left(\frac{3}{784}x - \frac{3}{280}x^2 + \frac{1}{140}x^3 \right) (\sin qx - qx \cos qx). \quad (4.138)$$

This result for σ_2^2 does not depend on the sample size, as it only depends on the size of the redshift range F_{max} , making it a measure of cosmic variance. By integrating numerically, we find that it scales roughly as F_{max}^{-8} and

$$\sigma_2^2 \sim 0.03 \left(\frac{z_{max}}{0.2} \right)^{-8}. \quad (4.139)$$

For comparison, Ref. [51] uses a sample of 115 supernovae up to a redshift $z_{max} = 1.01$, and they find an error from the data of $\Delta\Omega_\Lambda = -0.04$. For this same scenario, we estimate $|\Delta\Omega_\Lambda| \approx 0.01$, from the sum of Eqs. (4.134) and (4.139).

4.6 Consistency with Prior Results

The method of analysis that we have presented in the previous sections differs from that of Refs. [10, 11, 13, 14]. This is because of (i) a difference in gauge choice and (ii) a fundamental difference in the definition of what constitutes ‘‘acceleration’’. We have chosen to use the standard post-Newtonian gauge, and to define acceleration as being based on fitting the luminosity distance-redshift relation to

that of a homogeneous model containing dust and a cosmological constant. As this definition of acceleration is based only on observable quantities, performing our calculation in other gauges gives us the same results.

In contrast, Refs. [10, 11, 13, 14] calculate the cosmological expansion rate, averaged over a constant time slice. The motivation for doing this comes from the spatially-averaged Friedmann equations, also called the Buchert equations [71]. In particular, Ref. [10] defines the effective coarse-grained scale factor a_D in terms of the average matter density: $\langle \rho \rangle_D \propto a_D^{-3}$, where the angle brackets $\langle \rangle_D$, with subscript D , denote an average over a spatial hypersurface D at a given time. Then Ref. [11] defines the coarse-grained Hubble rate

$$H_D = \frac{\dot{a}_D}{a_D} = \frac{1}{3} \langle \theta \rangle_D \quad (4.140)$$

and the effective deceleration parameter

$$q = -\frac{\dot{H}_D}{H_D^2} - 1 . \quad (4.141)$$

These measures of acceleration are somewhat arbitrary since the deceleration parameter (4.141) depends on the spatial hypersurface over which one averages. Refs. [10, 11, 13, 14] use constant time slices in the comoving synchronous gauge. In this gauge, the perturbation to the the expansion θ is related quite simply to the perturbations to the trace of the connection; from Ref. [10],

$$\langle \theta_{(1)} \rangle_D = \frac{1}{a} \langle \Gamma_{ti(1)}^i \rangle_D , \quad (4.142)$$

and similarly for $\theta_{(2)}$. Ref. [14] claims that spatially averaged perturbations could become quite large, which implies that our perception of the expansion rate of the Universe is significantly affected by inhomogeneity. The culprit is the appearance

of terms in $\Gamma_{ti(2)}^i$ with large numbers of spatial gradients, which naturally appear in the synchronous gauge. These higher derivative terms, which do not appear in our method above, lead to a perturbative instability, wherein terms higher order in perturbation theory do not get smaller as expected.

Although the results of the previous sections appear to differ from the claims of Refs. [10, 11, 13, 14], in fact the large fitting effect claimed in those papers arises at a higher post-Newtonian order than we have computed. In this section we show that our results are consistent with theirs to the order we have computed. Our method of computation could be extended to higher post-Newtonian order, which would allow for a detailed confrontation with their claims.

However, we believe that our result of a small fitting effect is robust, in the sense that it will not be altered by the inclusion of effects that are higher order in ϵ and/or δ . This belief is based on the structure of the post-Newtonian expansion of Einstein's equations, and on the fact that we are computing a gauge-invariant observable. If this is true, then our conclusion is in disagreement with Refs. [10, 11, 13, 14].

We believe the most likely reason for the disagreement is that we compute a gauge-invariant observable that is directly and uniquely related to supernova observations, whereas the quantities computed in Refs. [10, 11, 13, 14] have some arbitrariness and are not directly related to observations. The proposal of Refs. [10, 11, 13, 14] that there might be a large backreaction effect in terms of q_D does not necessarily imply that observers will measure large deviations from FRW dynamics. As mentioned above, spatially averaged perturbations are dependent on one's coordinate choice, in the sense that a constant time hypersurface in one

coordinate system is most likely not going to be a constant time hypersurface in a different coordinate system. These averages are unlikely to be directly observable, and are not uniquely related to the cosmic acceleration inferred from cosmological observations. As Hirata and Seljak [27] remarked, we “cannot cover the entire universe with astronomers so as to measure spatially averaged quantities” such as H_D . It is possible that the measure of acceleration (4.141) could be large while the observed acceleration is small.

We now turn to showing consistency of our results with those of Refs. [10, 11, 13, 14] to the order we have computed. We take our metric (4.9) and transform it from the post-Newtonian gauge to the synchronous gauge. We then compute from the transformed metric the perturbation to the Hubble rate. The relative size of the difference between H_D and the expected FRW value H determines whether or not there will be a large fitting effect. As an example, we will now compute the ratio

$$\frac{H_D - H}{H} \equiv \frac{\Delta H}{H} = \frac{\langle \theta_{(1)} + \theta_{(2)} \rangle_D}{3H} \quad (4.143)$$

where the spatial average involves integrating with respect to the perturbed volume element $dV = \sqrt{g_{space}} d^3x$, where g_{space} is the determinant of the spatial part of the metric. Note that the quantity that we define as $\Delta H/H$ differs from what is computed in Refs. [10, 11, 13, 14], although we do find the same qualitative result at the end of the day. Below we show that this quantity is small to Newtonian order, in correspondence with what was found in [10], even though it involves a sum of terms that can be large individually. The reason these terms are large is that in synchronous coordinates metric perturbations can be of order δ , which may be of considerable size even though there are no large gravitational potentials anywhere

in the Universe. By contrast, in our calculation based on standard post-Newtonian coordinates, metric perturbations are at most of order $\epsilon^2\delta$, which is always small. In this sense, perturbation expansions are much better behaved in the standard post-Newtonian coordinates than in synchronous coordinates.

We start by reviewing the transformation from standard post-Newtonian coordinates (4.9) to synchronous coordinates; a detailed discussion is presented in Appendix A.4. Begin with the second order perturbed FRW metric in the gauge

$$ds^2 = a^2(\eta) \left[- (1 + 2\Phi_{(1)} + 2\Phi_{(2)}) d\eta^2 + (1 - 2\Phi_{(1)} - 2\Phi_{(2)}) \delta_{ij} dX^i dX^j \right] , \quad (4.144)$$

where we are now using conformal and Cartesian coordinates for simplicity, and we will only need to work to Newtonian order. We can then define the new coordinates τ and \tilde{x}^i by

$$\eta = \tau \left[1 - \frac{1}{3}\Phi_{(1)} - \frac{1}{5}\Phi_{(2)} + \frac{2\tau^2}{45} (\nabla\Phi_{(1)})^2 \right] + O(\tau_0\epsilon^4) + O(\tau_0\delta^3) \quad (4.145)$$

and

$$X^i = \tilde{x}^i - \frac{\tau^2}{6}\Phi_{(1),i} - \frac{\tau^2}{20}\Phi_{(2),i} + \frac{\tau^4}{120}\Phi_{(1),ij}\Phi_{(1),j} + O(\tilde{x}^i\epsilon^2) + O(\tilde{x}^i\delta^3) , \quad (4.146)$$

where these potentials are fixed physical quantities, evaluated at (τ, \tilde{x}^i) , and these spatial derivatives are in terms of the new coordinates. We are also assuming that we have the growing mode only, for which we have the power law scalings $\Phi_{(1)} \propto \tau^0$ and $\Phi_{(2)} \propto \tau^2$. Then the line element becomes, to lowest order in ϵ ,

$$\begin{aligned} ds^2 &= a^2(\tau) \left[-d\tau^2 + \tilde{g}_{ij} d\tilde{x}^i d\tilde{x}^j \right] \\ &= a^2(\tau) \left\{ -d\tau^2 + \left[\delta_{ij} - \frac{\tau^2}{3}\Phi_{(1),ij} - \frac{\tau^2}{10}\Phi_{(2),ij} + \frac{\tau^4}{60}\Phi_{(1),ijk}\Phi_{(1),k} \right. \right. \\ &\quad \left. \left. + \frac{2\tau^4}{45}\Phi_{(1),ik}\Phi_{(1),jk} + O(\epsilon^2) \right] d\tilde{x}^i d\tilde{x}^j \right\} , \quad (4.147) \end{aligned}$$

which is now in a synchronous gauge. Note that the metric now has perturbations of order $\varepsilon^0 \delta \sim \delta$, and these are the terms that will lead to the appearance of a large $\Delta H/H$. Then we find

$$\sqrt{g_{space}} = a^3(\tau) \left[1 - \frac{\tau^2}{6} \nabla^2 \Phi_{(1)} + O(\delta^2) \right]. \quad (4.148)$$

The spatial trace of the connection is

$$\Gamma_{\tau i}^i = \frac{1}{2a^2} \tilde{g}^{ij} (a^2 \tilde{g}_{ij})_{,\tau} \quad (4.149)$$

which receives the first and second order perturbations

$$\Gamma_{\tau i(1)}^i = a(\tau) \theta_{(1)} = \frac{1}{2} \delta^{ij} \tilde{g}_{ij(1),\tau} = -\frac{\tau}{3} \nabla^2 \Phi_{(1)} + O(\delta \varepsilon^2) \quad (4.150)$$

and

$$\begin{aligned} \Gamma_{\tau i(2)}^i = a(\tau) \theta_{(2)} &= \frac{1}{2} \tilde{g}^{ij(1)} \tilde{g}_{ij(1),\tau} + \frac{1}{2} \delta^{ij} \tilde{g}_{ij(2),\tau} \\ &= -\frac{\tau^3}{45} \Phi_{(1),ij} \Phi_{(1),ij} - \frac{\tau}{10} \nabla^2 \Phi_{(2)} + \frac{\tau^3}{30} (\nabla^2 \Phi_{(1)})_{,k} \Phi_{(1),k} \\ &\quad + O(\delta^2 \varepsilon^2). \end{aligned} \quad (4.151)$$

Using the Fourier transformation (4.92), taking an ensemble average, and using the result that $\langle \nabla^2 \Phi_{(2)} \rangle = 0$ (see Appendix A.3), we find from Eqs. (4.143) and (4.142)

$$\begin{aligned} \frac{\Delta H}{H} &\approx \frac{1}{3Ha} \left\langle \frac{\tau^3}{18} (\nabla^2 \Phi_{(1)})^2 - \frac{\tau^3}{45} \Phi_{(1),ij} \Phi_{(1),ij} + \frac{\tau^3}{30} (\nabla^2 \Phi_{(1)})_{,k} \Phi_{(1),k} \right\rangle \\ &= \frac{\tau^3}{135Ha} \left\langle (\nabla^2 \Phi_{(1)})^2 - \Phi_{(1),ij} \Phi_{(1),ij} \right\rangle \\ &= \frac{\tau^3}{135Ha} \left\langle [\Phi_{(1),i} \nabla^2 \Phi_{(1)} - \Phi_{(1),j} \Phi_{(1),ij}]_{,i} \right\rangle, \end{aligned} \quad (4.152)$$

which is consistent with the lowest order result of Ref. [10]. This spatial average is a boundary term, whose ensemble average vanishes.

Although (4.152) vanishes, it contains terms with two more powers of k/H_0 than what one would find in the post-Newtonian gauge. It is these terms that Refs. [11, 14] argue will lead to a large effect at higher order in perturbation theory. In other words, using the synchronous gauge and defining acceleration in terms of spatially averaged expansion parameters can lead to a conceivably large correction. This is in contrast to our earlier method, wherein we calculate the observable effect, which is very small. Note that our expansion (A.5) for $D_L(z)$ contains no four-derivative terms like those in (4.152).

4.7 Conclusions

We have computed the inhomogeneity-induced perturbations to the redshifts and luminosity distances that a comoving observer would measure to first post-Newtonian order, i.e. we have computed z and $H_0 D_L$ to order $\varepsilon^3 \sim (v/c)^3$, and to second order in the density perturbation $\delta = (\rho - \langle \rho \rangle) / \langle \rho \rangle$. Assuming a flat and matter-dominated background cosmology, the perturbed luminosity distance-redshift relation is given by Eq. (4.88). The perturbations to $D_L(z)$ depend on the correlation between the peculiar velocities at the observer and at the source. Roughly speaking, these perturbations are of order $\Delta D_L / D_L \sim 10^{-5}$ when $z \sim 0.1$. The luminosity distance-redshift relation was averaged over viewing angles and over an ensemble of realizations of the density perturbation. The result is gauge invariant, as it corresponds to a measurable quantity. We then fit this function to what one would expect in a homogeneous FRW cosmology, containing dust and a cosmological constant, to deduce the corresponding perturbation to the inferred cosmological constant density.

The inferred Ω_Λ depends on the limiting redshifts z_{min} and z_{max} of the sample, and we summarize the best-fit values of Ω_Λ for different values of these limiting redshifts in Figure 4.1 and Table 4.1. These ensemble averaged results indicate that we are justified in fitting low- z supernova data to homogeneous models, as long as we use supernova data that spans a large enough redshift range. For instance, assuming that we have luminosities and redshifts from $z_{min} = 0.02$ out to $z_{max} = 0.15$, the errors induced by the “fitting problem” are small: $\Omega_\Lambda \sim 0.004$. Such errors are not large enough to explain the measured value $\Omega_\Lambda \approx 0.7$. This is what we would expect, since we have other evidence to suggest that our universe contains dark energy from large scale structure surveys, from the CMB power spectrum, and from weak lensing.

In contrast to the small value of the best-fit Ω_Λ for the ensemble averaged luminosity distance-redshift relation, we find that relatively large errors are possible due to fluctuations in $D_L(z)$, specifically from terms that are linear in peculiar velocities. This effect was noted in Ref. [70] and then calculated in Ref. [51] for an actual nearby supernova data set. We find that the associated variance in Ω_Λ has two components, one that depends on the number of sources N , $\sigma_1^2 \sim (100/N)(z_{max}/0.2)^{-6}$, and one that does not, $\sigma_2^2 \sim 0.03(z_{max}/0.2)^{-8}$.

It should be stressed that our goal in this chapter was only to find a rough estimate of the fitting effect. One potential weakness of our analysis is that we have assumed that $\delta < 1$, and thus we do not address the effects of highly nonlinear structures. Such nonlinear modes could be included by using the full nonlinear power spectrum from N-body simulations [68], and we estimate that this would change the result by approximately a factor of two. Furthermore, we have assumed

that the observer is in a random location in the Universe, and has no knowledge of his/her own peculiar velocity. One can redo the calculation for an observer who knows and corrects for this velocity.

It has been claimed that there exists a perturbative instability, where successive orders in an expansion in powers of δ do not get smaller [10, 11, 14]. We do not see any indications of such an instability with our method. When one defines “acceleration” in terms of only directly observable quantities, as we did in Sections 4.2 through 4.5, the fitting effect one obtains is small.

Chapter 5

Summary of Results

5.1 Models Used in this Study

The aim of this thesis was to calculate systematic inhomogeneity-induced corrections to the measured luminosity distance-redshift relation $D_L(z)$, and then to find the impact that such corrections have on our interpretation of supernova data and the computation of best-fit cosmological parameters. We accomplished this task by evaluating a series of models for cosmological structure formation. Each of these models was matter dominated, flat on average, and with gravity dictated by general relativity; we addressed these models in order of increasing sophistication and realism.

In Chapter 2, we explored this problem in spherical symmetry, using LTB models. These are useful since they let us attack this problem non-perturbatively. However, these are only toy models as they require geocentricity so as to match the observed isotropy of the CMB.

We used a more realistic model of structure formation in Chapter 3, wherein we constructed a model for cosmological voids and sheets. In this model, we cut spheres out of an FRW background and then placed this matter in mass compensating shells at the boundaries.

In Chapter 4, we attacked this problem in full three dimensional generality, with a perturbative calculation. We computed the perturbed luminosity distance

and redshift to second order in the density contrast $\delta = \delta\rho/\rho$ and to third order in the fluid velocity v/c . We also assumed δ at a given time to be a homogeneous random process.

5.2 Systematic Corrections to $D_L(z)$ and Their Impact on the Assessment of Acceleration

Through this series of studies, we have found that local inhomogeneity does systematically affect the luminosity distance-redshift relation $D_L(z)$. Then we found that these systematic corrections could mimic dark energy, in principle, although such effects are expected to be very small in realistic models.

Our analysis of the spherically-symmetric LTB models showed that inhomogeneity could conceivably mimic dark energy. We found that inhomogeneity does in fact alter $D_L(z)$, and significant corrections are possible if one does not constrain the amplitudes or the wavelengths of density perturbations. If such supernova data are then interpreted in the framework of a flat homogeneous model, the deceleration parameter q and the effective equation of state parameter w_{eff} could both become negative, signaling acceleration. We found that it is very difficult to match the $D_L(z)$ of a Λ CDM model with an LTB model, although this has been accomplished recently [53].

In our void and sheet model, we find very different results. This is because this is a much more realistic model of structure formation, and also because we included only Newtonian effects. In this framework, we found that large voids and sheets

of matter do not affect redshifts, although they have a small nonzero effect on the magnification. However, taking the limit of an infinite number of sources, we found that there is no systematic effect on the luminosity distance-redshift relation to this order. This is in accordance with the results of Holz and Wald [50].

We then found the lowest order systematic effect with a perturbative post-Newtonian calculation, in full three dimensional generality, in Chapter 4. Here we found that redshifts and luminosity distances are affected by gravitational redshifts, the Doppler effect, gravitational lensing, and the integrated Sachs-Wolfe effect. We then found that the leading order correction to $D_L(z)$ depends on the two point velocity correlation function. This leads to a large effect for very small z and an order $\lesssim 10^{-5}$ effect for modest redshifts above $z \sim 0.01$. This perturbed relation is then fit to a homogeneous FRW model that contains matter and a cosmological constant with a density Ω_Λ . We find that the correction to the best-fit Ω_Λ is larger than expected: $\Omega_\Lambda \approx 0.004$, for a catalog that extends from a redshift $z_{min} = 0.02$ to a redshift $z_{max} = 0.15$. This is far too small to explain the current best-fit value $\Omega_\Lambda \sim 0.7$, although this is still a possibly important source of systematic error. We also found a significant variance in Ω_Λ , for a sample of N supernovae out to a redshift z_{max} : $\sigma_\Lambda^2 \sim (100/N)(v_{max}/0.2)^{-6} + 0.03(v_{max}/0.2)^{-8}$.

Appendix A

Details of the Calculation in Chapter 4

A.1 Combining the Redshift and Luminosity Distance Relations

Adding the redshift equations (4.77), (4.85), and (4.86) yields

$$\begin{aligned}
z(t, r, \theta, \phi) = & \left[\frac{2r}{3t} + \frac{r^2}{9t^2} + \frac{4r^3}{27t^3} + O(\varepsilon^4) \right] \\
& + \left[v_{s(1)}^r - v_{o(1)}^r + \Phi_{o(1)} - \Phi_{s(1)} + \frac{2r}{3t} (v_{s(1)}^r - v_{o(1)}^r) - 2 \int_0^r \dot{\Phi}_{(1)} dr' \right. \\
& \left. + \frac{2r}{3t} \Phi_{o(1)} - \frac{2r}{t} \Phi_{s(1)} - \frac{r^2}{9t^2} v_{o(1)}^r + \frac{r^2}{3t^2} v_{s(1)}^r + O(\varepsilon^4 \delta) \right] \\
& + \left\{ v_{s(2)}^r - v_{o(2)}^r + \Phi_{o(2)} - \Phi_{s(2)} + \frac{2r}{3t} (v_{s(2)}^r - v_{o(2)}^r) + \frac{1}{2} (v_{s(1)}^2 - v_{o(1)}^2) \right. \\
& + (v_{o(1)}^r)^2 - v_{o(1)}^r v_{s(1)}^r - 2 \int_0^r \dot{\Phi}_{(2)} dr' + \left(v_{\theta(1)} k_{(1)}^\theta + v_{\phi(1)} k_{(1)}^\phi \right)_o \\
& - \left(v_{\theta(1)} k_{(1)}^\theta + v_{\phi(1)} k_{(1)}^\phi \right)_s + \frac{2r}{3t} \Phi_{o(2)} - \frac{2r}{t} \Phi_{s(2)} - \frac{r^2}{9t^2} v_{o(2)}^r + \frac{r^2}{3t^2} v_{s(2)}^r \\
& + \frac{r}{3t} \left[(v_{s(1)})^2 - (v_{o(1)})^2 \right] + \frac{2r}{3t} \left[(v_{s(1)}^r)^2 + (v_{o(1)}^r)^2 - v_{s(1)}^r v_{o(1)}^r \right] \\
& + \Phi_{o(1)} v_{o(1)}^r + \Phi_{s(1)} v_{o(1)}^r + \Phi_{o(1)} v_{s(1)}^r - 3\Phi_{s(1)} v_{s(1)}^r + x_{(1)}^i v_{s(1),i}^r \\
& \left. + O(\varepsilon^4 \delta^2) \right\} + O(\varepsilon \delta^3) . \tag{A.1}
\end{aligned}$$

where the right hand side is evaluated at $r = r(\lambda) = -\lambda$ and $t = t(\lambda) = t_0 + \lambda$.

To point out a few of the above effects, the terms linear in velocity and linear in Φ correspond to the Doppler effect and the gravitational redshift, respectively.

We also see the second order Doppler shift with the v^2 terms, and the integrated Sachs-Wolfe effect with the integrated terms. The perturbed luminosity distance

is found from Eqs. (4.78), (4.82), and (4.83) to be

$$\begin{aligned}
D_L(t, r, \theta, \phi) = & \frac{(1+z)^2 2r}{H_0 3t} \left\{ \left[1 - \frac{r}{t} + \frac{8r^2}{9t^2} + O(\varepsilon^3) \right] \right. \\
& - \left[\int_0^r \frac{dr'}{r'^2} \int_0^{r'} (r'')^2 \nabla^2 \Phi_{(1)} dr'' + O(\varepsilon^3 \delta) \right] \\
& - \left[\int_0^r \frac{dr'}{r'^2} \int_0^{r'} (r'')^2 \nabla^2 \Phi_{(2)} dr'' + O(\varepsilon^3 \delta^2) \right] \\
& \left. + O(\varepsilon \delta^3) \right\}. \tag{A.2}
\end{aligned}$$

Here we can see the effects of weak gravitational lensing. Note that as the cosmological portion of the redshift goes to zero, and hence $r \rightarrow 0$, the luminosity distance also goes to zero, as expected.

By combining Eqs. (A.1) and (A.2), we can eliminate λ and compute D_L as a function of z , θ , and ϕ . This computation can be carried out explicitly by using the fact that the expressions are power series in ε and δ . This procedure gives

$$D_L(z, \theta, \phi) \approx D_L^a(z, \theta, \phi) + D_L^b(z, \theta, \phi), \tag{A.3}$$

where

$$\begin{aligned}
D_L^a(z, \theta, \phi) \equiv & \frac{(1+z)^2}{H_0} \left\{ z - \frac{7}{4}z^2 + \frac{19}{8}z^3 + \left(-1 + \frac{5}{2}z - \frac{33}{8}z^2 \right) (v_{s(1)}^r + v_{s(2)}^r) \right. \\
& + \left(1 - \frac{5}{2}z + \frac{29}{8}z^2 \right) (v_{o(1)}^r + v_{o(2)}^r) + \left(1 - \frac{1}{2}z \right) (\Phi_{s(1)} + \Phi_{s(2)}) \\
& + \left(-1 + \frac{5}{2}z \right) (\Phi_{o(1)} + \Phi_{o(2)}) + \left(\frac{1}{2} - \frac{5}{4}z \right) (v_{o(1)}^2 - v_{s(1)}^2) \\
& + \left(-\frac{7}{4} + \frac{29}{8}z \right) (v_{o(1)}^r)^2 + \left(-\frac{3}{4} + \frac{9}{8}z \right) (v_{s(1)}^r)^2 \\
& \left. + \left(\frac{5}{2} - \frac{23}{4}z \right) v_{o(1)}^r v_{s(1)}^r + \frac{1}{2} v_{o(1)}^r (\Phi_{o(1)} - \Phi_{s(1)}) \right\} \tag{A.4}
\end{aligned}$$

and

$$\begin{aligned}
D_L^b(z, \theta, \phi) \equiv & \frac{(1+z)^2}{H_0} \left\{ \frac{5}{2} v_{s(1)}^r (\Phi_{s(1)} - \Phi_{o(1)}) \right. \\
& - x_{(1)}^i v_{s(1),i}^r + \int_0^r \left(\dot{\Phi}_{(1)} + \dot{\Phi}_{(2)} \right) dr' + \left(v_{\theta(1)} k_{(1)}^\theta + v_{\phi(1)} k_{(1)}^\phi \right)_s \\
& \left(v_{\theta(1)} k_{(1)}^\theta + v_{\phi(1)} k_{(1)}^\phi \right)_o - (z + v_{o(1)}^r - v_{s(1)}^r) \int_0^r \frac{dr'}{r'^2} \int_0^{r'} (r'')^2 \nabla^2 \Phi_{(1)} dr'' \\
& - z \int_0^r \frac{dr'}{r'^2} \int_0^{r'} (r'')^2 \nabla^2 \Phi_{(2)} dr'' \\
& + (v_{s(1)}^r - v_{o(1)}^r) \left[z \frac{d}{dz} \int_0^r \frac{dr'}{r'^2} \int_0^{r'} (r'')^2 \nabla^2 \Phi_{(1)} dr'' - 2 \frac{d}{dz} \int_0^r \dot{\Phi}_{(1)} dr' \right] \\
& + \left[\Phi_{s(1)} - \Phi_{o(1)} + \left(1 + \frac{1}{2} z \right) (v_{o(1)}^r - v_{s(1)}^r) \right] \frac{d}{dz} \Phi_{s(1)} \\
& - \left[2 \int_0^r \dot{\Phi}_{(1)} dr' + \left(-1 + \frac{3}{2} z \right) \Phi_{o(1)} + \left(1 + \frac{1}{2} z \right) \Phi_{s(1)} \right. \\
& \left. + \left(1 - \frac{3}{2} z + \frac{13}{8} z^2 \right) v_{o(1)}^r + \left(-1 + \frac{3}{2} z - \frac{17}{8} z^2 \right) v_{s(1)}^r \right] \\
& \left. \times \frac{d}{dz} v_{s(1)}^r \right\}. \tag{A.5}
\end{aligned}$$

Here, $d/dz \approx (3t_0/2)\partial/\partial r$ to leading order, and we have had to split up D_L in a very unappealing way so that we do not leave too much white space and thus have an inappropriately-formatted thesis. The functions of r and t that appear on the right hand side of Eq. (A.5) are evaluated at $r = z/H_0$ and $t = t_0 - z/H_0$. Note that the redshift z here is the full redshift as measured by the observer. Next we need to average $D_L(z, \theta, \phi)$ over viewing angles in the observer's rest frame, and also take an ensemble average. In doing so, the averages of first order quantities will vanish. We also will find that we will only need the second order velocities and potentials to Newtonian order, so that we may compute the lowest-order effect.

A.2 Newtonian Second-Order Perturbation Theory

In terms of comoving coordinates $\mathbf{r} = \mathbf{x}/a(t)$ [33], the equations of Newtonian hydrodynamics are

$$\frac{\partial \delta}{\partial t} + \frac{1}{a} \nabla \cdot [(1 + \delta) \mathbf{v}_p] = 0 , \quad (\text{A.6})$$

$$\frac{\partial \mathbf{v}_p}{\partial t} + \frac{\dot{a}}{a} \mathbf{v}_p + \frac{1}{a} (\mathbf{v}_p \cdot \nabla) \mathbf{v}_p = -\frac{\nabla \Phi_p}{a} , \quad (\text{A.7})$$

and

$$\nabla^2 \Phi_p = 4\pi \rho_0 a^2 \delta , \quad (\text{A.8})$$

where $\mathbf{v}_p = \mathbf{v}_{(1)} + \mathbf{v}_{(2)} + \dots$ is the peculiar velocity, $\Phi_p = \Phi_{(1)} + \Phi_{(2)} + \dots$ is the perturbation to the Newtonian gravitational potential, the density contrast is $\delta = [\rho(\mathbf{r}, t) - \rho_0(t)]/\rho_0(t)$, and the zeroth order quantities are given in Section 4.2. The Newtonian first order results are very well known; for a detailed review, see Peebles [33]. For a Newtonian analysis to second order in δ , see Ref. [72].

The first order result is that the density contrast consists of mode that grows with time, and one that decays with time:

$$\delta_{(1)}(\mathbf{r}, t) = f(\mathbf{r})t^{2/3} + g(\mathbf{r})t^{-1} , \quad (\text{A.9})$$

where f and g are functions of the spatial coordinates. We will only consider the growing mode. It is useful to rewrite the hydrodynamic equations in terms of their Fourier modes. Writing

$$\delta = \int \frac{d^3 k}{(2\pi)^3} \delta_{\mathbf{k}} e^{i\mathbf{k} \cdot \mathbf{r}} \quad (\text{A.10})$$

and

$$\Phi_p = \int \frac{d^3 k}{(2\pi)^3} \Phi_{\mathbf{k}} e^{i\mathbf{k} \cdot \mathbf{r}} , \quad (\text{A.11})$$

Eq. (A.8) becomes

$$k^2\Phi_{\mathbf{k}} = 4\pi\rho_0a^2\delta_{\mathbf{k}}. \quad (\text{A.12})$$

The second order density contrast is

$$\delta_{(2)} = \frac{9t^4}{14a^4t_0^4} \left(\Phi_{(1),ij}\Phi_{(1),j} + \frac{5}{2}\nabla^2\Phi_{(1)}\Phi_{(1),i} \right)_{,i}; \quad (\text{A.13})$$

this result came from perturbing Eqs. (A.6)-(A.8) to second order and then solving these by using the first order solutions, Eqs. (A.9) and (A.11). It can be seen that the expected value of $\delta_{(2)}$ vanishes by substituting the mode expansion of $\Phi_{(1)}$ into Eq. (A.13): $\langle\delta_{(2)}\rangle = 0$. We also see from Eq. (A.12) that $\langle\Phi_p\rangle$ depends only on boundary conditions; we can choose to add overall constants to Φ at each order in δ , and it is natural to choose these constants to satisfy $\langle\Phi_{(1)}\rangle = \langle\Phi_{(2)}\rangle = 0$.

Assuming that we only have the growing mode solution of Eq. (A.9), we find that the first order peculiar velocity is related to the Newtonian potential,

$$\mathbf{v}_{(1)}(\mathbf{r}, t) = -\frac{t}{a(t)}\nabla\Phi_{(1)} = -t^{1/3}t_0^{2/3}\nabla\Phi_{(1)}. \quad (\text{A.14})$$

This averages to zero but its square does not. The second order velocity perturbation is

$$v_{(2)}^i = -\frac{3t^3}{14a^3}\Phi_{(1),ij}\Phi_{(1),j} \quad (\text{A.15})$$

which also averages to zero: $\langle v_{(2)}\rangle = 0$. Note that these averages are ensemble averages, not spatial averages.

A.3 Averaging the Luminosity Distance-Redshift Relation

Now we can scrutinize the terms of Eq. (A.5), so that we may find their angular and ensemble averages. Note that the angular averages will be performed with respect

to the observer's angles $(\tilde{\theta}, \tilde{\phi})$, and so we will need to use the Jacobian given in Eq. (4.70). The first three terms of Eq. (A.5) only depend on the background cosmology, and are unchanged after averaging, and all terms that are to first order in δ will have a vanishing ensemble average. As shown in Appendix A.2, terms that depend on $v_{(2)}^i$ and $\Phi_{(2)}$ also average to zero.

In addition, there are many terms that have vanishing ensemble averages because they contain an odd number of spatial derivatives of the potential, such as

$$\langle v_{o(1)}^r \Phi_{o(1)} \rangle = \langle v_{s(1)}^r \Phi_{s(1)} \rangle = 0 , \quad (\text{A.16})$$

$$\left\langle v_{s(1)}^r \frac{\partial}{\partial r} v_{s(1)}^r \right\rangle = 0 , \quad (\text{A.17})$$

$$\langle x_{(1)}^i v_{s(1),i}^r \rangle = 0 , \quad (\text{A.18})$$

$$\left\langle v_{s(1)}^r \frac{d}{dz} \int_0^r \dot{\Phi}_{(1)} dr' \right\rangle = 0 , \quad (\text{A.19})$$

et cetera. We also find that

$$\left\langle \left(v_{\theta(1)} k_{(1)}^\theta + v_{\phi(1)} k_{(1)}^\phi \right)_s - \left(v_{\theta(1)} k_{(1)}^\theta + v_{\phi(1)} k_{(1)}^\phi \right)_o \right\rangle \sim O(\varepsilon^4) , \quad (\text{A.20})$$

since $v_{\theta(1)} k_{(1)}^\theta \sim v_{\phi(1)} k_{(1)}^\phi \sim \varepsilon^3$, and taking the difference of the averages at the source and at the observer introduces another factor of $z \sim \varepsilon$.

We can further rewrite the average $\langle v_{s(1)}^2 \rangle$ by exploiting the power law scaling $v_{(1)}^2 \propto t^{2/3}$, to find

$$\begin{aligned} \langle v_{s(1)}^2 \rangle &= \left\langle \left(t_0^{2/3} t^{1/3} \nabla \Phi_{(1)} \right)^2 \right\rangle \approx \left\langle \left(t_0^{2/3} \nabla \Phi_{(1)} \right)^2 \right\rangle (t_0 - r)^{2/3} \\ &= \langle v_{o(1)}^2 \rangle [1 - z + \mathcal{O}(z^2)] . \end{aligned} \quad (\text{A.21})$$

We also use $\langle (v_{(1)}^r)^2 \rangle = \langle v_{(1)}^2 \rangle / 3$, and introduce the two point correlation function

$f(r)$,

$$\langle v_{s(1)}^r v_{o(1)}^r \rangle = \frac{1}{3} \langle v_{o(1)}^2 \rangle \left(1 - \frac{1}{2} z \right) [1 + f(r)] , \quad (\text{A.22})$$

where $f(r)$ is defined by

$$\langle \mathbf{n} \cdot \mathbf{v}(\mathbf{r}_0, t) \mathbf{n} \cdot \mathbf{v}(\mathbf{r}_0 + r\mathbf{n}, t) \rangle = \frac{1}{3} \langle v_{o(1)}^2 \rangle [1 + f(r)] , \quad (\text{A.23})$$

and \mathbf{n} is a unit vector that defines the viewing direction.

We can write this correlation function in terms of a more general correlation function $c_{ij}(r)$, using the Fourier transform of Eq. (A.11) and Eqs. (4.94)-(4.97):

$$\langle v_{o(1)}^2 \rangle c_{ij}(r) \equiv \langle v_i(\mathbf{r}_0, t_0) v_j(\mathbf{r}_0 + \mathbf{r}, t_0) \rangle = \frac{H_0^2}{4\pi} \int_0^\infty \frac{d^3 k k_i k_j \Delta^2(k) e^{-i\mathbf{k} \cdot \mathbf{r}}}{k^7} . \quad (\text{A.24})$$

This function can be rewritten as

$$\langle v_{o(1)}^2 \rangle c_{ij}(r) \equiv H_0^2 \left[\frac{1}{3} A(r) \delta_{ij} + \frac{r_i r_j}{r^2} B(r) \right] , \quad (\text{A.25})$$

where

$$\begin{aligned} A(r) &= \frac{3}{8\pi} \int_0^\infty \frac{d^3 k \Delta^2(k)}{k^5} [1 - (\mathbf{k} \cdot \mathbf{r})^2] e^{-i\mathbf{k} \cdot \mathbf{r}} \\ &= \int_0^\infty \frac{dk \Delta^2(k)}{k^3} [j_0(kr) + j_2(kr)] \end{aligned} \quad (\text{A.26})$$

and

$$\begin{aligned} B(r) &= \frac{1}{8\pi} \int_0^\infty \frac{d^3 k \Delta^2(k)}{k^5} [3(\mathbf{k} \cdot \mathbf{r})^2 - 1] e^{-i\mathbf{k} \cdot \mathbf{r}} \\ &= \int_0^\infty \frac{dk \Delta^2(k)}{k^3} [-j_2(kr)] , \end{aligned} \quad (\text{A.27})$$

and where we are using spherical Bessel functions of the first kind:

$$j_0(x) = \frac{\sin x}{x} \quad (\text{A.28})$$

and

$$j_2(x) = \left(\frac{3}{x^3} - \frac{1}{x} \right) \sin x - \frac{3}{x^2} \cos x . \quad (\text{A.29})$$

It follows that

$$\begin{aligned} \frac{1}{3}\langle v_{o(1)}^2 \rangle [1 + f(r)] &= \langle v_{o(1)}^2 \rangle n^i n^j c_{ij}(r) = H_0^2 \left[\frac{1}{3}A(r) + B(r) \right] \\ &= \frac{C^2 k_{eq}^2}{H_0^2} \int_0^\infty y dy T^2(y) \left[\frac{1}{3}j_0 \left(\frac{k_{eq}zy}{H_0} \right) - \frac{2}{3}j_2 \left(\frac{k_{eq}zy}{H_0} \right) \right], \end{aligned} \quad (\text{A.30})$$

where $k_{eq} = 1/\lambda_c \sim 10^3 H_0$. We plot $1 + f(r)$ in Figure 4.2; we see that it falls to approximately zero for $r \gg \lambda_c \sim 10$ Mpc, and thus we do not expect it to be important when measuring the distances to supernovae at redshifts $z \sim 0.1$. Note also that f becomes negative for large enough r .

Using these simplifications, we finally get

$$D_L(z) = \frac{z}{H_0} \left(1 + \frac{1}{4}z - \frac{1}{8}z^2 \right) + \Delta D_L^{rms}(z) + \Delta D_L^{corr}(z), \quad (\text{A.31})$$

where $\Delta D_L^{rms}(z)$ is the perturbation that depends on RMS quantities at a given point, which vanishes:

$$\Delta D_L^{rms}(z) = 0, \quad (\text{A.32})$$

and $\Delta D_L^{corr}(z)$ is the perturbation that depends on f . To subleading order, this is

$$\begin{aligned} \Delta D_L^{corr}(z) &\approx \frac{(1+z)^2 \langle v_{o(1)}^2 \rangle}{H_0} \left[\frac{3}{2}f \left(\frac{z}{H_0} \right) - \frac{1}{3H_0} f' \left(\frac{z}{H_0} \right) (1-2z) \right] \\ &+ O \left(\frac{f \varepsilon^3 \delta^2}{H_0} \right), \end{aligned} \quad (\text{A.33})$$

where the subleading terms are suppressed by a factor of $\lambda_c H_0$ or z . We will only use the lowest order piece,

$$\begin{aligned} \Delta D_L(z) &= \Delta D_L^{corr}(z) \approx -\frac{\langle v_{o(1)}^2 \rangle}{3H_0^2} f' \left(\frac{z}{H_0} \right) \\ &= \frac{C^2 k_{eq}^3}{H_0^4} \int_0^\infty dy T^2(y) \left[\frac{y \cos(k_{eq}zy/H_0)}{k_{eq}z/H_0} - 3 \frac{\sin(k_{eq}zy/H_0)}{(k_{eq}z/H_0)^2} - 6 \frac{\cos(k_{eq}zy/H_0)}{(k_{eq}z/H_0)^3 y} \right. \\ &\quad \left. + 6 \frac{\sin(k_{eq}zy/H_0)}{(k_{eq}z/H_0)^4 y^2} \right]. \end{aligned} \quad (\text{A.34})$$

A.4 Transforming from the Standard Post-Newtonian Gauge to the Synchronous Gauge

In the standard post-Newtonian gauge discussed in Section 4.2, we can rewrite the metric in terms of conformal coordinates,

$$ds^2 = a^2(\eta) \left[- (1 + 2\Phi_{(1)} + 2\Phi_{(2)}) d\eta^2 + (1 - 2\Phi_{(1)} - 2\Phi_{(2)}) \delta_{ij} dX^i dX^j \right] , \quad (\text{A.35})$$

where we will only need this to Newtonian order, and now the scale factor is $a(\eta) = (\eta/\eta_0)^2$. We will define $\eta_0 \approx 3t_0$ to be the conformal time today. This new time coordinate is related to that of Sections 4.2 - 4.5 by

$$\eta = 3 \left(\frac{t}{t_0} \right)^{-2/3} t \left[1 - \frac{r^2}{9t^2} + O\left(\frac{r^4}{t^4}\right) \right] = \frac{3}{a} t + O(t\varepsilon^2) , \quad (\text{A.36})$$

and the radial coordinates are related by

$$R = \left(\frac{t}{t_0} \right)^{-2/3} r \left[1 + \frac{r^2}{9t^2} + O\left(\frac{r^4}{t^4}\right) \right] = \frac{r}{a} + O(r\varepsilon^2) , \quad (\text{A.37})$$

where $R = \sqrt{(X^1)^2 + (X^2)^2 + (X^3)^2}$. Thus, we see that the potentials are the same as before, to Newtonian order, except that they now are in terms of comoving distance X^i and conformal time η . We also now use Cartesian coordinates for simplicity.

Our goal is to transform to the synchronous gauge, with new coordinates $\tilde{x}^\mu = (\tau, \tilde{x}^i)$, where the line element has the form

$$ds^2 = a^2(\tau) \tilde{g}_{\mu\nu} d\tilde{x}^\mu d\tilde{x}^\nu = a^2(\tau) \left[-d\tau^2 + \tilde{g}_{ij} d\tilde{x}^i d\tilde{x}^j \right] . \quad (\text{A.38})$$

In this gauge, $\tilde{g}_{\tau\tau} = -1$ and $\tilde{g}_{\tau i} = \tilde{g}_{i\tau} = 0$. We make the following ansatz for the new coordinates:

$$\eta = \tau + f_{(1)}(\tau, \tilde{x}) + f_{(2)}(\tau, \tilde{x}) + O(\tau_0\varepsilon^4) \quad (\text{A.39})$$

and

$$X^i = \tilde{x}^i + h_{(1)}^i(\tau, \tilde{x}) + h_{(2)}^i(\tau, \tilde{x}) + O(\tilde{x}^i \varepsilon^2) , \quad (\text{A.40})$$

where $h_{(1)}^i \sim \delta \tilde{x}^i$, $h_{(2)}^i \sim \delta^2 \tilde{x}^i$, $f_{(1)} \sim \delta \tau_0 \varepsilon^2$, $f_{(2)} \sim \delta^2 \tau_0 \varepsilon^2$, and $\tau_0 \sim \eta_0$ is the time today. We are also assuming that we have the growing mode only, for which we have the power law scalings $\Phi_{(1)} \propto \tau^0$ and $\Phi_{(2)} \propto \tau^2$.

In order to find the new metric, we will need the relations

$$a^2(\eta) = a^2(\tau) \left[1 + \frac{4}{\tau} f_{(1)} + \frac{4}{\tau} f_{(2)} + O(\varepsilon^4) \right] \quad (\text{A.41})$$

and

$$\begin{aligned} \Phi_{(1)}(\eta, X) + \Phi_{(2)}(\eta, X) &= \Phi_{(1)}(\tau, \tilde{x}) + \Phi_{(2)}(\tau, \tilde{x}) + \Phi_{(1),i} h_{(1)}^i \\ &+ O(\varepsilon^4) + O(\delta^3) . \end{aligned} \quad (\text{A.42})$$

Using these and the coordinate transformations (A.39) and (A.40), we find

$$\begin{aligned} \tilde{g}_{\tau\tau} &= - \left(1 + \frac{4}{\tau} f_{(1)} + \frac{4}{\tau} f_{(2)} + 2\Phi_{(1)} + 2\Phi_{(1),i} h_{(1)}^i + 2\Phi_{(2)} + 2\dot{f}_{(1)} + 2\dot{f}_{(2)} \right) \\ &\quad + \left(\dot{h}_{(1)} \right)^2 \\ &= -1 , \end{aligned} \quad (\text{A.43})$$

implying

$$\frac{2}{\tau} f_{(1)} + \Phi_{(1)} + \dot{f}_{(1)} = 0 \quad (\text{A.44})$$

and

$$\frac{4}{\tau} f_{(2)} + 2\Phi_{(1),i} h_{(1)}^i + 2\Phi_{(2)} + 2\dot{f}_{(2)} - \dot{h}_{(1)}^i \dot{h}_{(1)}^i = 0 . \quad (\text{A.45})$$

Similarly, the time-space component of the new metric is

$$\tilde{g}_{\tau i} = -f_{(1),i} - f_{(2),i} + \dot{h}_{(1)}^i + \dot{h}_{(2)}^i + h_{(1),i}^j \dot{h}_{(1)}^j + O(\varepsilon^3) = 0 \quad (\text{A.46})$$

and this implies

$$-f_{(1),i} + \dot{h}_{(1)}^i = 0 \quad (\text{A.47})$$

and

$$-f_{(2),i} + \dot{h}_{(2)}^i + h_{(1),i}^j \dot{h}_{(1)}^j = 0 . \quad (\text{A.48})$$

Equations (A.44), (A.45), (A.47) and (A.48) are solved by

$$f_{(1)} = -\frac{\tau}{3}\Phi_{(1)} + \frac{A}{\tau^2} , \quad (\text{A.49})$$

$$f_{(2)} = -\frac{\tau}{5}\Phi_{(2)} + \frac{2\tau^3}{45}(\nabla\Phi_{(1)})^2 + \frac{B}{\tau^2} - \frac{\tau}{6}h_0^i\Phi_{(1),i} , \quad (\text{A.50})$$

$$h_{(1)}^i = -\frac{\tau^2}{6}\Phi_{(1),i} + h_0^i(\tilde{x}) , \quad (\text{A.51})$$

and

$$h_{(2)}^i = -\frac{\tau^2}{20}\Phi_{(2),i} + \frac{\tau^4}{120}\Phi_{(1),ij}\Phi_{(1),j} - \frac{\tau^2}{12}\Phi_{(1),ji}h_0^j + \frac{\tau^2}{12}\Phi_{(1),j}h_{0,i}^j + \tilde{h}_0^i(\tilde{x}) , \quad (\text{A.52})$$

where the arbitrary constants A and B and functions $h_0^i(\tilde{x})$ and $\tilde{h}_0^i(\tilde{x})$ represent residual gauge freedoms associated with synchronous coordinates. Setting A and B to zero will give us comoving coordinates. We can imagine comoving coordinates to be fixed on some spacelike hypersurface from which the worldlines of freely falling particles emanate. If we set all of the clocks carried by these particles to the same time on this spacelike hypersurface, then $A = B = 0$. The residual functions h_0^i and \tilde{h}_0^i correspond to simply changing the coordinates on the spacelike hypersurface from which worldlines emanate, and we will set $h_0^i = \tilde{h}_0^i = 0$. Using this solution for the appropriate coordinate transformation, we find the spatial part of the new

metric to be

$$\begin{aligned}
\tilde{g}_{ij} &= \delta_{ij} \left[1 + \frac{4}{\tau} f_{(1)} + \frac{4}{\tau} f_{(2)} - 2\Phi_{(1)} - 2\Phi_{(2)} - 2\Phi_{(1),k} h_{(1)}^k \right] - f_{(1),i} f_{(1),j} + h_{(1)i,j} + h_{(1)j,i} \\
&\quad + h_{(2)i,j} + h_{(2)j,i} + h_{(1)k,i} h_{(1)k,j} + \left[\frac{4}{\tau} f_{(1)} - 2\Phi_{(1)} \right] [h_{(1)i,j} + h_{(1)j,i}] + O(\varepsilon^4) + O(\delta^3) \\
&= \delta_{ij} - \frac{\tau^2}{3} \Phi_{(1),ij} - \frac{\tau^2}{10} \Phi_{(2),ij} + \frac{\tau^4}{60} \Phi_{(1),ijk} \Phi_{(1),k} + \frac{2\tau^4}{45} \Phi_{(1),ik} \Phi_{(1),jk} \\
&\quad + O(\varepsilon^2) + O(\delta^3) .
\end{aligned} \tag{A.53}$$

BIBLIOGRAPHY

- [1] A. G Riess *et al.*, *Astron. J.* **116**, 1009 (1998).
- [2] S. Perlmutter *et al.*, *Astrophys. J.* **517**, 565 (1999).
- [3] M. M. Phillips, *Astrophys. J.* **413**, L105 (1993).
- [4] R. Miquel, astro-ph/0703459.
- [5] E. V. Linder, *Phys. Rev. Lett.* **90**, 091301 (2003).
- [6] P. Coles and F. Lucchin, *Cosmology*, 2nd ed. (John Wiley and Sons, 2002).
- [7] C. L. Bennett *et al.*, *Astrophys J. Suppl.* **148**, 1 (2003).
- [8] P. J. E. Peebles and B. Ratra, *Rev. Mod. Phys.* **75**, 559 (2003).
- [9] S. M. Carroll, V. Duvvuri, M. Trodden, and M. S. Turner, *Phys. Rev. D* **70**, 043528 (2004).
- [10] E. W. Kolb, S. Matarrese, A. Notari, and A. Riotto, *Phys. Rev. D* **71**, 023524 (2005).
- [11] E. W. Kolb, S. Matarrese, and A. Riotto, astro-ph/0506534.
- [12] E. W. Kolb, S. Matarrese, and A. Riotto, astro-ph/0511073.
- [13] S. Räsänen, *JCAP* **0402**, 003 (2004).
- [14] A. Notari, astro-ph/0503715.
- [15] G. F. R. Ellis, Invited papers 10th int. conf. on general relativity and gravitation, p. 215 (1984).
- [16] G. F. R. Ellis and W. Stoeger, *Class. Quant. Grav.* **4**, 1697 (1987).
- [17] This idea from É. Flanagan, private communication.
- [18] Ya. B. Zel'dovich, *Soviet Astronomy* **8**, 13 (1964).
- [19] C. C. Dyer and R. C. Roeder, *Astrophys. J.* **174**, L115 (1972).
- [20] H. Bondi, *MNRAS* **107**, 410 (1947).
- [21] Y. Nambu and M. Tanimoto, gr-qc/0507057.
- [22] J. W. Moffat, astro-ph/0505326.
- [23] R. Mansouri, astro-ph/0512605.

- [24] C.-H. Chuang, J.-A. Gu, and W.-Y. P. Hwang, astro-ph/0512651.
- [25] H. Alnes, M. Amazguioui, and Ø. Grøn, astro-ph/0506449.
- [26] E. E. Flanagan, Phys. Rev. D **71**, 103521 (2005).
- [27] C. M Hirata and U. Seljak, Phys. Rev. D **72**, 083501 (2005).
- [28] N. Mustapha, B. A. Bassett, C. Hellaby, and G. F. R. Ellis, MNRAS **292**, 817 (1997).
- [29] N. Sugiura, K. I. Nakao, and T. Harada, Phys. Rev. D **60**, 103508 (1999).
- [30] M. N. Célérier, Astron. and Astrophys. **353**, 63 (2000).
- [31] H. Iguchi, T. Nakamura, and K. Nakao, Prog. of Theo. Phys. **108**, 809 (2002).
- [32] F. J. Tipler, Phys. Lett. **64A**, 8 (1977).
- [33] P. J. E. Peebles, *The Large-Scale Structure of the Universe*, 1st ed. (Princeton University Press, 1980), Ch. 10.
- [34] H. Alnes, M. Amazguioui, and Ø. Grøn, astro-ph/0512006.
- [35] J. Schneider and M. N. Célérier, Astron. and Astrophys. **348**, 25 (1999).
- [36] B. A. Benson *et al.*, Astrophys.J. **592**, 674 (2003).
- [37] J. R. Bond, L. Kofman, and D. Pogosyan, Nature **380**, 603 (1996).
- [38] A. Einstein and E. G. Straus, Rev. Mod. Phys. **17**, 120 (1945).
- [39] E. Schucking, Zs. f. Phys. **137**, 595 (1954).
- [40] R. Kantowski, Astrophys. J. **155**, 89 (1969).
- [41] L. Amendola, J. A. Frieman and I. Waga, MNRAS **309**, 465-473 (1999).
- [42] N. Sugiura, K. Nakao, D. Ida, N. Sakai, and H. Ishihara, Prog. of Theo. Phys. **103** 73 (2000).
- [43] N. Brouzakis, N. Tetradis, and E. Tzavara, astro-ph/0703586.
- [44] W. Israel, Nuovo Cimento **44B**, 1 (1966).
- [45] E. Poisson, *An Advanced Course in General Relativity*, draft of January 2002.
- [46] R. D. Blandford and R. Narayan, Annu. Rev. Astron. Astrophys. **30**, 311-358 (1992).
- [47] S. Weinberg, Ap. J. **208**, L1-L3 (1976).

- [48] A. Babul and M. H. Lee, MNRAS **250**, 407-413 (1991).
- [49] J. A. Frieman, Comm. in Astrophys. **18**, 323 (1996).
- [50] D. E. Holz and R. M. Wald, Phys. Rev. D. **58**, 063501 (1998).
- [51] J. D. Neill, M. J. Hudson, and A. Conley, arXiv:0704.1654.
- [52] C. Gordon, K. Land, and A. Slosar, arXiv:0705.1718.
- [53] D. Garfinkle, Class. and Quant. Grav. **23**, 4811 (2006).
- [54] T. Biswas and A. Notari, astro-ph/0702555.
- [55] T. Kai, H. Kozaki, K. Nakao, Y. Nambu, and C. Yoo, Prog. of Theo. Phys. **117**, 229 (2007).
- [56] N. Brouzakis, N. Tetradis, and E. Tzavara, JCAP **0702**, 013 (2007).
- [57] N. Brouzakis, N. Tetradis, and E. Tzavara, astro-ph/0703586.
- [58] C. Bonvin, R. Durrer, and M. A. Gasparini, Phys. Rev. D **73**. 023523 (2006).
- [59] E. Barausse, S. Matarrese and A. Riotto, Phys. Rev. D **71**, 063537 (2005).
- [60] M. Kasai, H. Asada, and T. Futamase, Prog. of Theo. Phys. **115**, 827 (2006).
- [61] N. Li and D. J. Schwarz, gr-qc/0702043.
- [62] P. J. E. Peebles, Am. J. Phys. **37**, 410 (1969).
- [63] C. W. Misner, K. S. Thorne, and J. A. Wheeler, *Gravitation*, Freeman, San Francisco, CA (1973)
- [64] R. Sachs, Proc. R. Soc. A **264**, 309 (1961).
- [65] L. Hui and U. Seljak, IAUS **173**, 89H (1996).
- [66] H. Tanaka and T. Futamase, astro-ph/0612151.
- [67] J. M. Bardeen, J. R. Bond, N. Kaiser, and A. S. Szalay, Astrophys. J. **304**, 15 (1986).
- [68] R. E. Smith *et al.*, MNRAS **341**, 1311 (2003).
- [69] R. A. Vanderveld, É. É Flanagan, and I. Wasserman, Phys. Rev. D **74**, 023506 (2006).
- [70] L. Hui and P. B. Greene, Phys. Rev. D **73**, 123526 (2006).
- [71] T. Buchert, Gen. Rel. Grav. **32**, 105 (2000).
- [72] S. Zaroubi and Y. Hoffman, Astrophys. J. **414**, 20 (1993).